UNIVERSITY OF SOUTHAMPTON

LASER ACTION IN NEODYMIUM DOPED SILICA FIBRE

by

IAN PETER ALCOCK

A thesis submitted for the degree of Doctor of Philosophy

Department of Physics

Faculty of Science

September 1988

UNIVERSITY OF SOUTHAMPTON

ABSTRACT

FACULTY OF SCIENCE

PHYSICS

Doctor of Philosophy

LASER ACTION IN NEODYMIUM DOPED SILICA FIBRE

by Ian Peter Alcock

This thesis describes an investigation into the suitability of neodymium doped monomode optical fibre as a gain medium for miniature laser systems.

Characterisation of the material and parameters required for quantitative analysis of such laser systems are presented in a spectroscopic analysis carried out in the first part of the thesis. Measurements performed in this section also indicate that at room temperature the wide fluorescence bands of the neodymium doped silica fibre are spectrally broadened by a homogeneous process.

The behaviour of a longitudinally pumped continuous-wave fibre laser is modelled in the next section followed by the design and realisation of a

practical system. Efficiencies of approximately 6% and threshold pump powers of 8–12 mW have been obtained, even under narrow linewidth operation. Tunability over ranges of 45–60nm has also been demonstrated.

The thesis is concluded by experiments on pulsed fibre lasers. Q–switching the laser has achieved peak powers of several watts in pulses 180ns wide with good agreement between the results obtained and predicted values. Shorter pulses 450ps wide have been realised by mode–locking a fibre laser. Suggestions for reducing the pulse width further and the effects of material dispersion are also given. Finally modulated pump sources have been investigated and it is shown that synchronous pumping with short pulses has limitations due to dispersion, while resonantly pumping relaxation oscillations is a simple means of obtaining a pulsed output.

CONTENTS

CHAPTER 1

Introduction

Recent experiments have demonstrated the possibility of incorporating impurities such as rare–earth ions in the core of monomode optical fibres without impairing the high optical quality of such fibres [1]. These doped fibres not only allow passive but also active devices such as lasers [2,3] or amplifiers [4] to be constructed. Monomode fibre lasers of this type have several novel features which make them an interesting class of miniature lasers; the waveguide geometry readily lends itself to efficient longitudinal laser pumping and the ability to achieve high gains whilst minimising thermal problems. Also the broad fluorescence bands characteristic of impurity ions in glass lead to tuning of laser output over wide ranges [5,6], generation of short pulses [7], or broadband amplifiers. Other physical properties of the impurity ions can fulfill the requirements of sensor applications such as the temperature sensors based on the variation of absorption coefficient or fluorescence lifetime with temperature [8].

The work in this thesis outlines the assessment of neodymium doped fused silica as the gain medium in fibre lasers and it has formed the basis of several publications, and conference papers. It includes the first demonstration of Q–switching and mode–locking of fibre lasers; continuous–wave operation on the $^4F_{3/2}$ – $^4F_{9/2}$ transition of neodymium is also reported for the first time in a glass host.

Qualitative analysis of fibre laser performance requires a knowledge of various parameters such as absorption and emission cross–sections, quantum–efficiency

and transition lifetimes. Some of these parameters are difficult to measure in the fibre geometry because reabsorption can affect fluorescence spectra, the effect of spatial variations of fields across the doped core needs to be considered and the low concentration of dopant ions makes it difficult to determine the concentration independently eg by EPMA. Moreover, the composition of the glass host [9,10] affects the dopant ion spectra and there is plenty of evidence to suggest that rare–earth ions in fused silica are spectroscopically different to those in silicate glass. Therefore, this thesis also contains reports of the energy levels deduced from absorption and emission spectra, and lifetime and cross–section measurements. Any techniques relevant to measuring these parameters in fibres are also discussed.

Doped fibres are also spectroscopically interesting media because the dopant ions can be used to obtain information about the dynamics of the glass host. Previous experiments using bulk materials have been complicated by the variety of glass compositions studied and interactions between dopant ions. The long optical interaction lengths available in fibres allow low concentrations of dopant ions to be employed thereby minimising ion–ion interactions and fused silica is a relatively simple glass. Therefore, some brief measurements on the neodymium doped silica are also described along with some conclusions deduced from the results.

The remainder of this chapter will explain the basic features of optical waveguides followed by a summary of the use of rare–earth doped glass as a laser host and early work on fibre lasers. Then the optical properties of rare–earth ions in a glass matrix will be discussed with a brief reference to the dynamics of glass matrices.

Chapter two contains a description of the spectroscopic measurements performed on the Nd^{3+} doped fused silica including the equipment used. Chapter three outlines the design and alignment of a c.w. fibre laser cavity, followed by an assessment of the results obtained. The ability to tune neodymium doped fibre lasers is also demonstrated. Chapter four discusses pulsed fibre lasers including Q–switching and mode–locking.

1.1 Optical Fibre Waveguides

This section introduces the concepts behind optical waveguides and explains the terms which are used later on. The optical fibre consists of a central region, known as the core, which is surrounded by the cladding (figure 1.1). If light rays are to remain bound in the core by total internal reflection then the refractive index of the core must be higher than that of the cladding. However, the refractive index profile across the core can either be constant (step index) or variable (graded index).

Reflection at the core–cladding interface is governed by Snell's law and only those rays which subtend an angle relative to the fibre axis (figure 1.1) less than the complementary critical angle θ_c, will undergo total internal reflection. The complementary critical angle is defined by

$$\theta_c = \cos^{-1}\left(\frac{n_{cl}}{n_{co}}\right) = \sin^{-1}\left(\frac{n_{co}^2 - n_{cl}^2}{n_{co}^2}\right)^{1/2} \qquad (1.1)$$

n_{co} – refractive index of the core

n_{cl} – refractive index of the cladding

Applying Snell's law to the end face of the fibre one can see that the maximum angle a ray can make relative to the normal of the face, if it is to remain bound in the core is

$$\sin\theta_m = n_{co}\sin\theta_c = (n_{co}^2 - n_{cl}^2)^{1/2} \qquad (1.2)$$

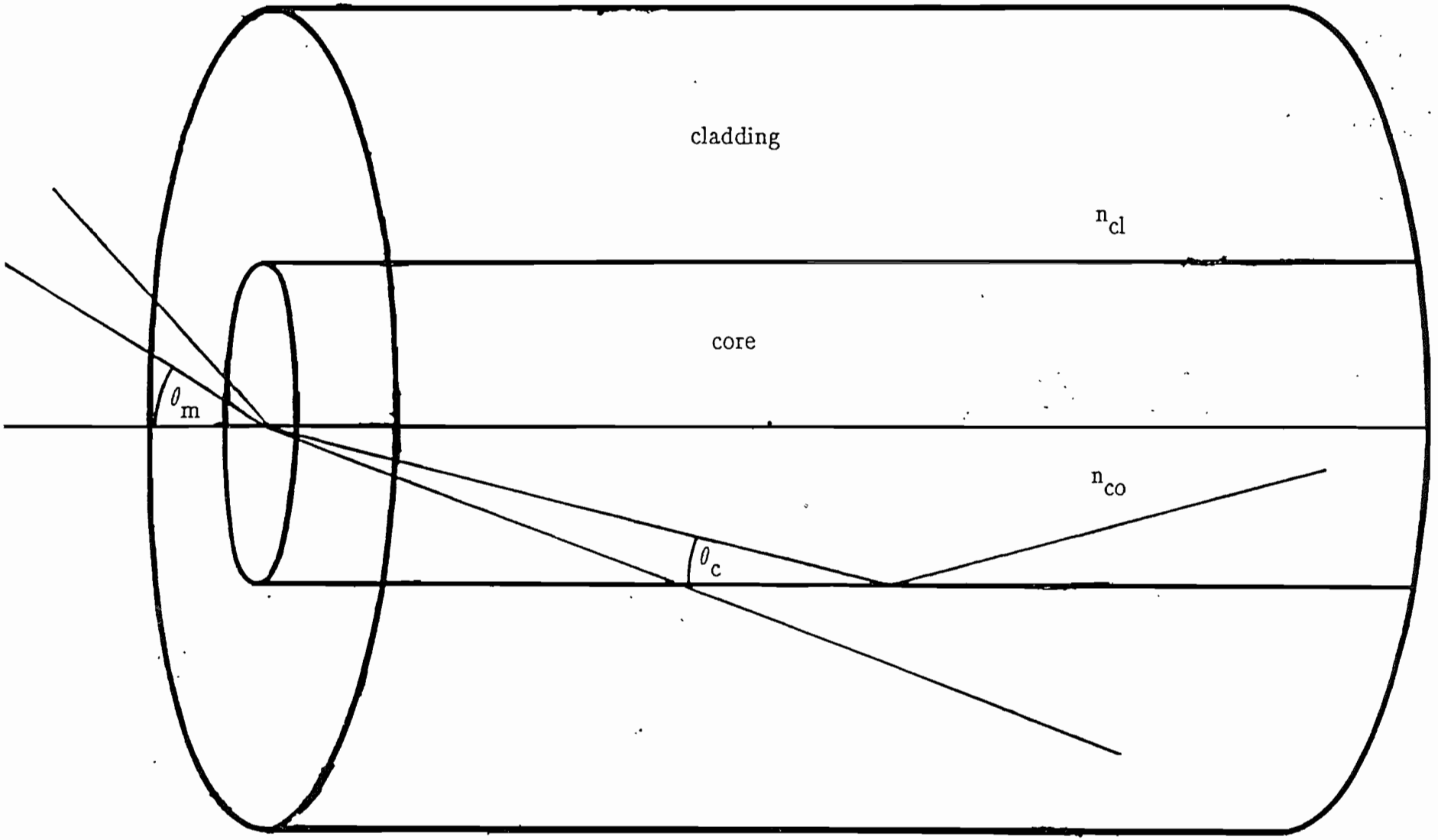

Figure 1.1

Bound and unbound rays in an optical fibre

Clearly this is a measure of the light collecting power of the fibre and is often called the numerical aperture (N.A).

This simple ray model is adequate for large core diameter fibres, but when the dimensions become small, the wave nature of the light must be taken into account and interference between the plane wave components of each ray and the phase shifts experienced at each reflection would have to be incorporated into the model.

If the effects of interference were considered for various combinations of all the possible bound rays then one could imagine that the interference patterns produced would depend on the combination chosen. As the numerical aperture of the fibre becomes smaller, the range of bound rays would be reduced and eventually only one interference pattern would be produced. These patterns are solutions to Maxwells equations applied to the fibre and are known as modes. The point at which light, whose wavelength is above a critical value, will only propagate in one mode is known as cut–off and the fibre is termed monomode.

The profile of the electric field inside the core, ie mode profile, of a step index fibre is described by a Bessel function of the first kind [11]. If the numerical aperture of the fibre is small, the fibre is said to be weakly guiding and the mode can be approximated by a Gaussian profile [11].

A dimensionless parameter known as the waveguide parameter is useful to characterise the fibres and can be used to determine mode sizes and distributions, or whether a fibre is multimode or monomode.

The parameter V is given by [11]

$$V = \frac{2\pi\rho}{\lambda}(NA) \qquad (1.3)$$

ρ = core radius

λ = vacuum wavelength of the light

The value of V at which cut–off occurs is found from the first zero of the Bessel function describing the lowest order mode and is 2.405 for a step–index fibre.

Within the Gaussian approximation the mode size is given by [11].

$$r = (2 \cdot \ln V)^{-1/2} \qquad (1.4)$$

From (1.4) it is apparent that as V gets smaller, ie the waveguide becomes more monomode, the mode size get larger. Consequently more energy propagates in the cladding, as the evanescent wave, and if only the core is doped then fewer photons see any dopant ions. Since this behaviour is not predicted using the simple ray model, it is obvious that these effects should be borne in mind when examining doped fibres.

1.2 Rare earth doped glass as a laser host material and early work on fibre lasers

Glass has been used extensively as a laser host material [12] for several reasons. Commercially it is desirable because it can be made cheaply in large sizes and pressed or moulded into various shapes while retaining excellent optical quality; the broad optical linewidths available from ions doped into glass allow the possibility of producing tunable solid–state lasers and short mode–locked pulses. Absorption of pump radiation from broadband sources can also be more efficient on account of the broad linewidths. However, this is accompanied by a reduction in stimulated emission cross–sections, which can either be viewed as an advantage or disadvantage. On the one hand it enables efficient amplification and energy storage to be achieved since amplified spontaneous emission is reduced, but it also increases the pump power required to produce lasing action.

Since heat is generated by the energy difference between the absorbed and emitted photons, and non–radiative processes, this raising of the threshold pump power increases the amount of thermal energy which must be dissipated. The outer surface of the material is likely to be cooled more effectively than the centre, thereby causing a large thermal gradient to be set up if the material has a low thermal conductivity. The parabolic radial temperature profile produced in a uniformly pumped rod can be used to some advantage. If the material has a temperature dependant refractive index then a parabolic refractive index profile will be also produced and it will act as a waveguide.

However, associated with the temperature profile are stresses induced by the resulting differential expansion. Since the conductivity of glasses is generally

low, this imposes a limit on the pump power that can be used before fracture of the material occurs. Therefore, limitations on permissible pump powers, and small emission cross–sections have made c.w. operation of glass lasers difficult.

A solution to the problem is to reduce the thermal gradient and stresses by reducing the material dimensions.

Assuming a uniform deposition of heat in the material allows the maximum stress generated in a rod to be given by [13]

$$\sigma_{max} = \frac{2 \quad P_a \alpha \, E}{8\pi L \, K \, (1 - \nu)}^{1/2} \qquad (1.5)$$

α = thermal expansion coefficient

E = Youngs modulus

K = thermal conductivity

ν = Poissons ration

L = length of rod

P_a = absorbed pump power

If fracture is to be avoided then this must be smaller than the rupture stress σ_r. Therefore, replacing σ_{max} by σ_r in expression (1.5) one can obtain an upper limit for the absorbed pump power permissible. However, if laser operation is to occur then assuming 4 'level' behaviour, the absorbed pump power must exceed the threshold value given by [Appendix A]

$$P_{th} = \frac{h \nu_p}{\sigma_e \tau} \cdot \frac{\gamma}{\eta} \cdot \pi \, r^2 \qquad (1.6)$$

h = Plancks constant

ν_p = pump frequency

γ = logarithmic cavity loss

σ_e = stimulated emission cross section

τ = lifetime of upper laser level

η = fraction of excited electrons which end up in the upper laser level

r = radius of rod

Combining expressions (1.5) and (1.6) allows the maximum rod diameter possible before fracture occurs, to be calculated.

eg.

$\nu_p = 366$ THz

$\gamma = 0.1$

$\sigma_e = 1.6\times10^{-24}$ m^2

$\tau = 480$ μs

$\eta = 0.75$

$E = 7.3\times10^{10}$ Nm^{-2} [14]

$\nu = 0.17$ [14]

$\alpha = 3\times10^{-6}$ K^{-1} [14]

$k = 1.1$ $Wm^{-1}k^{-1}$ [14]

$\sigma_r = 4\times10^{7}$ Nm^2 [14]

gives a maximum radius of 1.1mm for a 6cm long rod. This approach of reducing the material dimensions was successfully exploited by Young [15] who demonstrated the first c.w. glass laser, with the medium in the form of a short length of multimode cladded glass fibre. The same technique was used by Uchida et al [16] to produce c.w. oscillation in a Kr lamp pumped SELFOC Nd^{3+} doped glass rod.

An alternative approach to reducing the thermal gradient is to reduce the pumped area by end pumping with a laser. If a rod, radius r_2, is subjected to uniform pumping over a radius r_1, only, then the maximum stress now becomes [13]

$$\sigma_{max} = \frac{2^{1/2} P_a \alpha E}{8\pi L K (1 - \nu)} \cdot \left[2 - \left[\frac{r_1}{r_2}\right]^2\right] \qquad (1.7)$$

and the radius in expression (1.6) is now r_1.

Therefore, if $r_1 < r_2$ the stress generated for a given P_a is approximately twice that of the previous case but the value of P_a required to reach threshold is reduced by $\left[\frac{r_1}{r_2}\right]^2$.

This means that either the stress at threshold is reduced by $2\left[\frac{r_1}{r_2}\right]^2$ by end pumping a radius r_1, rather than r_2 or a cavity which is $\frac{1}{2}\left[\frac{r_2}{r_1}\right]^2$ times more lossy can reach threshold before fracture occurs. This latter approach allowed Kishida et al [17] to achieve the first c.w. oscillation in Nd^{3+} doped phosphate glass using an Ar^+ ion pump laser. A combination of both techniques was utilised by Stone and Burrus [18] when they end pumped a multimode, cladded glass fibre with an Ar^+ ion laser. It is also obvious that the material parameters affect the permissible pump powers and Quartz has an expansion coefficient which is typically an order of magnitude smaller than most other glasses.

Diffraction losses in the resonator will increase if either technique is employed unless total internal reflection or waveguide techniques are used to confine the radiation. Hence, many of the aforementioned studies had the gain medium in the form of some type of waveguide. Indeed cladded glass fibre lasers were reported as far back as the early 1960's by Koester and Snitzer [19] who also employed the novel variation of a passive core surrounded by an active cladding to provide amplification by the evanescent wave [20]. However, the details of the experiments are somewhat sparse and appear to have mainly been performed using side pumped multimode fibres. Now that the ability to grow high quality doped monomode fibres has been developed [1], the ability to take the reduction in pumped area to the extreme by end pumping a doped monomode fibre can be realised [2,13]. This results in a pumped area of only a few μm^2 and an overall fibre diameter of approximately $110\mu m$ so that fracture from thermal loading is virtually non–existent.

The nature of a monomode fibre waveguide ensures that only the lowest order transverse mode will be supported, to be contrasted with the previous experiments, and inherently stable devices can be made. Also full compatibility with fibre optic device technology and telecommunications grade fibres is ensured. Utilisation of existing fibre technology enabled a fibre ring laser to be constructed [2], which required no optical alignment other than launching the pump into the doped core.

Further advantages are that guidance of the pump allows long interaction lengths to be achieved and the small dimensions of the doped core, $2 \rightarrow 6$ μm, results in very intense pumping.

There are, however, several factors unique to these fibre lasers which must be

carefully considered if the systems are to be fully optimised. Although longitudinal pumping the fibre geometry has many advantages, the variation of the pump intensity down the fibre must be taken into account if reabsorption is to be avoided in 'three level' systems; the intrinsic mismatch in the overlap of the pump and laser modes must also be examined in order to determine the limitations on the efficiency of these devices and to optimise the fibre design. Moreover, the unusual cavities used in fibre lasers can result in non–linear and dispersive materials almost filling the entire cavity and possibly impose a limit on short pulse generation using fibre lasers. However, incorporating long lengths of doped non–linear materials in cavities could be a natural extension to the demonstration of c.w. Raman oscillation in a Nd^{3+}:YAG intra–cavity fibre laser [21], where lengths of quartz fibre were inserted in a c.w. Nd^{3+}:YAG laser cavity to provide a Raman gain medium.

1.3 Spectroscopic Properties of Rare–earth Ions in a Glass Host

Optical transitions in rare–earth doped hosts correspond to transitions within the manifold of 4f electrons of the rare–earth ions. Since the states involved have the same parity then transitions should only occur by even parity processes such as magnetic–dipole or electric–quadrupole. However, an electric dipole process is generally responsible and is allowed by the ligand field of the host mixing states of different parity into the 4f states [22].

The ligand field has both static and dynamic components, both of which contribute to the spectroscopic properties of the ion.

The static component is responsible for the splitting of the free ion levels and radiative transitions between levels. If the host is not uniform, such as is the case in a glass, then the local field at each rare–earth site will be slightly different, resulting in a distribution of energy levels. This will effectively broaden any spectral lines and this type of broadening is termed inhomogeneous on account of its non–uniformity. The variation of the local field at each rare–earth ion site can also cause lifetimes of levels to vary from site to site. This is particularly evident when fluorescence following pulsed excitation decays non–exponentially because a distribution of exponentially decaying sites is observed [23].

The dynamic component of the ligand field causes dephasing and multiphonon non–radiative decay. The latter can be observed when a fluorescence lifetime which is shorter than that expected by radiative decay or one which has a temperature dependent value is measured.

Associated with each spectral line lying inside the inhomogeneous profile is an intrinsic linewidth determined by the dephasing rate and finite lifetime of levels involved. This broadening is termed homogeneous because it is similar at each rare–earth ion site and can be smaller or greater than the inhomogeneous contribution. Since this type of broadening is partially due to the dynamic component of the ligand field, its magnitude is temperature dependent while the inhomogeneous linewidth generally is not.

From the preceding paragraphs it should be apparent that energy differences, transition rates, linewidths between levels are intimately related to the ion–host coupling. Therefore by measuring absorption and emission spectra, one ought to be able to calculate parameters such as transition cross–sections, excited state lifetimes, quantum efficiencies. A summary of how these parameters can be calculated is given below [22].

The absorption cross–section $\sigma_a(\nu)$ of a transition is related to the absorption coefficient $k(\nu)$ by

$$k(\nu) = N\ \sigma_a(\nu) \qquad (1.8)$$

where N is the population density of the lower level.

If the transition is assumed to be homogeneously broadened and has a Lorentzian line profile, one can calculate the cross–section at the peak of the line using

$$\sigma_{ap} = \frac{2}{\pi\Delta\nu}\,\frac{1}{N}\int k(\nu)d\nu \qquad (1.9)$$

with

$$\sigma_a(\nu) = \sigma_{ap} \cdot \frac{1}{1 + \left(\frac{2(\nu - \nu_p)}{\Delta\nu}\right)^2} \qquad (1.10)$$

$\Delta\nu$ = line width defined as F.W.H.M.

ν_p = frequency of the line centre

Hence by measuring $k(\nu)$ one can calculate $\sigma_a(\nu)$ with a knowledge of N.

Similarly the emission cross–section can be found in a similar manner by measuring the gain coefficient. However, the inversion must be known and this may prove difficult to measure accurately. Therefore, the emission cross–section can be found from the absorption cross–section using

$$\sigma_e(\nu) = \frac{g_1}{g_2}\, \sigma_a(\nu) \qquad (1.11)$$

where g_1 and g_2 are the degeneracies of the lower and upper levels.

The lifetime associated with spontaneous radiative decay from one level to another can be calculated from

$$\frac{1}{\tau_{rad}} = \frac{8\pi}{\lambda^2} \frac{g_1}{g_2} \frac{n^2}{N} \int k(\nu) d\nu \qquad (1.12)$$

n = refractive index of the material

If the upper level decays to more than one lower level then the total radiative lifetime of the level is found by summing over the other transitions.

$$\frac{1}{\tau_{rad}} = \sum_i \frac{1}{\tau_{rad\ i}} \qquad (1.13)$$

The branching ratio for the transitions is given by

$$\beta_i = \frac{1/\tau_i}{\sum_i 1/\tau_i} \qquad (1.14)$$

or it can be found by measuring the intensity of the fluorescence from each transition and calculating the fraction of emitted photons per transition ie

$$\beta_i = \frac{I_i / \nu_i}{\sum I_i / \nu_i} \qquad (1.15)$$

The radiative quantum efficiency of the level can be found by comparing the calculated radiative lifetime to the measured fluorescence lifetime.

$$\eta = \frac{\tau_{fl}}{\tau_{rad}} \qquad (1.16)$$

Finally if the transition is homogeneously broadened, with a Lorentzian profile then the peak emission cross–section can be found from expressions (1.9), (1.11) and (1.12).

$$\sigma_{ep} = \frac{\lambda^2}{4\pi^2 n^2 \Delta\nu\ \tau_{rad}} \qquad (1.17)$$

So far only the coupling between the impurity ion and static component of the host ligand field has been considered, primarily with the aim of calculating parameters required for the assessment of optical gain media. However, a

wealth of information about dynamical modes of the host can be derived by studying the homogeneous linewidth of impurity ions since it reflects the interaction between the dynamic component of the host field and the impurity ion.

Various high resolution laser techniques such as Fluorescence Line Narrowing (F.L.N.)[24–26], Spectral Hole Burning [27] and Optical Coherent Transients [28] have been used to measure the homogeneous contribution to the linewidth of 'probe' ions doped into glasses. These experiments have shown that the homogeneous linewidth of these 'probe' ions at low temperatures is 10^2–10^3 times broader than that of the same ion in crystals. These observations have been partially explained by proposing a coupling between the probe ions and low frequency, localised disorder modes peculiar to amorphous structures. The existence of these modes, pictured as an ensemble of 'two level systems' was first postulated to account for the anomalous thermal properties of glass at low temperature [29,30]. However, this model has not been entirely successful in explaining the results of optical linewidth measurements unless various coupling schemes are involved [31–34]. This may be partly due to the large combination of different 'probe' ions and glass hosts studied [24–27] over various temperature ranges.

One would, therefore, like to obtain data on a simple glass such as high purity fused silica over a large temperature range, 0.1 → 300K. As in previous studies of inorganic glasses, a rare–earth ion will be chosen as the probe ion because its spectral lines are sharp. In particular a Nd^{3+} ion has been chosen because a low temperature experiment 0.1 – 1K [35] has already been performed on Nd^{3+} doped fused silica which yielded a previously unreported, for an inorganic glass, homogeneous linewidth temperature dependence of $T^{\frac{4}{3}}$ and one would like to extend the temperature range covered.

CHAPTER 2

2. Spectroscopic measurements of the Nd^{3+} ion in a fused silica host

2.1 Apparatus and Samples

The lasers used throughout the studies were a Coherent Innova 90 Ar^{+} ion laser and a Coherent 599 c.w. tunable dye laser. The dye laser was supplied with a birefringent filter which not only allowed tuning over the gain of the dye but also limited the output bandwidth to approximately 20GHz. For some experiments this bandwidth was too large and so the laser was modified to allow single longitudinal mode operation using an intra–cavity assembly, consisting of two etalons and a Brewster plate mounted on a galvanometer drive, loaned by Coherent UK.

An external temperature stabilised cavity provided a reference which the dye laser could be locked to (figure 2.1). Any drift of the laser with respect to the reference cavity produced an error signal and the drift was corrected by tilting the Brewster plate and moving one of the mirrors using a piezo crystal. The stabilisation made a bandwidth of approximately 1MHz possible.

The stabilised laser could also be scanned over a 30MHz range by varying the length of the reference cavity with a tipping Brewster plate.

The samples were provided by S.B. Poole (Fibre Optics Group at Southampton University) using a Modified Chemical Vapour Deposition technique [1] in which dopants are added as volatile chlorides and deposited onto the inside of a high quality fused silica tube. The tube is then collapsed

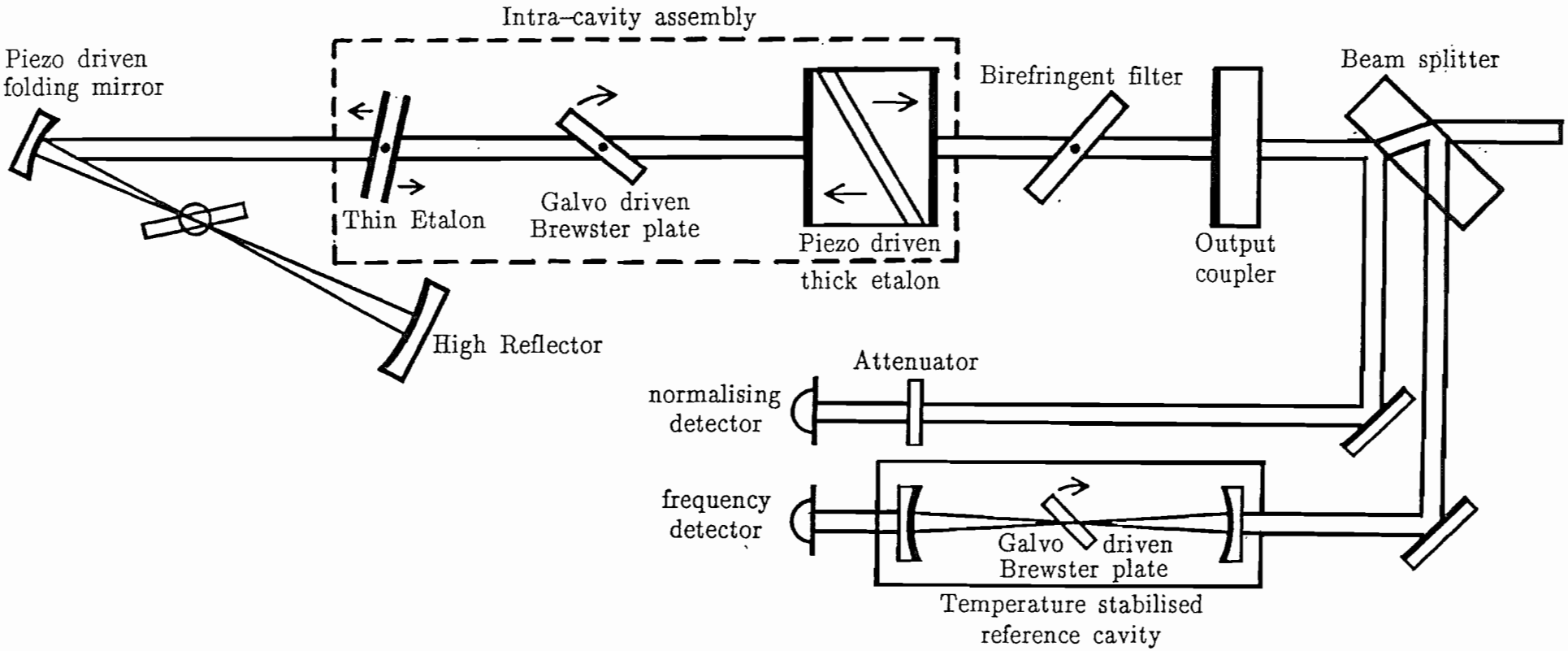

Figure 2.1

Schematic of stabilised, single–mode dye laser

forming a rod, known as the preform, whose central core contains the dopant ions, which can then be drawn into optical fibres if required.

All of the samples studied were cut or drawn from the same preform and had a Nd^{3+} dopant ion concentration of approximately 300ppm (S.B. Poole). The geometry of the sample, ie fibre or preform, was selected to optimise the measurements.

Temperature control of fibres is in principle much easier than conventional samples because their long length allows heat to be dissipated more efficiently and reduces the possibility of localised heating due to pump absorption. However, in practice getting the fibre into a cryostat and coupling light in and out is more difficult, especially if the fibre is not to be stressed or damaged during liquid He transfers.

The surface strain of a fibre, radius a, wound onto a former of radius R (figure 2.2) is

$$\text{strain} = \frac{((R + 2a)-(R+a))\delta\theta}{(R+a)\delta\theta} = \frac{a}{R + a} \qquad (2.1)$$

Assuming Young's Modulus 10^{11} Nm^{-2} and a fracture stress of $\sim 10^{9}$ Nm^{-2} for fused silica, a minimum former radius of 6mm is calculated ($a \sim 60\mu m$) if fracture of the fibre is not to occur. In practice a 3.5cm radius former was used because it was the largest that would fit into the crystal and smaller formers, 5–10mm radius, resulted in the fibres cracking after 5–10 temperature cycles. Coupling light into the doped fibre was most easily achieved by splicing it to undoped fibre tails epoxied into a home–made, leadthrough on the cryostat top flange. The undoped tails also ensured that all of the doped fibre could be cooled.

Figure 2.2

Strain on a fibre wound around a former, radius R.

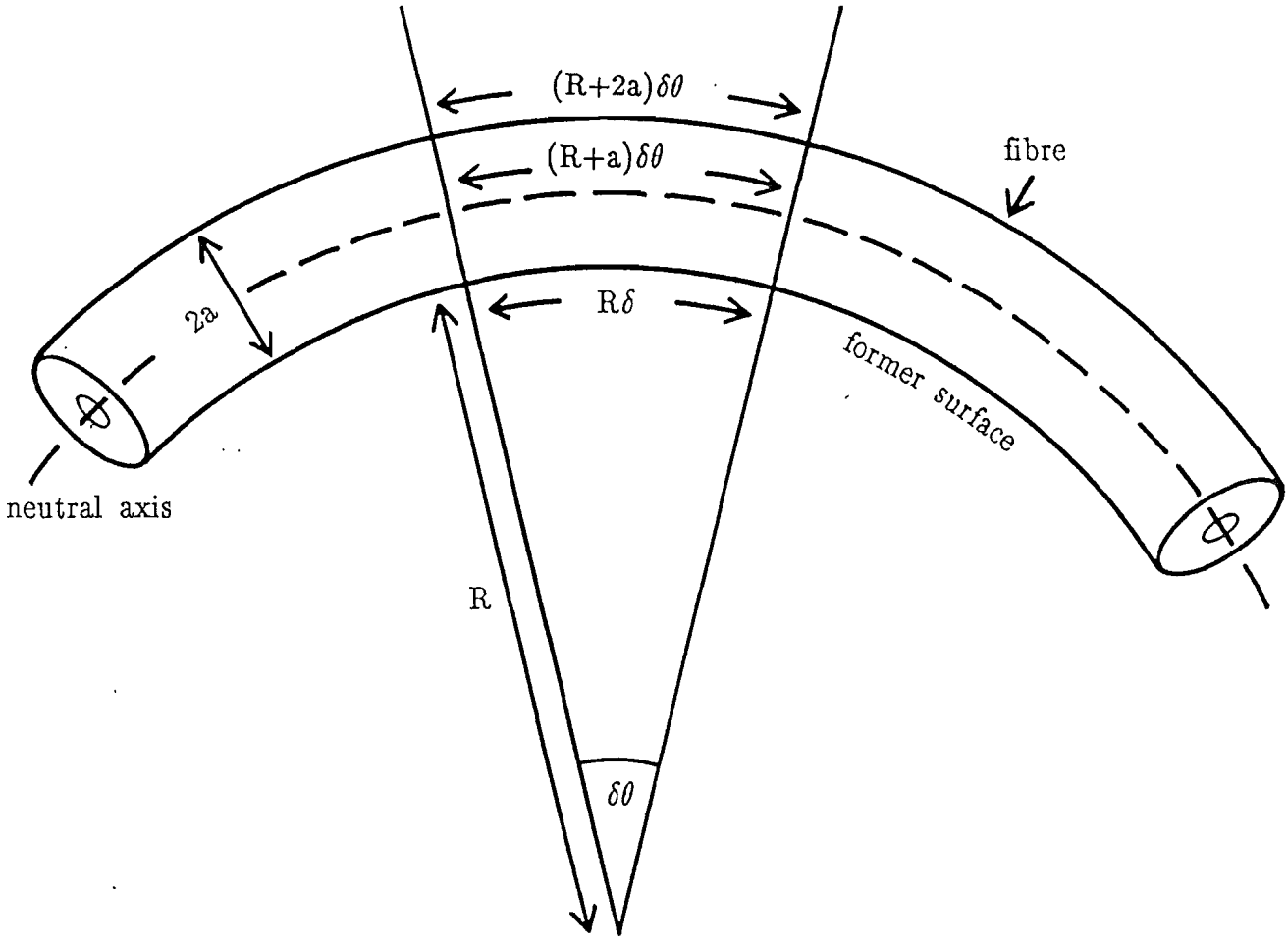

Commercial three axis micropositioners allowed the fibres to be positioned to within 0.1μm of the image produced by the focussing microscope objective. In section 1.1 it was shown that there is a maximum angle that an incoming ray can make with the fibre axis if it is to remain bound in the core. For a circular fibre this defines the maximum cone of light that can be accepted by the fibre. However, if the cone is tilted (figure 2.3) with respect to the fibre axis then all of the rays will no longer remain bound. In the case of monomode fibres energy will be coupled into higher order modes which are not supported by the waveguide and it will be radiated into the cladding. This situation can occur if the axes of the incident light, focussing lens or fibre are tilted or offset with respect to each other. Therefore, the positioners were attached to mounts which could be raised and tilted using three orthogonal adjusting screws.

Because there were no windows in the cryostat, the previous arrangement was not suitable for experiments which require fluorescence to be collected transversely. For experiments of this type a gas flow cryostat was used and the size of its tail required that the samples were short lengths of doped preform. Although transverse collection of the fluorescence may be easier using pieces of preform it is apparent that the shorter lengths compared to fibres will reduce the emitted fluorescence power and be a disadvantage. However, the higher collection efficiencies possible using the preform can largely offset this potential disadvantage.

An estimate of the amount of collected fluorescence can be made from

$$P_f = P_l \, \eta_l \, \eta_q \, \eta_c (1 - e^{-\alpha l}) \qquad (2.2)$$

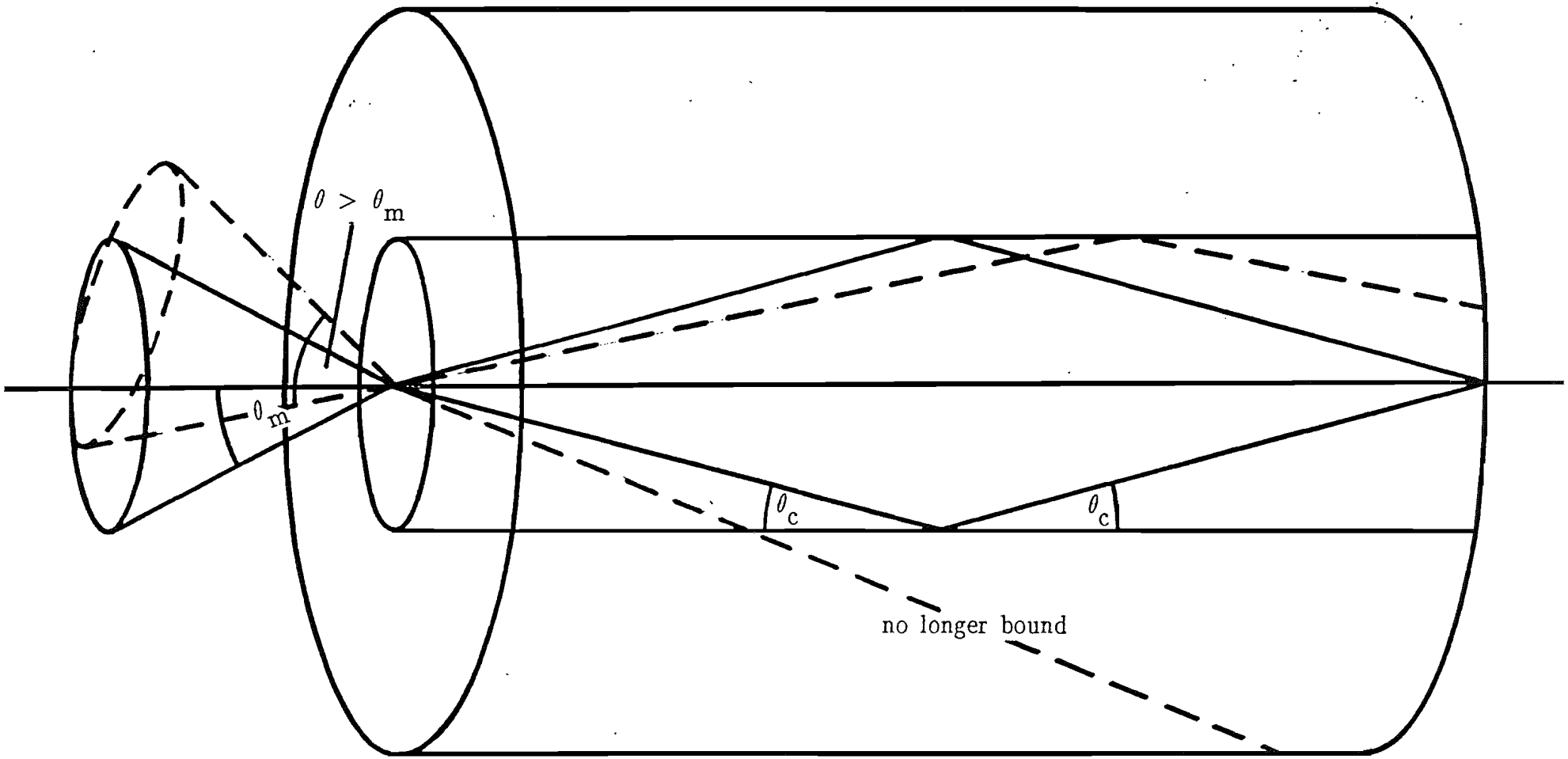

Figure 2.3

The effect of tilting an incident cone of light on the bound rays

P_l = Pump power

η_l = coupling efficiency of the pump power into the doped sample

η_q = ratio of emitted to pump photons

η_c = collection efficiency

α = absorption coefficient

l = sample length

For fibre samples η_l depends on the launch efficiency into the undoped pigtail and the transmission of the pigtail to sample splice. The collection efficiency can be split into three parts, the first being the transmission of the sample to pigtail splice. The second contribution occurs because the fluorescence is emitted uniformly in all directions and only a small fraction will be captured and remain bound in the core. This fraction is approximately given by

$$\frac{1}{4}\left[\frac{\text{N.A.}}{n_{co}}\right]^2 \qquad (2.3)$$

The final contribution depends on how many of the bound rays that the collimating or focussing lens will collect. If the N.A. of the lens is larger than that of the fibre then this term will be unity (neglecting reflection losses at the lens surfaces).

Even though the pigtail fibre was carefully matched to the doped fibre, the splices typically had transmission of less than 50% and launch efficiencies of 40% were obtainable. Therefore, a 1.3m fibre with an absorption coefficient of 4.52cm^{-1} and an N.A. of 0.21, would give a collected amount of fluorescence of approximately

$$P_f \sim 5.2\times10^{-4}\, P_l \eta_q$$

In the case of the preform the only contributions are from the launch efficiency of the pump into the preform and the collection properties of the collimating or focussing lens. The larger doped core enabled launch efficiencies of around 80% to be achieved and collecting lenses with an N.A. of ~ 0.25 can be used. This gives

$$P_f \sim 1.3\times10^{-2}\ P_l \eta_q (1 - e^{-\alpha l})$$

and hence only a 10mm long preform sample would give the same P_f for a given pump power. Therefore, even for experiments in which reabsorption is not a problem, collecting fluorescence transversely from a piece of preform is comparable to using a longer length of fibre viewed end on.

2.2.(a) Fluorescence and Absorption Measurements

A 1.3m length of doped fibre, which was found to give a reasonable amount of absorption was spliced to two lengths of undoped fibre whose numerical aperture and core diameter had been carefully matched to the doped fibre. It was then hung inside a bath cryostat so that all of the doped fibre could be cooled to the same temperature. Broadband light from a tungsten halogen lamp was launched into the fibre and the transmitted light was passed through a grating monochromator onto an extended infra–red response silicon photodiode. The signal from the diode was amplified using a Stanford instruments SR10 lockin amplifier before being recorded on a chart recorder. The absorption bands around 890 nm were studied in detail at 290K, 77K and 4.2K using a cooled S1 photomultiplier tube as the detector. The absorption curves obtained are shown in figures 2.4–2.5.

The fluorescence measurements required that any fluorescence was collected transversely in order to avoid the effects of reabsorption. For reasons mentioned earlier in the chapter this was most easily achieved using a short length of preform (8mm long, core diameter of 0.5mm) mounted in a gas flow cryostat. The preform had two flat surfaces ground and polished on it so that the fluorescence could be imaged more easily and scattered laser light reduced. In order to aid the alignment of the laser with the small doped core, a copper foil baffle centred about the core was held against one face. An Argon ion pump laser operating at 514nm was used to pump the sample and the collected fluorescence image was rotated by 90° using a Dove prism (figure 2.6). This ensured that the image was parallel to the slits of the grating monochromator. An extended infra–red response silicon photodiode was used to detect the bands at 0.906 μm and 1.08 μm while a Germanium photodiode was used at 1.36 μm. The signal from the detector was amplified using a

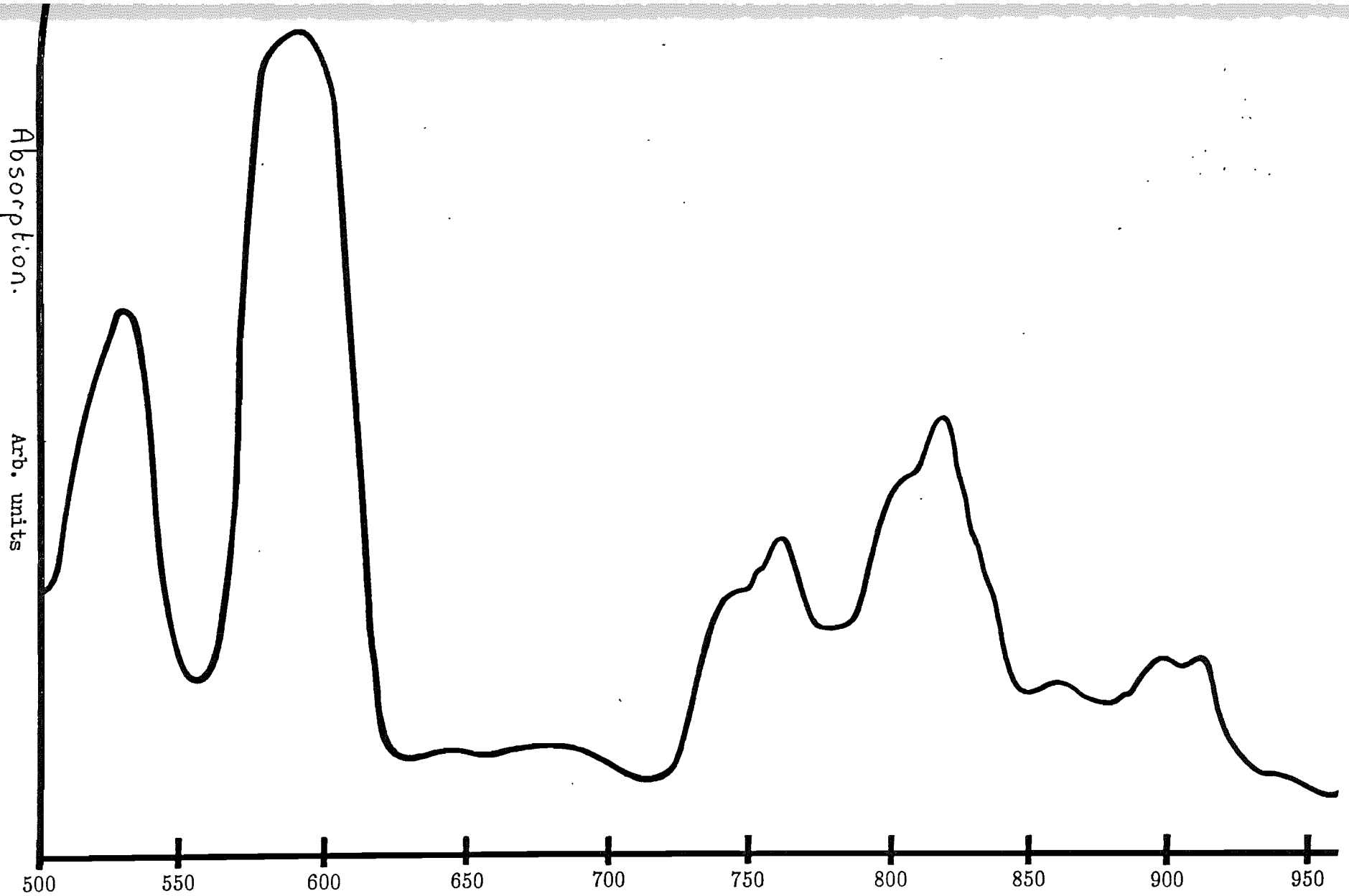

Figure 2.4

Absorption spectra of Nd^{3+} doped silica fibre

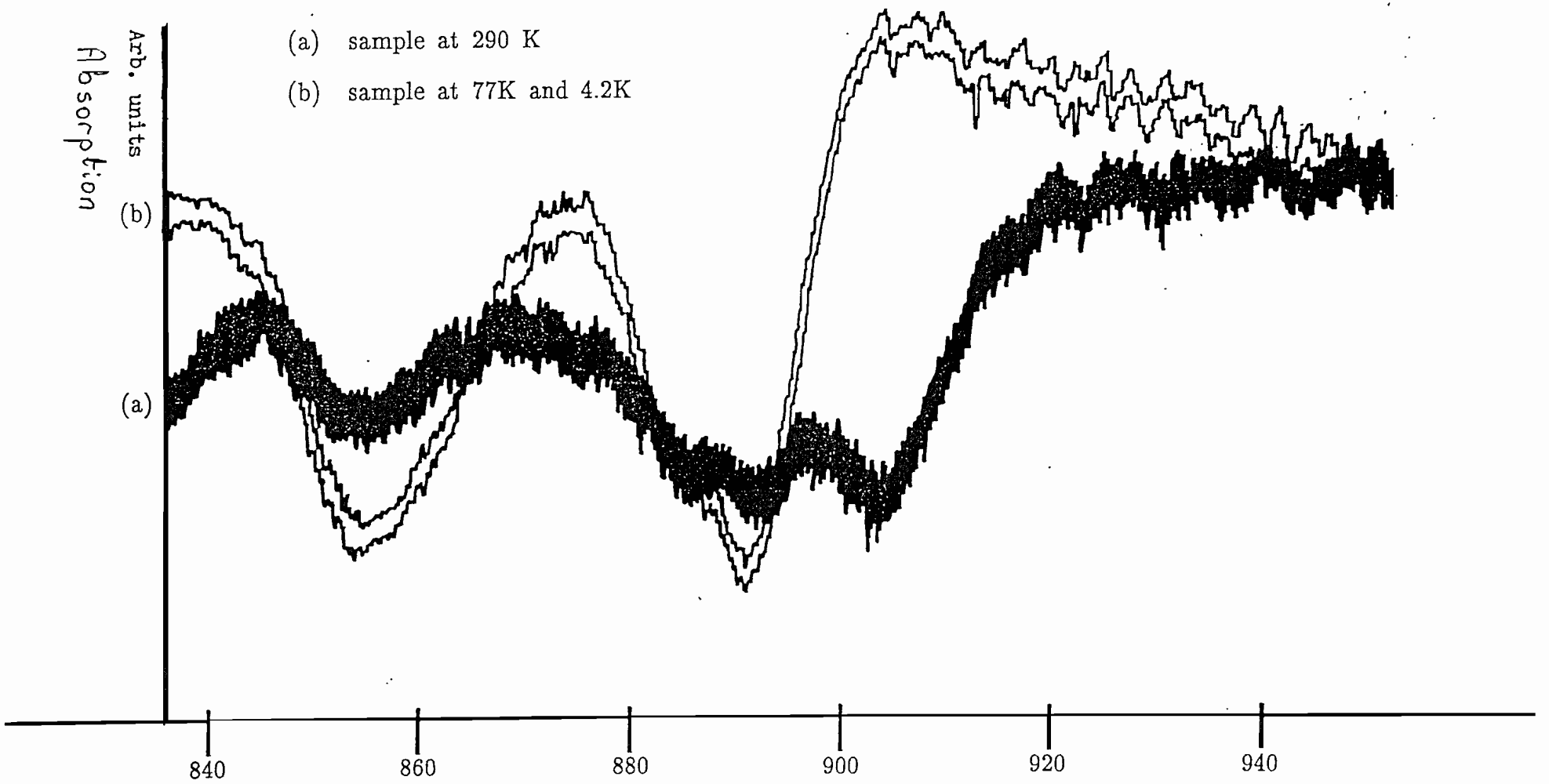

Figure 2.5

Absorption spectra of Nd^{3+} doped silica fibre

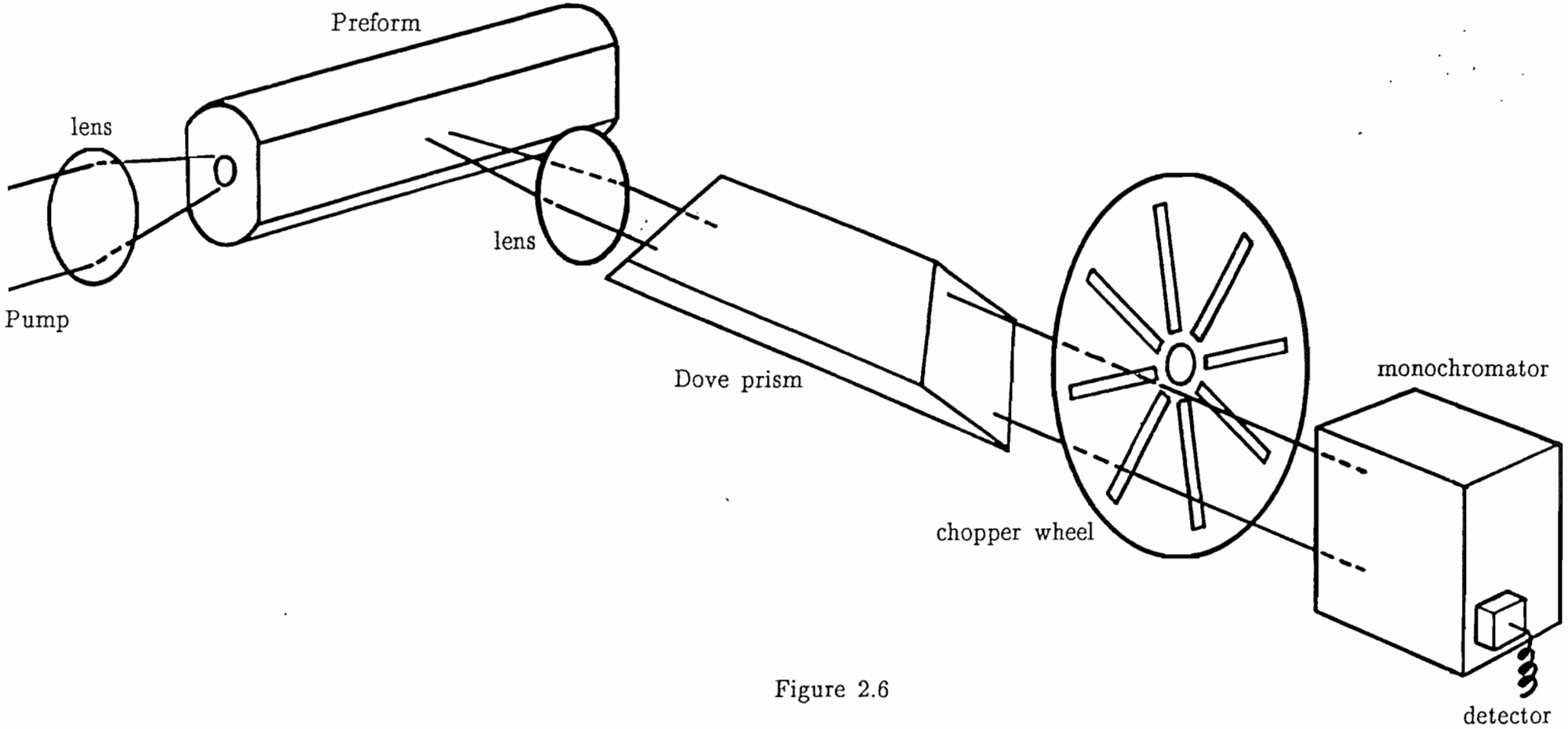

Figure 2.6

Experimental configuration for Fluorescence measurements

Stanford Instruments SR10 lockin amplifier and recorded using a chart recorder. The lockin amplifier could produce an output which was the ratio of two inputs and so any drift in the laser power could be compensated for using a reference channel. The spectra obtained are shown in figures 2.7–2.9.

In addition, the bands at 0.906 μm measured with the sample cooled to 77K and 4.2K using a cooled S1 photomultiplier tube, figure 2.7.

Interpretation of Results

The lack of symmetry of the electrostatic field at the rare–earth site in the glass host not only produces inhomogeneous broadening but also removes the degeneracy, other than Kramers degeneracy, of the states of the free Nd^{3+} ions; the removal of the free ion degeneracy results in the $^4F_{3/2}$ level being Stark split into two components and the $^4I_{9/2}$ level into five components. If rapid relaxation occurs from these levels then they will be thermally populated in accordance with a Maxwell Boltzmann distribution; this will also be true for the upper components of the $^4F_{3/2}$ level because the lifetime of the lower component is long enough to allow thermalisation to take place.

When the sample is at 4.2K only the lowest components of the $^4F_{3/2}$ and $^4I_{9/2}$ levels will be populated and so the two absorption peaks in figure 2.5 must be from the lowest component of $^4I_{9/2}$ to the two components of $^4F_{3/2}$. This gives a splitting of 460cm^{-1} for the $^4F_{3/2}$ level which is in good agreement with that published by Hegarty et al [35]. The fluorescence peaks in figure 2.7 must then correspond to transitions from the lowest component of the $^4F_{3/2}$ to the three lowest components of $^4I_{9/2}$.

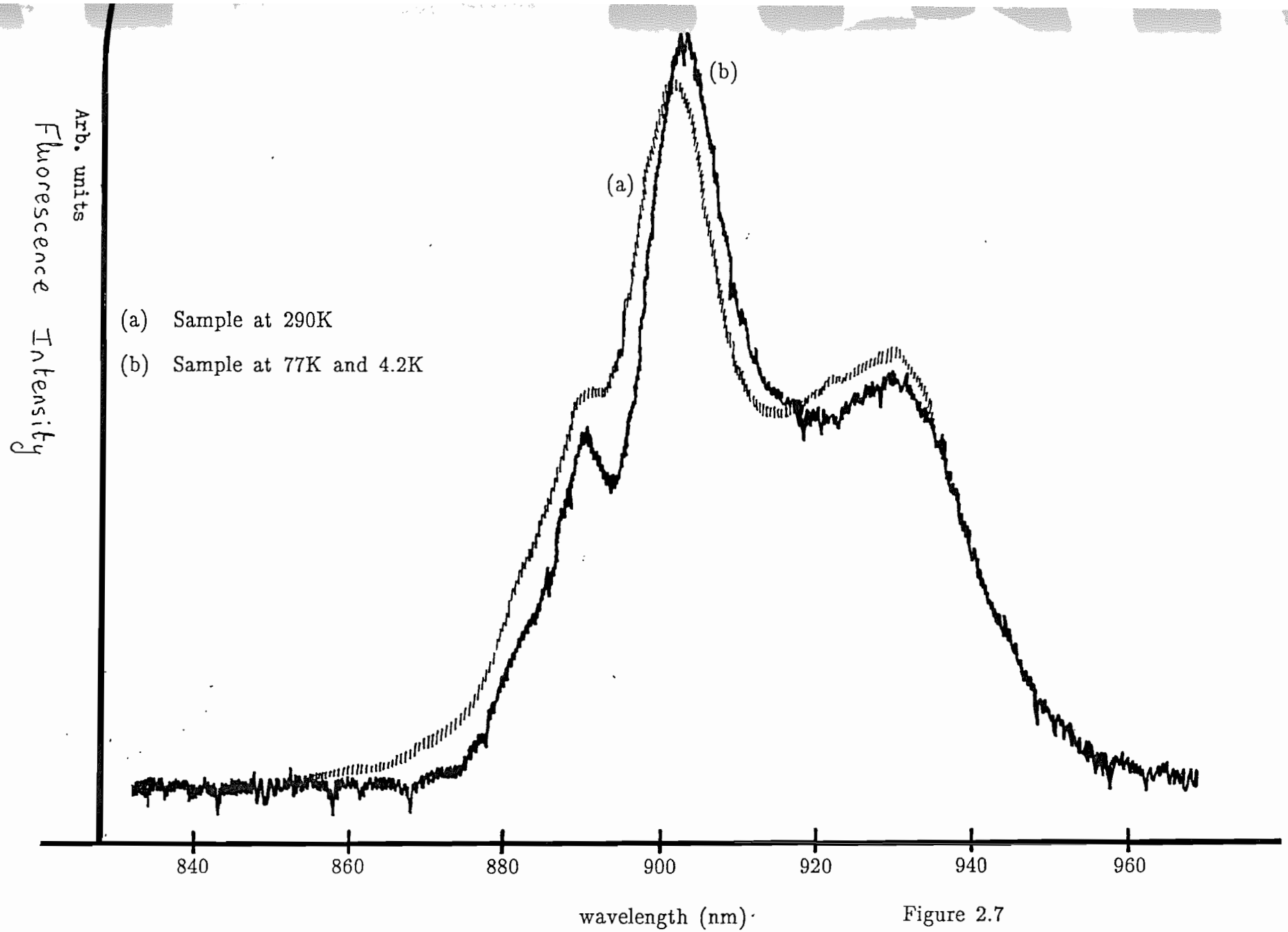

Figure 2.7

$^4F_{3/2} - {}^4I_{11/2}$ Fluorescence Spectra of Nd^{3+} doped silica

Figure 2.8

$^4F_{3/2} - {}^4I_{11/2}$ Fluorescence spectra of Nd^{3+} doped silica

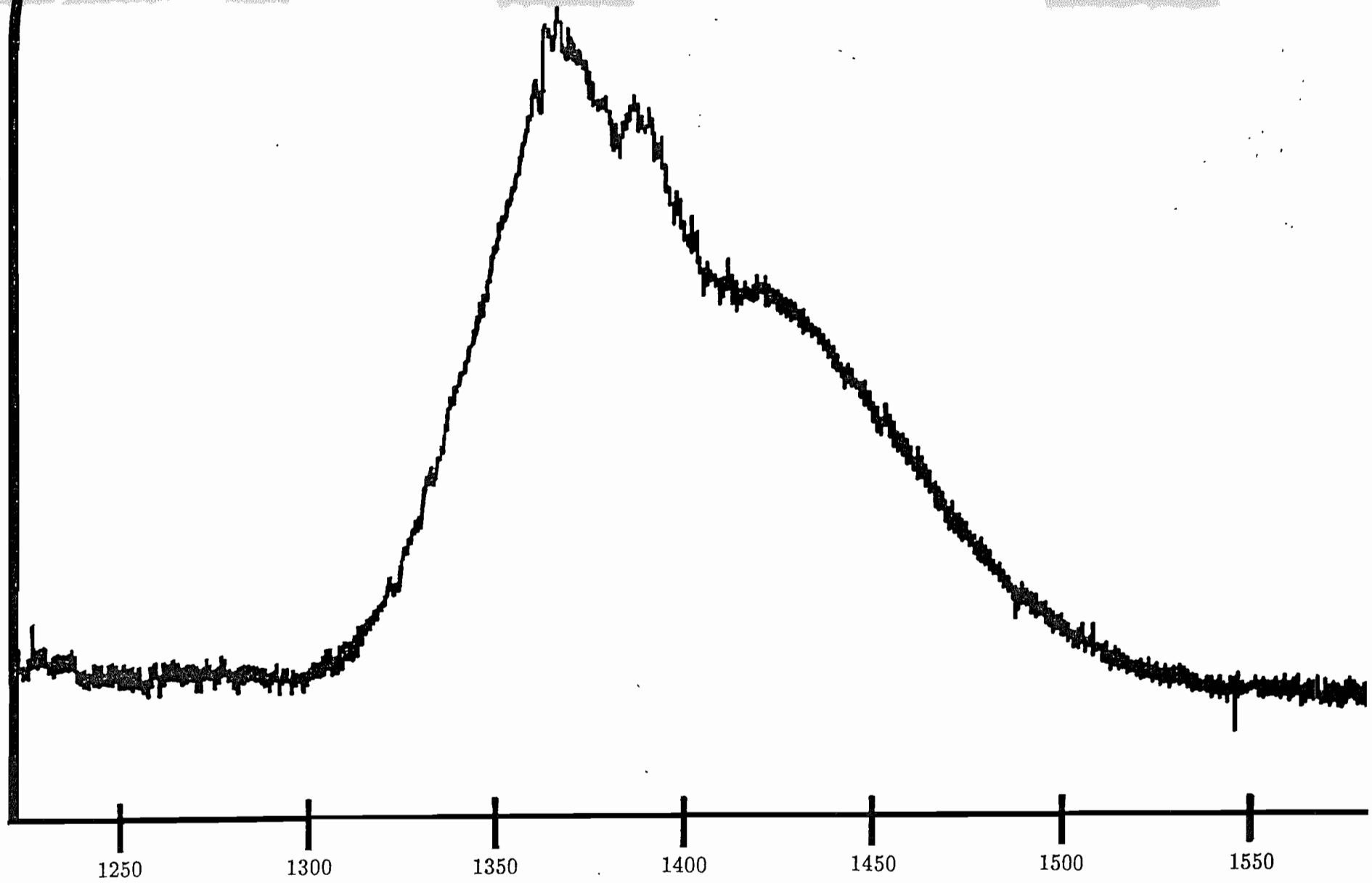

Figure 2.9

$^4F_{3/2} - {}^4I_{13/2}$ Fluorescence spectra for Nd^{3+} doped silica

As the temperature of the sample is increased, additional absorption peaks begin to appear, figure 2.5, which correspond to the fluorescence peaks of figure 2.7. These additional peaks occur because the lower components begin to become thermally populated; although the population of the component at $552cm^{-1}$ is only 7% even at 290K and is therefore, weakly absorbing. Similarly little fluorescence is observed from the upper component of $^4F_{3/2}$ because this component has only some 11% of the population of the lower component at 290K. A 'shoulder' can be seen on the short wavelength side of the peak at 890nm (figure 2.5) which is attributed to an unresolved component of the $^4I_{9/2}$ ground state. Peaks corresponding to transitions to the fifth component of the $^4I_{9/2}$ level are not seen either because they are unresolved or the transition is weak.

Similar conclusions about the energy levels involved in the $^4F_{3/2}$ - $^4I_{11/2}$, $^4I_{13/2}$ transitions can be made from figures 2.8, 2.9, although few components were resolved and no absorption peaks were seen. Figure 2.10 summarises the deduced energy levels for the Nd^{3+} ion in a fused silica host.

A temperature sensor has been demonstrated by Farries et al [8] which was based on the change of absorption of the Nd^{3+} ion at 904nm with temperature. Their results can be explained by a thermally induced population variation of level (b) in figure 2.10.

The room temperature spectra are similar to other published spectra [18, 36, 37] for Nd^{3+} doped fused silica, although the emission around 1.34 μm does not appear to have been reported. It is interesting to note that the transitions occur at longer wavelengths than in other Nd^{3+} doped glasses; therefore, a fused silica host may be able to extend the spectral range offered by other Nd^{3+} doped hosts. Also by adding other dopants one could alter

Figure 2.10

Ground state and Excited state energy levels of Nd^{3+} in silica

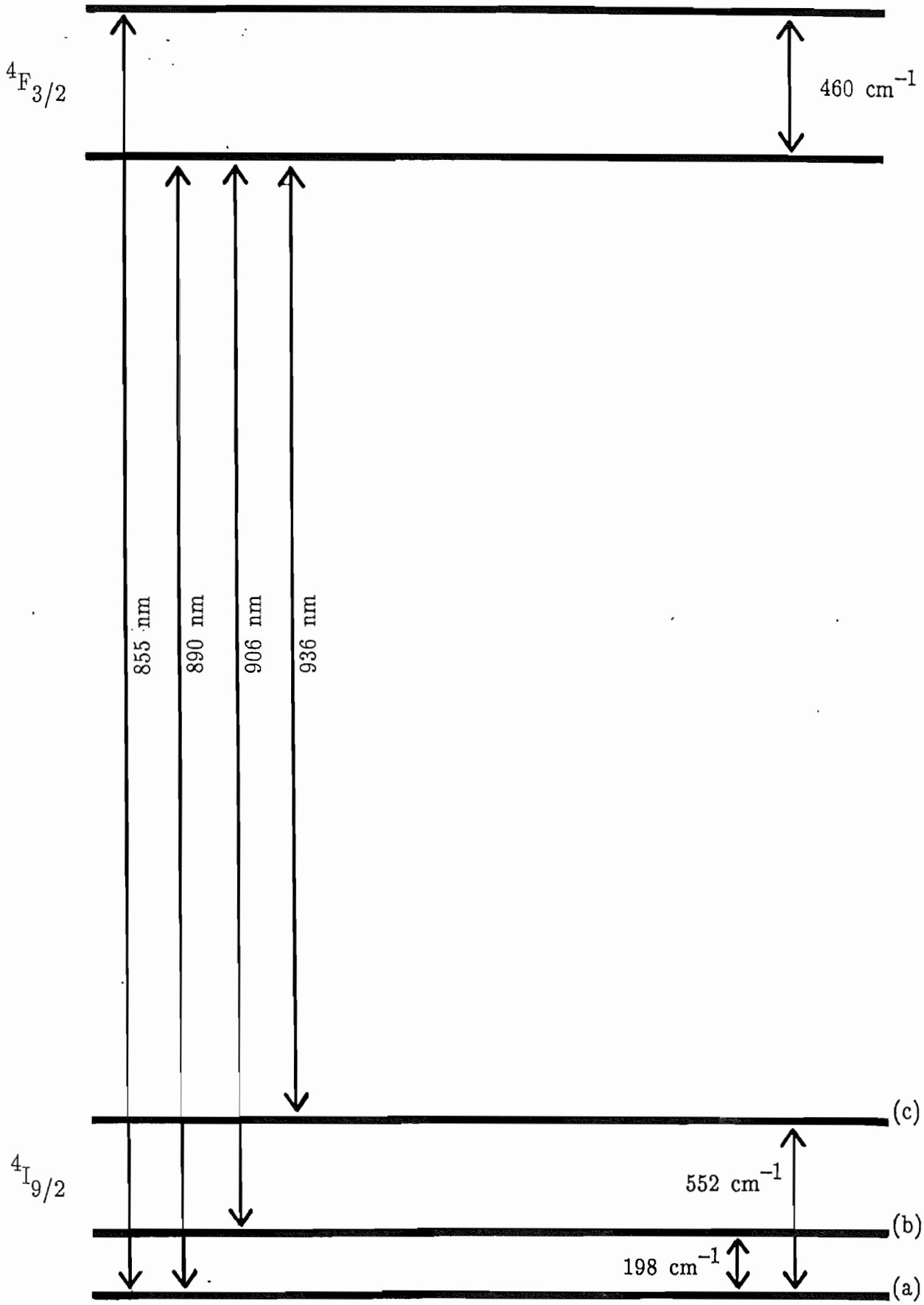

the transition rates or frequencies [10, 38, 39] to suit a particular application. This could be important, as will be shown in chapter 3, for operation at 1.3 μm.

2.2 (b) Absorption Coefficient Measurements

The absorption measurements from the previous experiments did not yield absolute values for the absorption lengths, only relative values. The following experiment provided an absolute measurement at 890nm and 590nm.

An Argon ion laser operating at 514nm pumped a Rhodamine 6G dye laser tuned to 590nm. The dye laser was launched into a length of doped fibre and the transmitted power was measured as a function of the fibre length under the same launch conditions. Any drift in the laser power was eliminated using the ratio facility on the lockin amplifier. The drift in the launch was less than 5%. A similar experiment was performed using the Argon ion laser running on all lines to pump a Styryl 9 dye laser tuned to 890nm.

The attenuation of the pump laser (see Appendix A) is given by

$$\ln\left[\frac{I_p(o)}{I_p(l)}\right] + \frac{I_p(o) - I_p(l)}{\frac{h\nu_p}{\sigma_p \tau}} = \alpha l \qquad (2.4)$$

Providing that there is little or no saturation of the absorption band, the pump intensity will decay exponentially as it propagates down the fibre. Therefore, a logarithmic plot of the pump intensity against fibre length should yield a straight line from which α, the absorption coefficient, can be calculated.

Because all of the power flow in the fibre was not confined to the core, a correction to the measured value must be made. This correction can be made by defining [40] an effective absorption coefficient.

$$\alpha' = \alpha \, \eta_p$$

α = plane wave absorption coefficient

η_p = fraction of power in the core, which may be deduced from a knowledge of the waveguide parameter, V

Figure 2.11 shows the results for 590nm and a reasonably good straight line was obtained. A least squares fit to the data gave a value of $\alpha' = 4.52$ m^{-1}. The fibre core radius was 1.7 μm and the N.A. was 0.21 (deduced from data given by S.B. Poole). This gave a value of V = 3.8 at λ = 590 nm from which a value of $\eta_p = 0.94$ was found using tables in [11].

Therefore, a value of $\alpha = 4.81$ m^{-1} at 590 nm was obtained.

A similar calculation using the data in figure 2.12 gave a value of $\alpha = 0.71$ m^{-1} at 890 nm.

The Nd^{3+} concentration was estimated to be 300ppm (S B Poole) of which approximately 60% would be in the ground state, neglecting depopulation due to the pump rate, at 290K. This corresponds to a ground state ion concentration of 4×10^{18} ions/cm^3.

Using expression 1.9, the absorption cross–sections at 590nm and 890nm were calculated to be 1.21×10^{-24} m^{-2} and 1.79×10^{-25} m^{-2} respectively.

The results are summarised in table 2.1.

Figure 2.11

Logarithmic Plot of laser intensity

as a function of length $\lambda = 590$ nm

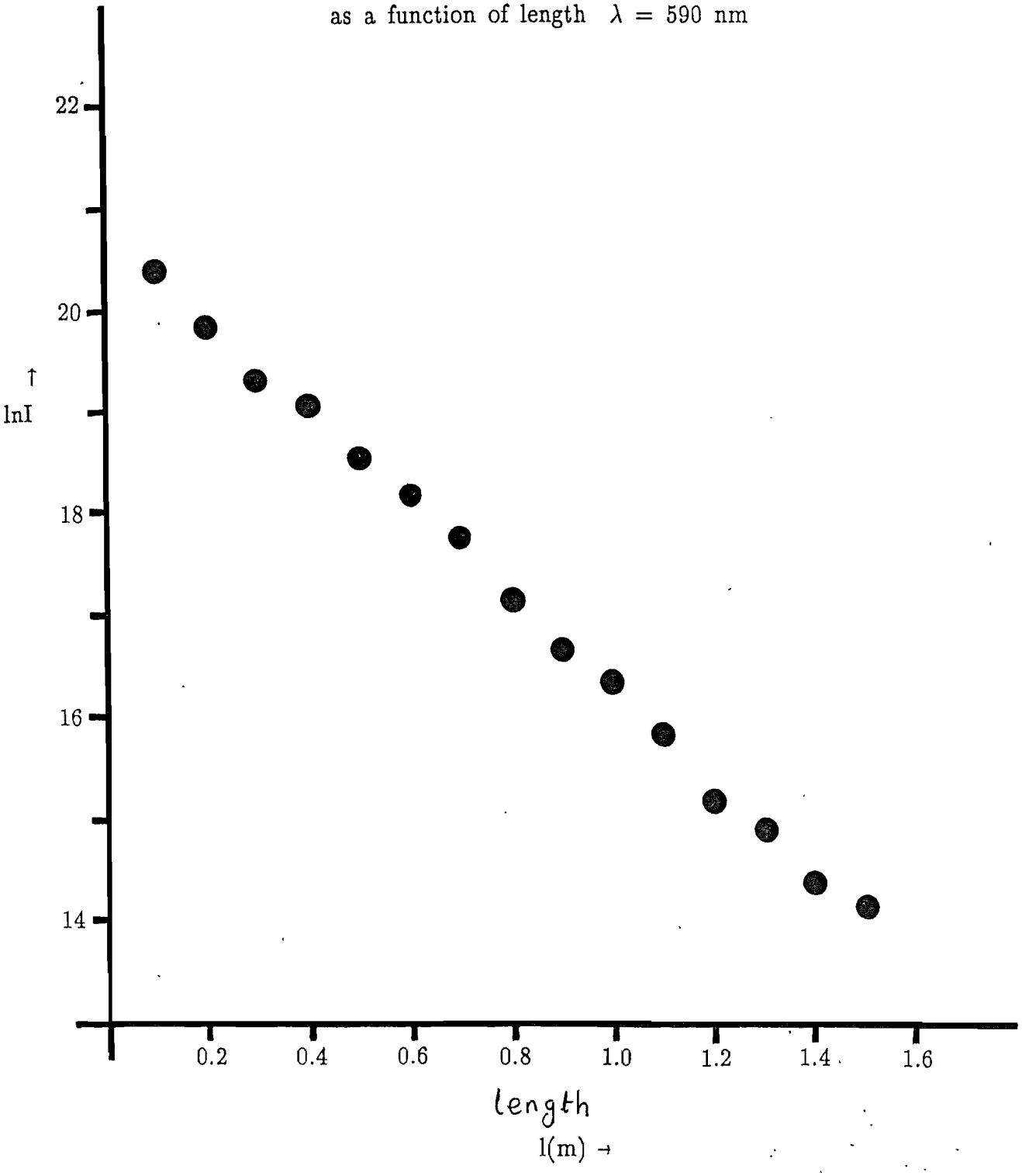

Figure 2.12

Logarithmic plot of laser intensity as a function of length $\lambda = 890$ nm.

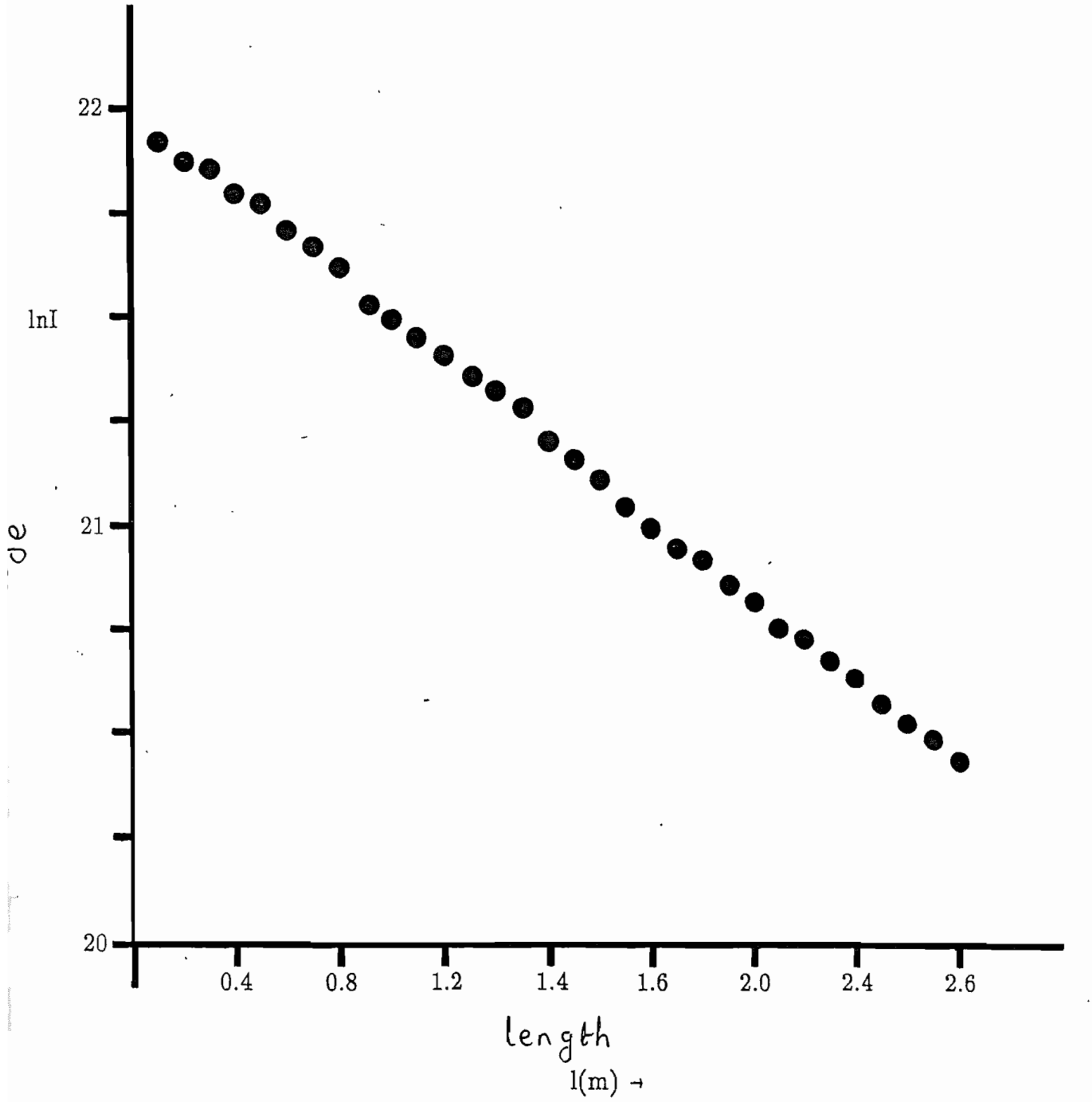

Table 2.1

Summary of parameters used to calculate the absorption cross-sections at $\lambda = 590nm$ and $\lambda = 890nm$

λ (nm)	590	890
ρ (μm)	1.7	1.7
V	3.80	2.52
η	0.94	0.84
α' (m^{-1})	4.52	0.60
α (m^{-1})	4.81	0.71
N_t (cm^{-3})	$6.67 \cdot 10^{18}$	$6.67 \cdot 10^{18}$
N_g (cm^{-3})	$4 \cdot 10^{18}$	$4 \cdot 10^{18}$
σ_p (m^2)	$1.21 \cdot 10^{-24}$	$1.79 \cdot 10^{-25}$

2.3 Lifetime Measurement

The experimental configuration is similar to that used in the fluorescence measurements except that the cooled S1 photomultiplier was terminated into a 10 kΩ load and amplified using a Tektronix 7A22 plug-in amplifier. The amplified signal was then averaged using a Tektronix 7D20 digitising plug-in and stored on disc via an I.E.E.E. interface controlled by a BBC microcomputer.

Both a fibre and preform were used as samples and gave identical results. However, care had to be taken when using high pump intensities with the fibre sample because sufficient gain could be created to cause a shortening of the lifetime. A 1 kHz test signal was used to calibrate the time axis of the plots.

The decay obtained after averaging 8 samples is shown in figure 2.13. From this plot the 1/e and $1/e^2$ decay times were determined to be 475 ± 20 μs and 960 ± 20 μs respectively. A logarithmic plot of the intensity as a function of time is shown in figure 2.14 and indicates that a roughly exponential decay is observed over 2 × 1/e decay times. A least squares fit to the data over this region gives a 1/e decay time of 480 ± 30 μs which is in fair agreement with the published values [1, 36, 37, 38].

The near exponential decay infers that the rare-earth in-host coupling at each site is similar and the transition may be homogeneously broadened.

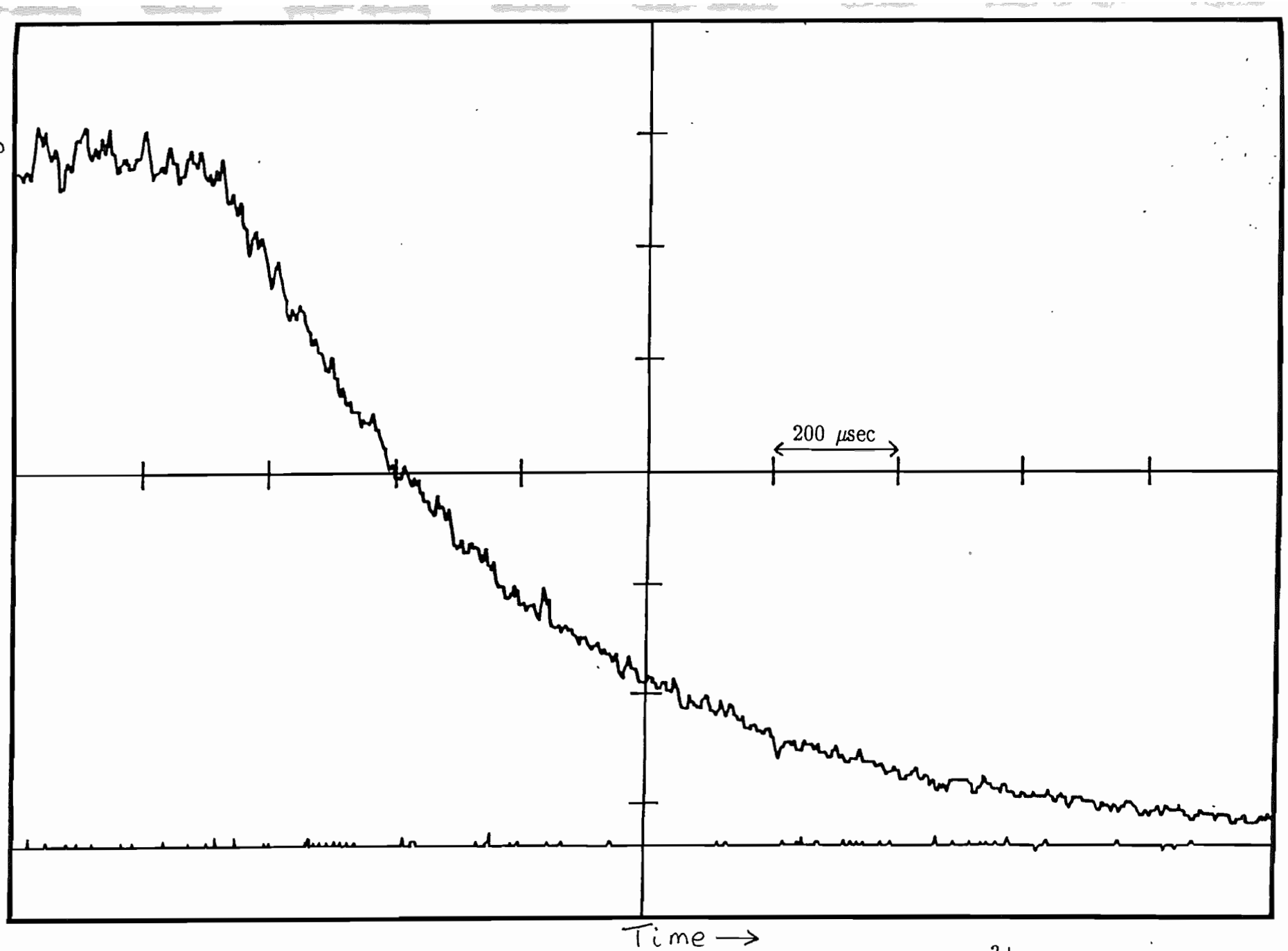

Figure 2.13 Fluorescence decay of Nd^{3+} in silica

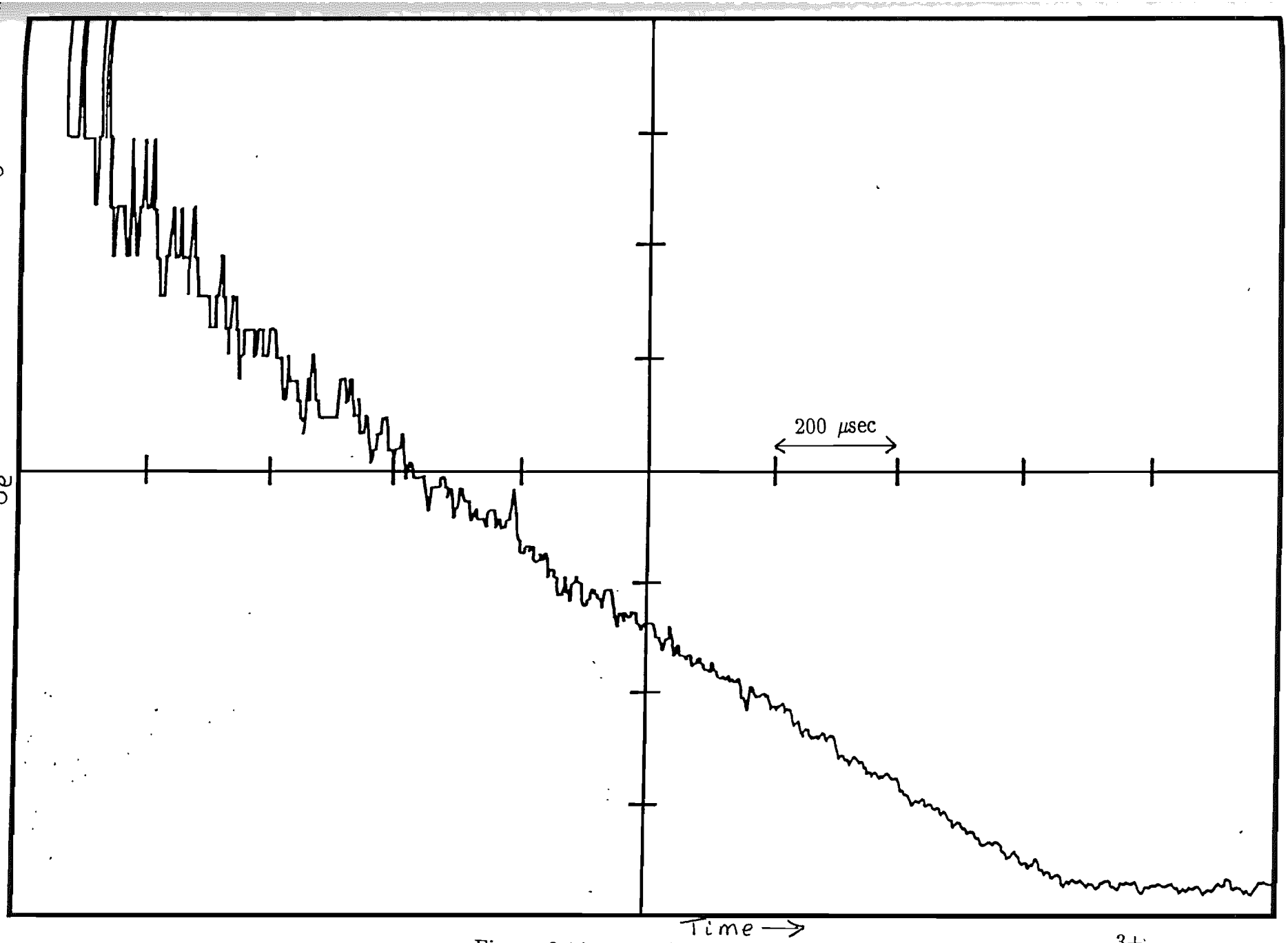

Figure 2.14 Logarithmic plot of fluorescence decay of Nd^{3+} in silica

2.4 Linewidth Measurements

Introduction

In the preceding sections some of the energy levels of the Nd^{3+} ions were deduced from the absorption and fluorescence spectra and inferences made about the possible spectral broadening mechanisms involved. This section outlines the experiments performed to determine the broadening mechanism and measure transition linewidths to provide information about the dynamics of the glass host.

The transitions were probed using a method known as Fluorescence Line Narrowing (F.L.N.). The technique relies on the narrow linewidth of a laser exciting a homogeneously broadened subset of sites inside an inhomogeneously broadened transition (figure 2.15) and measuring the spectrum of the emitted radiation. However, the results may not solely contain information about the homogeneous broadening because accidental degeneracy can result in an inhomogeneous component also being measured unless certain precautions are taken. This situation is depicted in figure 2.16 and occurs when impurities at different host sites accidentally have two of their energy levels in resonance and contribute to the measured spectrum. Therefore, if ambiguous data is to be avoided only sites which resonantly absorb and fluoresce must be probed.

If the pump and emitted fluorescence are at the same wavelength then gating of the excitation and detector is necessary if the scattered laser light is not to swamp the fluorescence signal and saturate or damage the detector.

Figure 2.15

Homogeneously broadened line lying inside an inhomogeneous profile

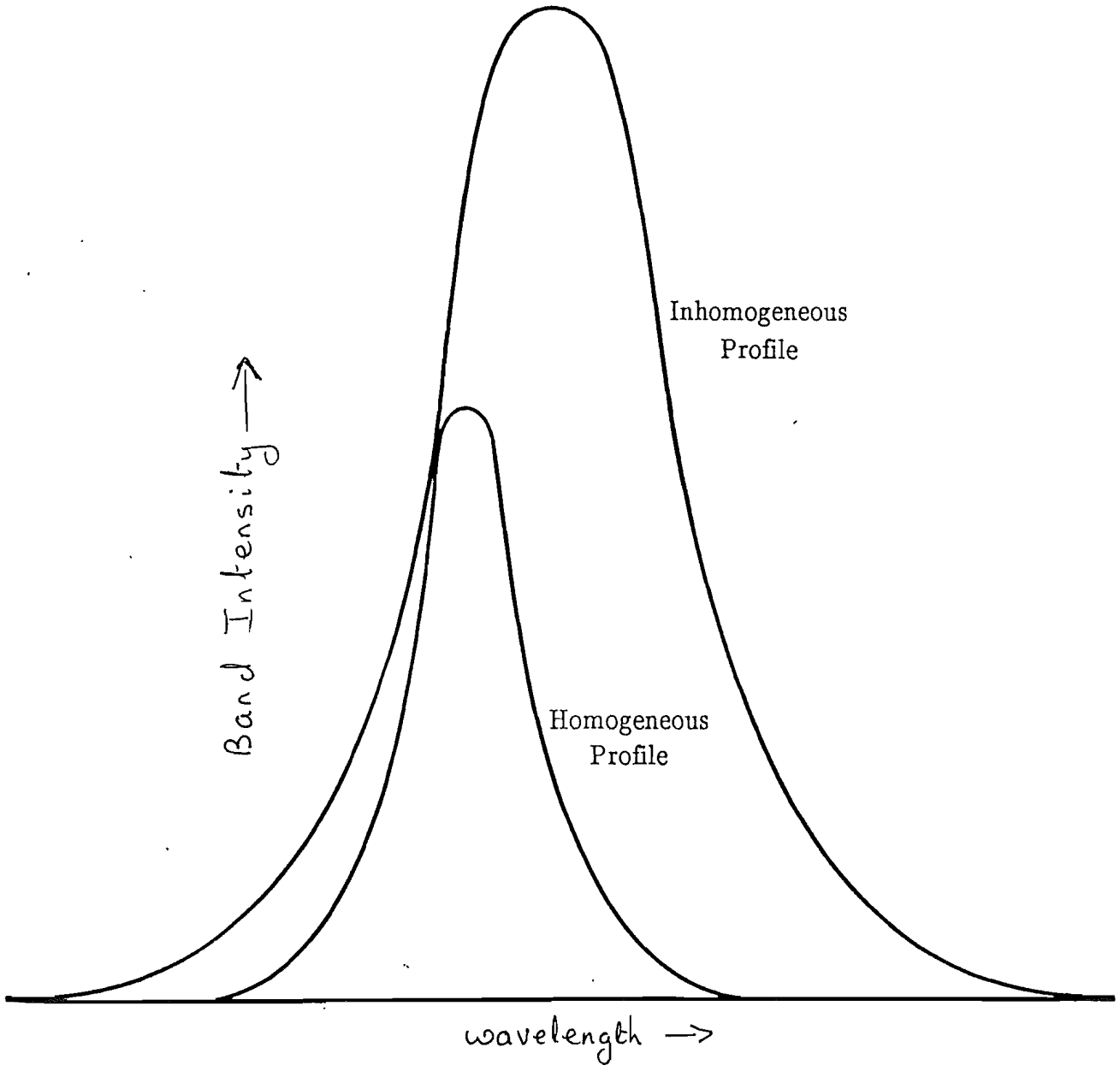

Figure 2.16

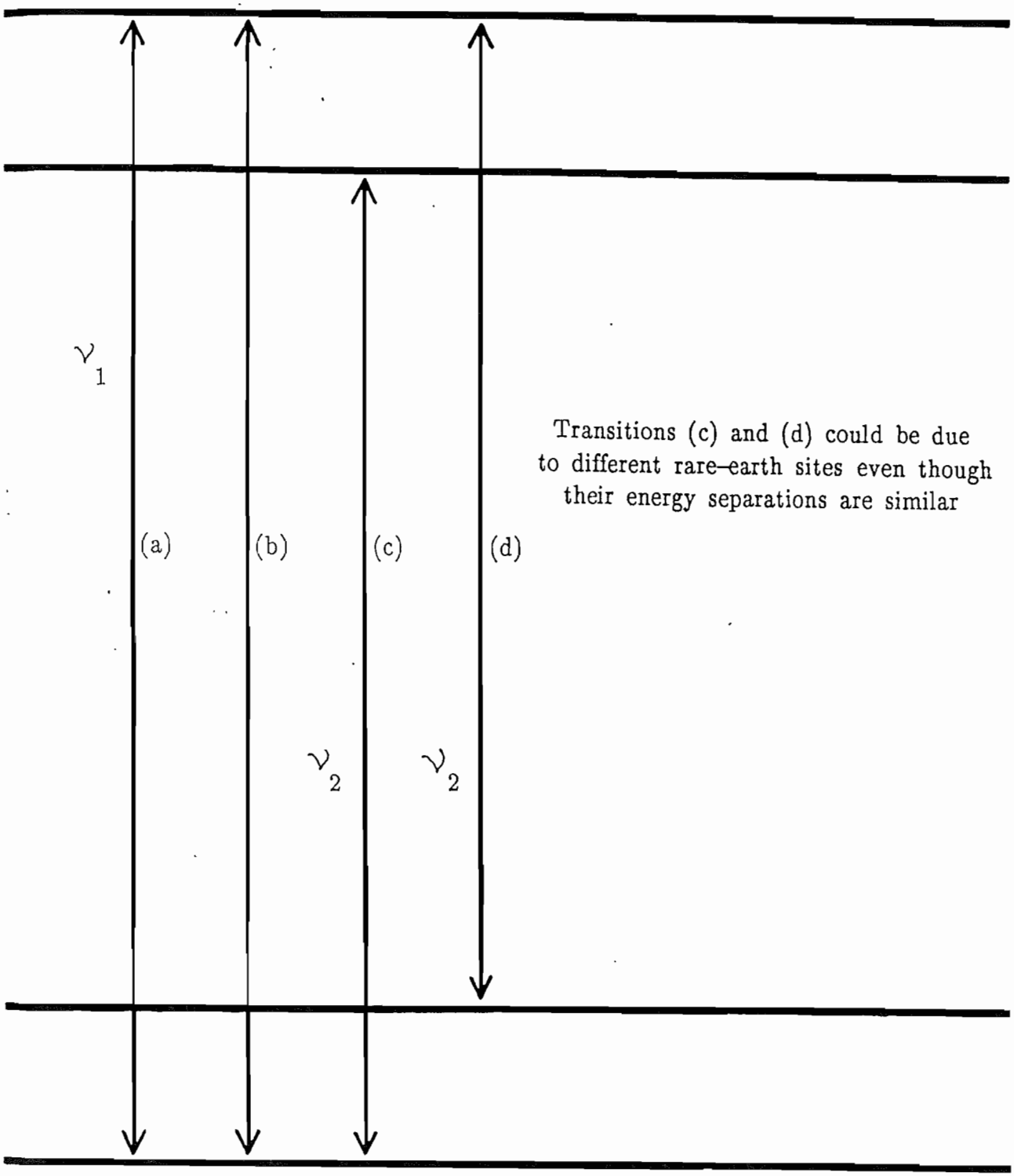
ν_1
(a)
(b)
(c)
(d)
ν_2
ν_2
Transitions (c) and (d) could be due to different rare–earth sites even though their energy separations are similar

Experimental configuration

Initially gating the detector and laser was attempted using two optical choppers; one switching the laser and the other the fluorescence signal. A phase locked loop provided a control signal to synchronise one of the choppers to the other. However, the time response of the motors was not fast enough to provide a rapid correction to any drift and so there would often be a hunting period before synchronous operation was resumed. Therefore, an acousto–optic modulator and chopper were used to provide the gating.

The Styryl 9 dye laser was gently focussed through the acousto–optic modulator and the first order diffracted spot was focussed into the doped core of the preform. The zero order spot was not used because complete on/off switching of the laser could not be achieved. The chopper acted as a shutter in front of the monochromator slits and allowed the detector to be blocked (figure 2.17). A reference signal obtained from the chopper was used to trigger a variable duty cycle drive signal for the acousto–optic modulator. By altering the phase between the unblocking of the detector and the reference signal, a window when the laser is turned off can be used to detect the fluorescence.

The spectrum obtained by resonantly pumping the sample (λ_p = 890 nm) at room temperature was the same as that obtained from broadband pumping. Since spectral narrowing was not observed one may conclude that at room temperature the broadening is homogeneous, as inferred by the near exponential decay rate.

When the sample was cooled to 77K a line narrowed peak was seen (figure 2.18) whose deconvolved F.W.H.M. was 200GHz. There was some doubt as to

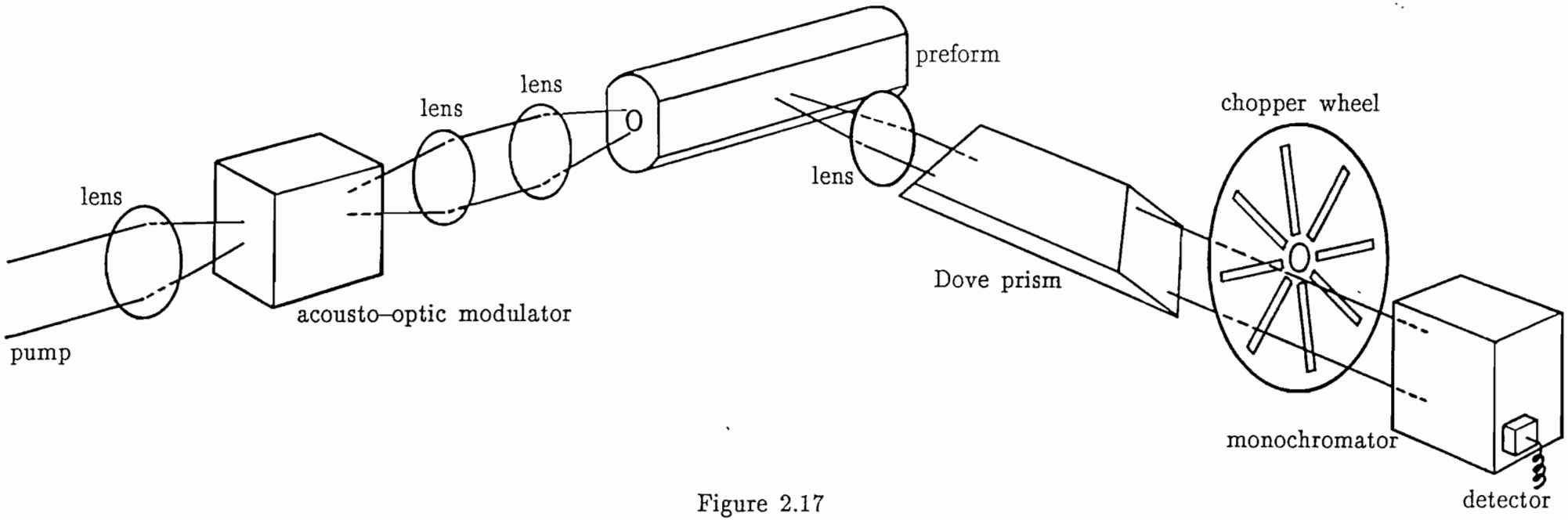

Figure 2.17

Experimental configuration for Fluorescence Line Narrowing measurements

Figure 2.18

Line narrowed peak, sample at 77K

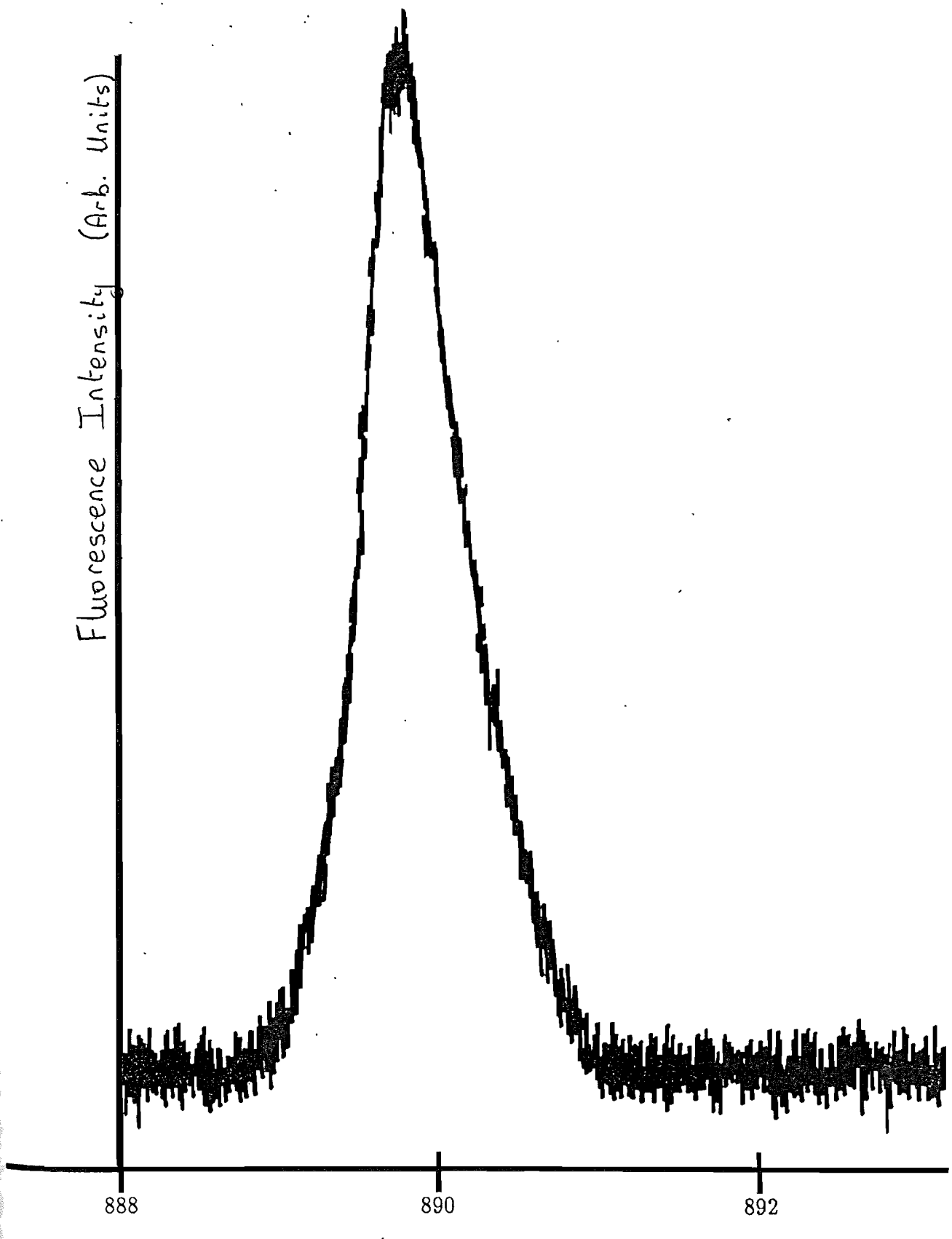

whether the peak was genuine or an artifact due to scattered laser light breaking through. This was clarified by looking at the time response of the peak's signal. The slow decay observed was consistent with a fluorescent decay rather than a fast switching of scattered laser light.

Once the sample was held at liquid helium temperatures the instrumental broadening was too large (approximately 175GHz) to make any linewidth measurements. One could either use a high finesse Fabry–Perot or a different technique to measure the linewidths to the required resolution. A high finesse Fabry–Perot has the disadvantage that the optical throughput is low and so a different technique was employed.

The alternative technique chosen was Optical Hole–burning. This technique also relies on exciting a subset of ions inside the inhomogeneous profile which then decay such that they are no longer in resonance with the laser, thereby reducing the number of electrons in resonance with the laser. By scanning the laser one can then sweep through the 'hole' burned in the absorption band and measure the linewidth of the transition.

For this experiment the Styryl 9 dye laser was actively stabilised and run on a single longitudinal mode using the intra–cavity components described in section 2.1. The laser output was gently focussed into the doped core of the sample. The absorption of the laser was monitored by measuring the amount of emitted fluorescence as this is a more sensitive method of measuring small variations. Although a hole was burned and observed with the laser at 4.2K, problems associated with scanning the laser over the required range cast a doubt about the validity of the result. The experiments were never successfully repeated or extended to different temperatures because of problems with the laser stability and insufficient time.

2.5 Stimulated Emission Cross-sections

The peak stimulated emission cross-sections for 906nm, 934nm and 1.088μm and 1.36μm were calculated using expression (1.17) and the necessary parameters measured in sections 2.2 and 2.3. The only other parameters required were the branching ratios required to calculate the radiative lifetime for each transition using expression (1.14). These were estimated using expression (1.15), measured emission intensities and assuming that the spectral response of the Germanium photodiode was similar to the one given by the manufacturer. The values were similar to the ones reported in reference 38; the latter values were probably more accurate and were used in the calculations.

The results together with the values used in the calculations are summarised in table 2.2.

The values corrected for power flow within the core of the fibres used are also given.

Table 2.2

Summary of parameters used to calculate emission cross-sections at $\lambda = 906\,nm$, $\lambda = 934\,nm$, $\lambda = 1088\,nm$ and $\lambda = 1360\,nm$

λ (nm)	906	934	1088	1360
β	0.44	0.44	0.47	0.08
τ (μs)	480	480	480	480
τ_{rad} (ms)	1.09	1.09	1.02	6.00
n	1.45	1.45	1.45	1.45
$\Delta\nu$ (THz)	7.3	8.1	9.0	8.1
σ_{ep} (m^2)	$1.24 \cdot 10^{-24}$	$1.19 \cdot 10^{-24}$	$1.55 \cdot 10^{-24}$	$4.59 \cdot 10^{-25}$
V	2.48	2.40	2.06	1.65
η	0.84	0.83	0.75	0.62
σ'_{ep} (m^2)	$1.04 \cdot 10^{-24}$	$9.88 \cdot 10^{-25}$	$1.16 \cdot 10^{-24}$	$2.84 \cdot 10^{-25}$

CHAPTER 3

3. Continuous–wave Fibre Lasers

Some of the advantages of longitudinal pumping were outlined in chapter 1. Other advantages are that it is ideally suited to laser pumping since good coupling between the pump and signal modes can be achieved. Also all of the pump radiation can be absorbed, resulting in highly efficient devices. However, the pump intensity will decay as it propagates down the fibre and so the gain will be non–uniform. This non–uniformity could become important for a system in which self–absorption can take place. Therefore, the first part of this chapter examines the behaviour of the pump and signal intensity down the fibre and discusses methods of obtaining the lowest threshold pump powers or maximising output power for given pump rates. Then the design of a fibre laser cavity is described followed by the results obtained from typical systems.

3.1 Theory

3.1.1 Behaviour below threshold

3.1.1 (a) Four level systems

If the effects of stimulated emission are ignored then the pump level at which threshold is reached can be expressed as (Appendix A)

$$I_p(o) - I_p(l) = \frac{\gamma\, h\, \nu_p}{\eta\, \sigma_e\, \tau} \qquad (3.1)$$

with $$\ln\left[\frac{I_p(o)}{I_p(l)}\right] + \eta\frac{\left[I_p(o) - I_p(l)\right]}{\frac{h\nu_p}{\sigma_p \tau}} = N_t \sigma_p l \qquad (3.2)$$

$I_p(z)$	is the pump intensity at a point z in the medium
N_t	is the dopant concentration
η	is the fraction of excited electrons which decay into the upper level
σ_p	is the pump absorption cross–section
σ_e	is the stimulated–emission cross–section
τ	is the fluorescence lifetime
γ	represents the cavity losses

From the two expressions it can be seen that possible ways of minimising the initial pump intensity required to reach threshold are to reduce $I_p(l)$, the cavity losses, or use pump photons of lower energy.

The final pump intensity $I_p(l)$ can be reduced by either increasing the dopant concentration N_t or the length of the gain medium. Increasing N_t can have detrimental effects since this can increase the possibility of an interaction between neighbouring dopant ions and a reduction of the luminescence efficiency. If the length of the gain medium is increased then strong absorption of the pump can still take place even for weakly absorbing or dilute systems. With conventional gain medium geometries it becomes difficult to maintain a non–divergent intense pump beam through the material. However, because the pump radiation is guided along the doped core of a fibre then very long interaction lengths can be achieved without the problems associated with a diverging beam.

Cavity losses can be attributed to several causes including diffraction losses, coupling losses and absorption and scattering in the gain medium and other optical components. Losses due to coupling and scattering in optical components are common to all types of cavity and can be minimised by careful cavity design and the use of good quality components. However, doped optical fibre waveguides can reduce diffraction losses and their high optical quality reduces losses due to material absorption and scattering (eg.approximately 3 dB/km at 1.08 μm).

Equation (3.1) can be re–arranged to give the absorbed threshold pump power.

$$P_{abs} = \frac{h \nu_p}{\sigma_e \tau} \frac{\gamma}{\eta} A \qquad (3.3)$$

A is the active area of the gain medium.

Since A is very small for fibres then once more their use as gain media should allow very low pump power thresholds to be realised. The following example indicates just how small threshold pump powers could be for a low loss fibre laser

eg. $\gamma = 0.1$

$A \sim 10\times10^{-12}\ m^2$

$\sigma_e = 1.16\times10^{-24}\ m^2$

$\nu_p = 366\ THz$

$\tau = 480\ \mu s$

$\eta = 0.75$

A value of $I(o) \sim 5.8\times10^{7}\ W/m^2$ is required for laser action which corresponds to an absorbed pump power threshold of $\sim$ 0.6 mW.

3.1.1 (b) Systems with population in the terminal laser level

Assuming that the terminal laser level is thermally populated one can express the criterion to reach threshold by (Appendix A)

$$I_p(o) - I_p(l) = \frac{h\,\nu_p}{\sigma_p \tau \eta} \left\{ \frac{g_2}{g_1}\, e^{-\Delta\epsilon/kT} \ln\left(\frac{I_p(o)}{I_p(l)}\right) + \frac{\sigma_p}{\sigma_e}\,\gamma \right\} \qquad (3.4)$$

$\Delta\epsilon$ is the energy separation of the terminal laser level and the ground–state.

g_1 and g_2 are the degeneracies of the terminal and upper laser levels.

If $\Delta\epsilon$ is large, ie four level type behaviour, (3.4) reduces to (3.1) and for true three level behaviour, ie $\Delta\epsilon = 0$, it reduces to

$$I_p(o) - I_p(l) = \frac{h\,\nu_p}{\sigma_p \tau \eta} \left\{ \frac{g_2}{g_1} \ln\left(\frac{I_p(o)}{I_p(l)}\right) + \frac{\sigma_p}{\sigma_e}\,\gamma \right\} \qquad (3.5)$$

By comparing (3.4) and (3.5) with (3.1) one can see that there is an additional term which determines the intensity required to reach threshold for these systems. This term arises from the requirement that the population in the upper level must be the same as that in the lower level before any inversion can be produced, ie partial or full saturation of the absorption is required.

Therefore, in order to minimise the initial intensity required to reach threshold, one not only has to take the same steps as in the four level case but also needs to reduce this additional term.

It can be shown that for any distance z along the fibre inversion can only be created if

$$I_p(z) > \frac{g_2}{g_1} \frac{h\,\nu_p}{\sigma_p \tau \eta} e^{-\Delta\epsilon/kT} \qquad (3.6)$$

Therefore, the maximum total inversion in a length l occurs when

$$I_p(l) = \frac{h\,\nu_p}{\sigma_p \tau} \frac{g_2}{g_1} \frac{e^{-\Delta\epsilon/kT}}{\eta} \qquad (3.7)$$

since any additional length will result in reabsorption taking place.

Combining (3.6) and (3.7) gives

$$I_p(o) - \frac{h\,\nu_p}{\sigma_p \tau \eta} e^{-\Delta\epsilon/kT} \frac{g_2}{g_1} \ln I_p(o) = \frac{h\,\nu_p}{\sigma_p \tau \eta} \left\{ \frac{g_2}{g_1} e^{-\Delta\epsilon/kT} \left[1 - \ln \frac{g_2}{g_1} \frac{h\,\nu_p}{\sigma_p \tau \eta} e^{-\Delta\epsilon/kT} \right] + \frac{\sigma_p}{\sigma_e} \gamma \right\} \qquad (3.8)$$

from which a numerical solution for the minimum $I_p(o)$ can be obtained. The length of fibre required can then be deduced using (3.5). It is apparent from (3.7) that $I_p(l)$ is reduced not only by reducing the pump energy but also by choosing pump transitions with a large σ_p.

eg $\gamma = 0.1$

$A = 10\times10^{-12}\ m^2$

$\sigma_e = 1.04\times10^{-24}\ m^2$

$\Delta\epsilon = 4\times10^{-21}\ J$

$\tau = 480\ \mu s$

$\eta = 0.75$

If a Rhodamine 6G dye laser pump is considered with

$$\nu_p = 508 \text{ THz}$$
$$\sigma_p = 1.14\times10^{-24} \text{ m}^2$$

then one would require $I_p(o) \sim 6.2 \times 10^8$ W/m^2 which translates to a pump power of 6.2mW. Approximately 3.8mW would be absorbed in an optimum 23cm length of fibre (assuming Nd^{3+} concentration of approximately 300ppm).

However a pump source operating at 810nm, such as a semiconductor diode laser has

$$\nu_p = 370 \text{ THz}$$
$$\sigma_p = 3.6\times10^{-25} \text{ m}^2$$

and would require $I_p(o) \sim 10 \times 10^8$ W/m^2. This corresponds to a pump power of 10mW of which 3.8mW would be absorbed in 33cm.

3.1.2 Behaviour above threshold

In the preceding sections the effect of stimulated emission was neglected. This approximation is valid until threshold is reached since the number of emitted photons is small. However, when threshold is reached the number of stimulated transitions rapidly builds up and depletion of the inversion can occur. Therefore, when threshold is exceeded a balance between creating and depleting inversion by pump and emitted photons must be taken into account.

The output power is given by

$$P_{out} = \frac{(1 - R_2)}{R_2^{1/2}} \frac{h \nu_e}{\sigma_e \tau} A(x - 1) \qquad (3.9)$$

R_2 is the reflectivity of the output coupler

x is the fractional number of times the threshold pump rate is exceeded

and is similar to the expression derived by Koechner [41].

For four level systems

$$x = \frac{I_p(o) - I_p(l)}{I_p(o) - I_p(l)\Big|_{threshold}} \qquad (3.10)$$

whilst for systems where there is population in the terminal laser level

$$x = \frac{\frac{\eta}{\Gamma_{sp}} \left[I_p(o) - I_p(l)\right] - \frac{g_2}{g_1} e^{-\Delta\epsilon/kT} \ln\left[\frac{I_p(l)}{I_p(o)}\right]}{\frac{\eta}{\Gamma_{sp}} \left(I_p(o) - I_p(l)\right) - \frac{g_2}{g_1} e^{-\Delta\epsilon/kT} \ln\left(\frac{I_p(l)}{I_p(o)}\right)\Big|_{threshold}} \qquad (3.11)$$

In order to maximise the output power there exists an optimum value of R_2 which strikes a balance between allowing more light to pass through the output coupler and reducing the cavity losses. This value is given by

$$R_{2\ opt} = 1 - \gamma'(x_{min}^{1/2} - 1) \qquad (3.12)$$

x_{min} is the ratio of the actual pump rate to that required for minimum threshold (ie the pump rate to reach threshold for zero output coupling, $R_2 = 1$).

γ' represents all of the cavity losses excluding those associated with transmission losses through the output coupler.

It is apparent from Appendix A that as the geometric mean intensity in the cavity changes with variations of R_2, the value of $I_p(l)$ and hence x, will change for a given $I_p(o)$ and l.

For a four level system this effect can be reduced by choosing a sufficiently long enough length of fibre such that $I_p(l)$ is always small.

In a system where there is population in the terminal laser level the situation is more complicated. If the initial intensity required to reach threshold is to be minimised then a length of fibre which allows 3.7 to be satisfied, must be used. One would also like this equality once the system is above threshold in order to eliminate reabsorption losses. Clearly it is unlikely that this can be achieved using the same length of fibre required to reach threshold.

3.2 (a) The Optical Cavity of a Fibre Laser

The basic cavity is shown in figure 3.1. The pump source is launched through a mirror, which is highly reflecting at the lasing wavelength but essentially transparent at the pump wavelength, into the fibre core using a microscope objective. The high reflector is optically butted up to the cleaved fibre end and provides feedback.

The microscope objective could be used in between the high reflector and the fibre end to launch both the pump and any reflected radiation back into the fibre core. However, the objective would introduce additional losses into the cavity and because of differing beam divergences and chromatic aberrations, could focus the two beams in slightly different places.

The output of the fibre is collimated using an intra–cavity microscope objective and this creates a region inside the cavity where additional intra–cavity elements such as tuning elements or modulators can be inserted. If fibre–optic versions of these elements had been available the output coupler could have been butted up to the fibre, thereby eliminating the intra–cavity objective.

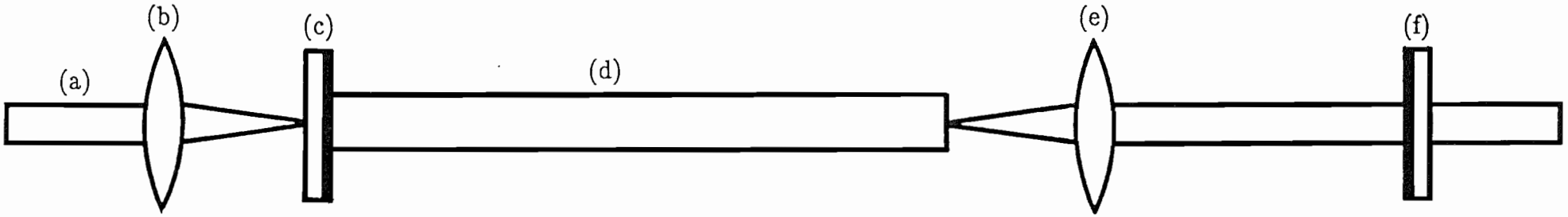

(a) Pump beam

(b) Focusing lens

(c) High reflector

(d) Doped fibre

(e) Intra–cavity microscope objective

(f) Output coupler

Figure 3.1

Basic fibre laser cavity

3.2 (b) Cavity Alignment Procedure

The pump launch is maximised by moving the fibre end using a micropositioner while monitoring the output from the fibre with a photodiode. Optical filters ensure that only radiation of the required lasing wavelength is monitored by the photodiode. When the launch has been maximised the high reflector is moved towards the fibre end using a small mount which was attached to the micropositioners. The optical contact of the mirror with the fibre end can be observed by an increase in the detector signal of a factor of two or more (a doubling is seen because radiation which would have been lost from one end is reflected back, and any further increase is due to gain).

Once this has been achieved the output coupler must be aligned so that it completes the cavity. An infra–red viewer can be used to see when the fibre output is focussed onto the output coupler and is reflected back onto the fibre end. Alternatively any residual pump light can be used to give a rough alignment. When lasing action occurs, the intra–cavity microscope position and output coupler tilt can be adjusted to maximise the laser output.

3.3 Broadband C.W. Systems

The cavity described in the previous section was used for all of the transitions studied with slight variations in the mirror reflectivities and fibre lengths used. The pump source was an Argon ion pumped Rhodamine 6G dye laser. A x20 intra–cavity microscope objective, whose N.A. of 0.25 was sufficiently large to collect the fibre output, was used.

A calibrated four plate variable attenuator between the pump and fibre laser allowed the pump rate to be varied accurately and reproducibly. Also relaxation oscillations on the fibre laser output could be driven by modulating the pump source with an optical chopper. From a knowledge of the pump rate and relaxation oscillation period [42], the cavity lifetime and hence the cavity loss could be calculated using

$$\tau_c = \tau_{rel}^2 \frac{(x - 1)}{4\pi^2 \tau} \qquad (3.13)$$

$$\gamma = \frac{L_{opt}}{c\tau_c} \qquad (3.14)$$

τ_c is the cavity lifetime
τ_{rel} is the relaxation oscillation period
L_{opt} is the optical length of the cavity.

3.4 (a) Operation on the $^4F_{3/2} - {}^4I_{11/2}$ Transition

The cavity parameters are summarised in table 3.1. The fibre length of 1.8m was chosen because reabsorption at the lasing wavelength was not a problem and this length ensured almost complete absorption of the pump. The internal loss calculated from the parameters in table 3.1 and expressions (3.13), (3.14) was $\gamma' = 0.22$. An optimum output coupler reflectivity of 62% was then calculated using expression (3.12). The nearest reflectivity available was 70% and this output coupler replaced the previous one of R = 98%. Figure 3.2 and table 3.1 summarise the characteristics of this arrangement.

The results in table 3.1 indicate that the calculated threshold is lower than the measured values. Some of the discrepancy could be due to the model not fully accounting for the coupling between the pump and signal modes.

In section 1.1 it was explained that the mode size and profile depend on the waveguide parameter and wavelength of the light in the fibre. Therefore, the shape and size of the modes at the pump and lasing wavelengths are likely to be different (figure 3.3); such a mismatch will reduce the system efficiency. This picture assumes passive waveguide solutions and no interaction between the pump and laser modes. However, in reality we have an active fibre whose pump and laser modes will interact. The inversion, and again, in the fibre have the same profile as the pump mode within the doped core. Consequently the laser mode will only see gain in this region and may become smaller than the passive solutions infer. This 'gain focussing' has been assumed to reduce the modal mismatch. (By adding a spatial variation of the signal and pump intensities in Appendix A one could numerically find a self consistent solution and fully take into account the effect described. Such a calculation would be very lengthy, especially to optimise all of the variables). The validity of this

Table 3.1

Summary of parameters and results for a fibre laser operating at $\lambda = 1.08\mu m$ with two different reflectivity output couplers.

x	12.73
τ_{rel} (μs)	8
L_{opt} (m)	2.76
γ	0.23
R_2	0.98
γ'	0.22

	Output coupler reflectivity R = 0.98	Output coupler reflectivity R = 0.70
R_2	0.98	0.70
σ_p (m^2)	$1.14 \cdot 10^{-24}$	$1.14 \cdot 10^{-24}$
σ_e (m^2)	$1.16 \cdot 10^{-24}$	$1.16 \cdot 10^{-24}$
ν_p (THz)	508	508
ν_e (THz)	276	276
A (m^2)	$9.08 \cdot 10^{-12}$	$9.08 \cdot 10^{-12}$
η	0.75	0.75
τ (μs)	480	480
P_{abs}(calculated) (mW)	1.7	2.9
P_{abs}(measured) (mW)	3.3	8.0

Figure 3.2

$^4F_{3/2} - {}^4I_{11/2}$

Variation of output power with number of times above threshold

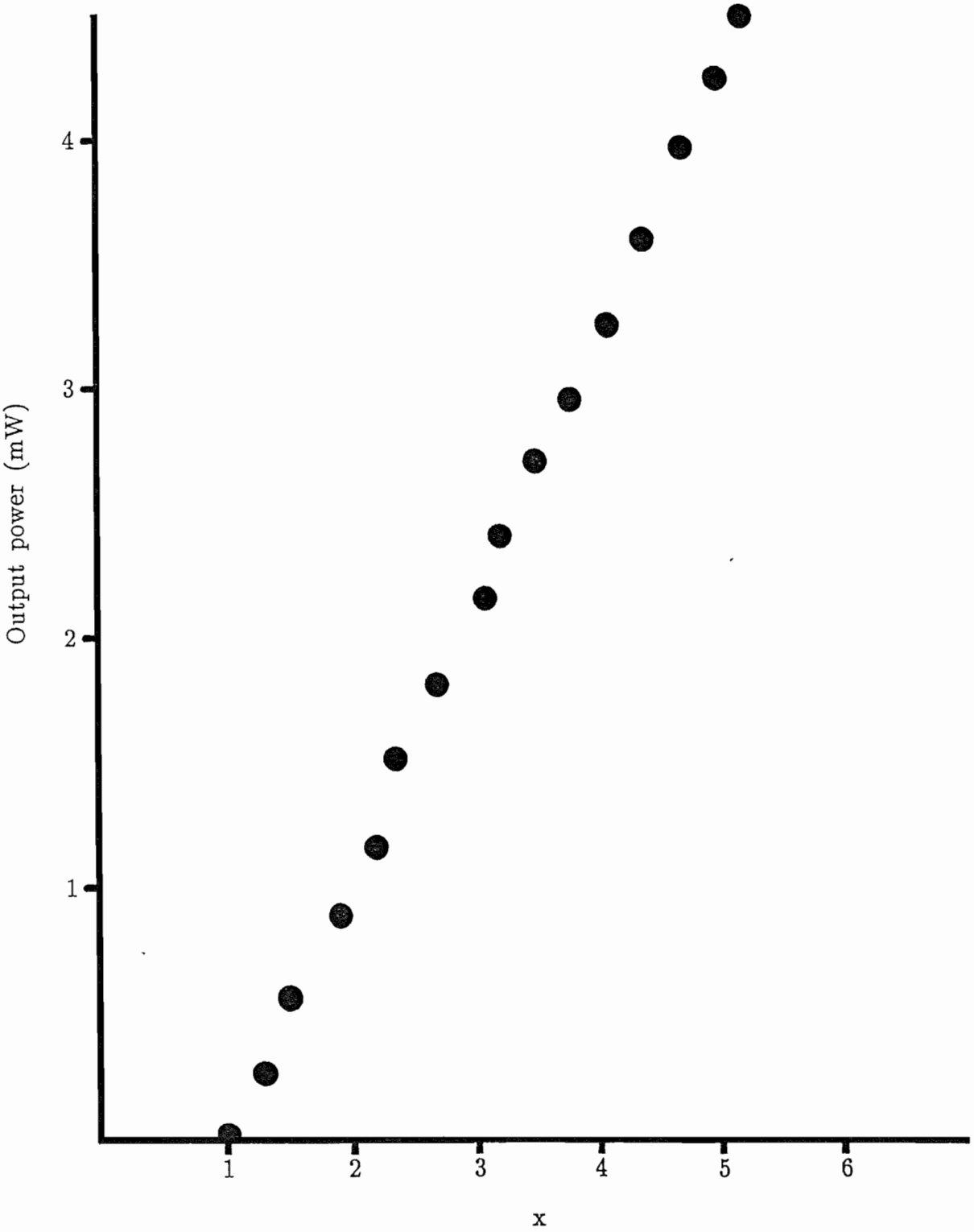

Figure 3.3

Pump and laser mode profiles in a passive fibre

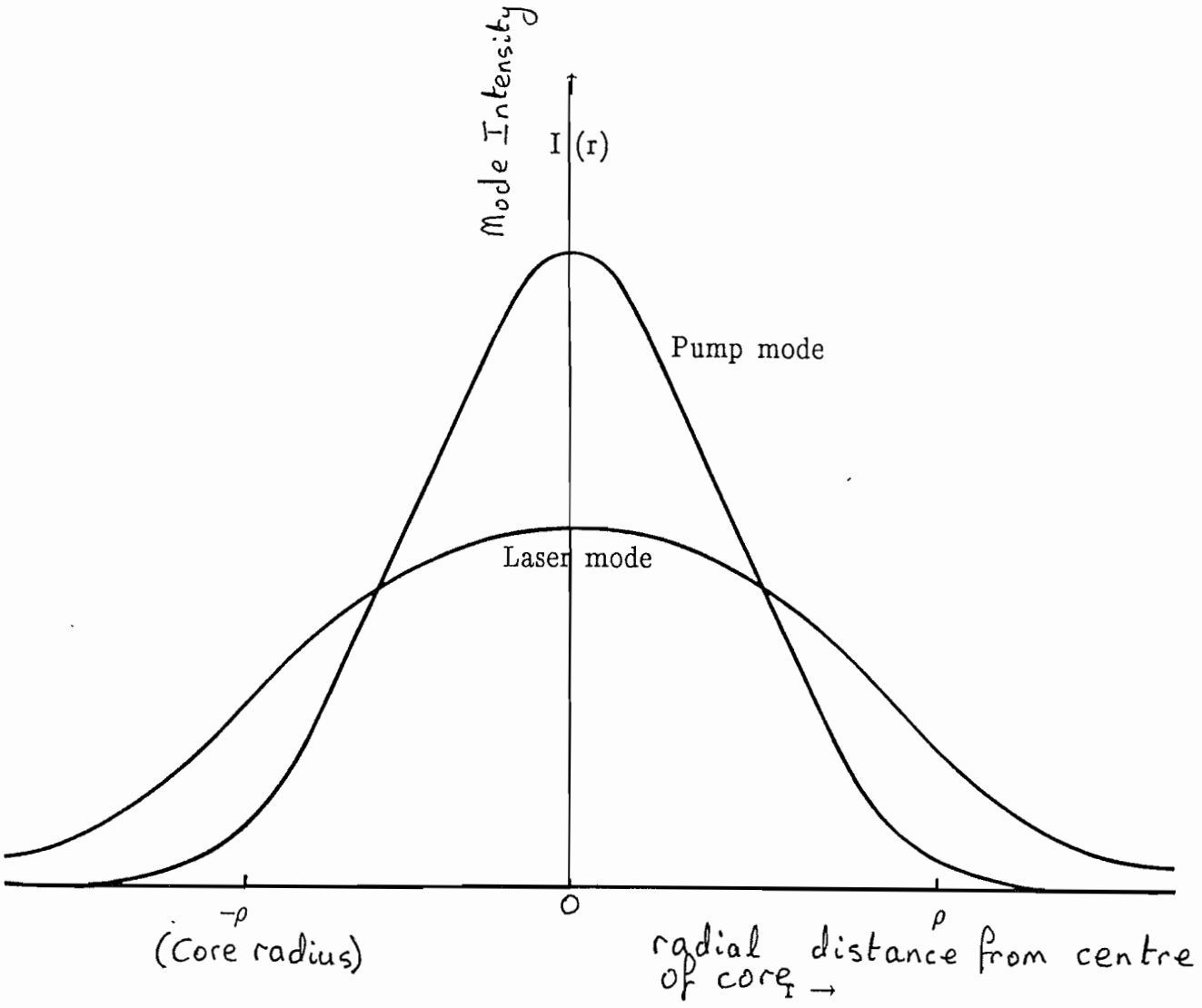

assumption or insensitivity on the mode profiles can be demonstrated with data from other studies using a Semi–conductor diode laser pump [43] and an Argon ion pump [44]. In the latter case any mismatch would be worse but as the results in table 3.2 show, the agreement between calculated and measured thresholds is quite good.

An alternative reason for the discrepancy is excited state absorption of the pump. Other studies on Nd^{3+} doped crystalline hosts have shown that excited state absorption of pump wavelengths ~ 590 nm can occur [45]. As a test for this, the dye laser was tuned throughout the absorption band of the ion in the hope that the pump would no longer be resonant with any possible higher levels. The small variations in the fibre laser output observed were consistent with the change in pump power as the dye laser was tuned. Although no direct evidence of excited state absorption was observed it is a strong possibility that the broad nature of the transitions could allow excited and ground state absorption bands to overlap.

Table 3.2

Summary of results obtained by [43, 44] for a fibre laser operating at $\lambda = 1.08\,\mu m$ with pump wavelengths of $\lambda = 820nm$ and $514nm$.

	Pump at 820nm	Pump at 514nm
γ	0.29	0.15
σ_e (m^2)	$1.16 \cdot 10^{-24}$	$1.16 \cdot 10^{-24}$
ν_p (THz)	366	584
ν_e (THz)	276	276
A (m^2)	$9.08 \cdot 10^{-12}$	$12.6 \cdot 10^{-12}$
η	0.75	0.75
τ (μs)	480	480
P_{abs}(calculated) (mW)	1.53	1.75
P_{abs}(measured) (mW)	1.3	2.0

3.4 (b) Operation on the $^4F_{3/2} - {}^4I_{9/2}$ Transition

The cavity parameters are summarised in table 3.3. The reflectivity of the mirrors at 1.08 μm, 15% and 12%, had to be low in order to discriminate against the $^4F_{3/2} - {}^4I_{11/2}$ transition. In view of the conflicting requirements on the length of fibre required to give lowest threshold and largest output power for this transition with population in the terminal laser level, the length was not rigorously calculated. A 1m length of fibre and an output coupler reflectivity of approximately 70% were experimentally found to give a reasonable compromise between output power and threshold. Laser action was supported on the two fluorescence peaks at 906nm and 934nm. The output could be switched from one to the other by altering the focus of the intra-cavity microscope objective by $\sim$ 5 μm. This behaviour is explained by the different mode size for the two wavelengths requiring its own location of the microscope objective to achieve mode matching.

The system operating at 906nm had significantly more population in the lower laser level than that at 934nm. The performance for the two wavelengths is summarised in tables 3.3 and figures 3.4, 3.5.

Once again the calculated threshold is smaller than that measured and is attributed to excited state absorption of the pump. There has been no other known study of c.w. laser operation on this transition in glass hosts and so no comparison with other workers' results can be made.

Table 3.3

Summary of parameters and results for a fibre laser operating at $\lambda = 906$ nm and $\lambda = 934$ nm.

	$\lambda = 906$ nm	$\lambda = 934$ nm
R_2	0.80	0.70
γ	0.33	0.4
ν_p (THz)	508	508
ν_e (THz)	331	321
σ_p (m^2)	$1.14 \cdot 10^{-24}$	$1.14 \cdot 10^{-24}$
σ_e (m^2)	$1.04 \cdot 10^{-24}$	$9.88 \cdot 10^{-25}$
η	0.75	0.75
τ (μs)	480	480
A (m^2)	$9.08 \cdot 10^{-12}$	$9.08 \cdot 10^{-12}$
$e^{-\Delta\epsilon/kT}$	0.38	0.07
P_{abs}(calculated) (mW)	11.23	5.41
P_{abs}(measured) (mW)	22.5	8.0

Figure 3.4

$^4F_{3/2} - {}^4I_{9/2}$ (λ = 906 nm)

Variation of output power with number of times above threshold

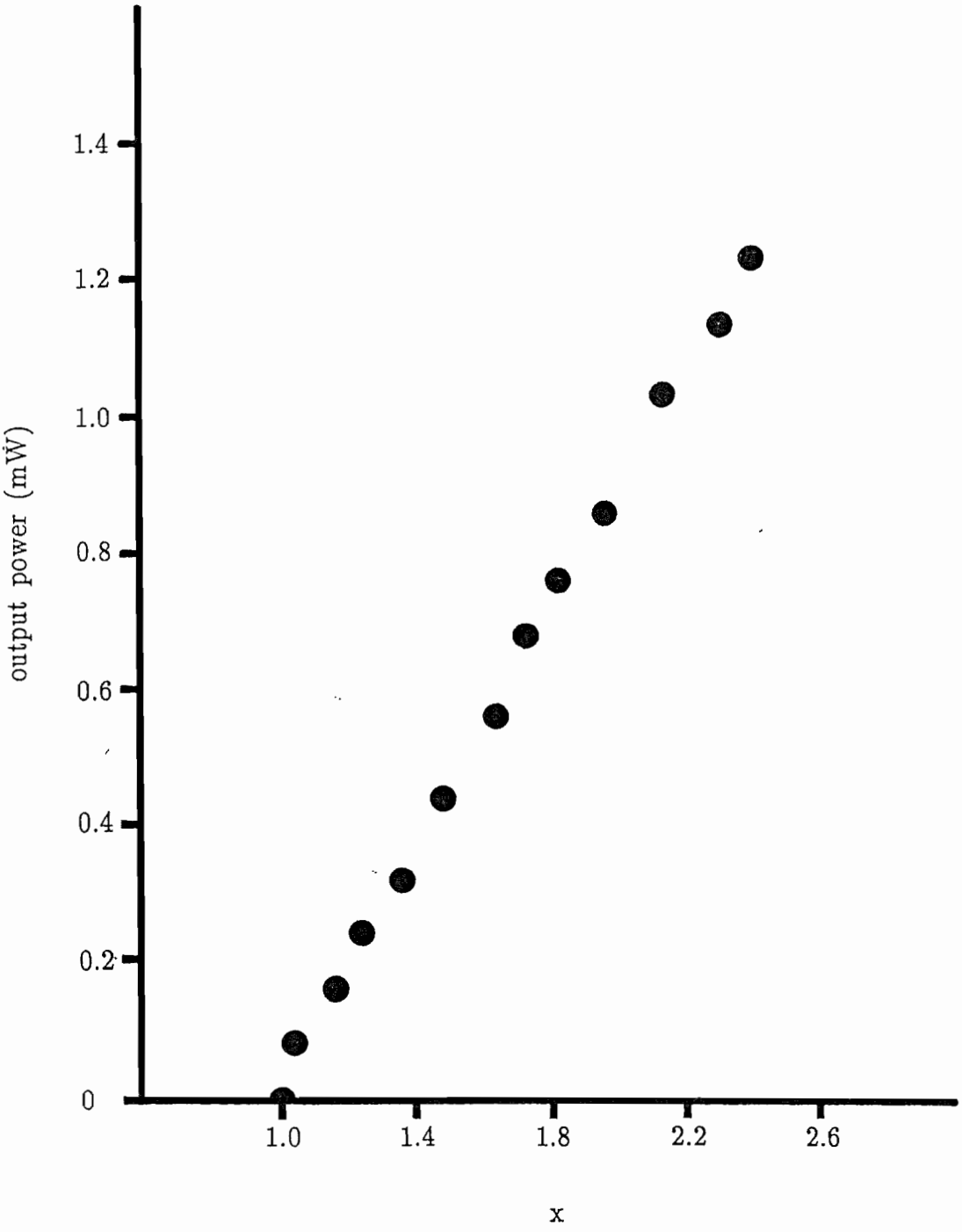

Figure 3.5

$^4F_{3/2} - {}^4I_{9/2}$ (λ = 934nm)

Variation of output power with number of times above threshold

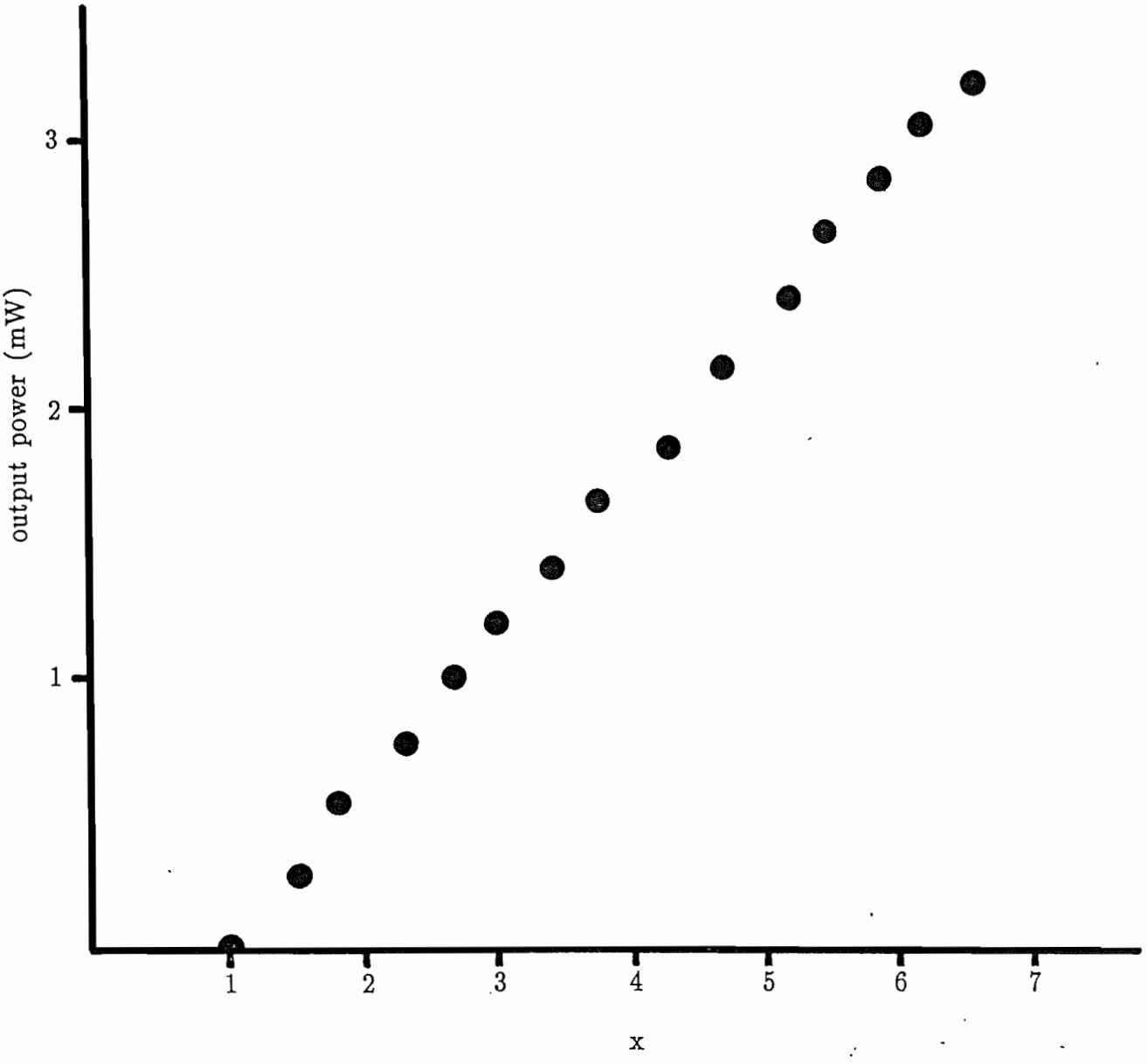

3.4 (c) Operation on the $^4F_{3/2} - {}^4I_{13/2}$ Transition

Although the intensity of this transition is weaker than the $^4F_{3/2} - {}^4I_{9/2}$, $^4I_{11/2}$ transitions it was felt that based on the previous results, laser action on this transition should be feasible. A cavity similar to those in the previous sections was constructed with a high reflector and output coupler reflectivity of 99% but laser action was not observed.

In an attempt to minimise cavity losses, the intra–cavity microscope objective was removed and a double butted mirror arrangement unsuccessfully tried. It was thought at these longer wavelengths any mismatch between the pump and signal modes may become important. Therefore a length of fibre with a longer cut off wavelength ($\sim$ 1.3 μm) was pulled from the same perform. Although this would help to concentrate the laser mode in the doped core, laser action still did not occur. The only alternative explanation seemed to be excited state absorption of the 1.3 μm radiation.

To check whether absorption was present, a probe beam from a miniature, diode pumped Nd^{3+}:YAG laser operating on the $^4F_{3/2} - {}^4I_{13/2}$ transition was used. The transmission of this probe beam (which was either at 1.32 μm or 1.34 μm) through the fibre was monitored while the pump beam was modulated by a mechanical chopper (figure 3.6). Absorption at both probe wavelengths was observed giving direct evidence of excited state absorption with the $^4F_{3/2} - {}^4G_{7/2}$ transition as the most probable assignment (see figure 3.7).

The absorption at 1.32 μm was much stronger, where approximately 40% absorption for an absorbed pump power of $\sim$ 20 mW was observed, while at 1.34 μm approximately 12% absorption was seen under similar conditions.

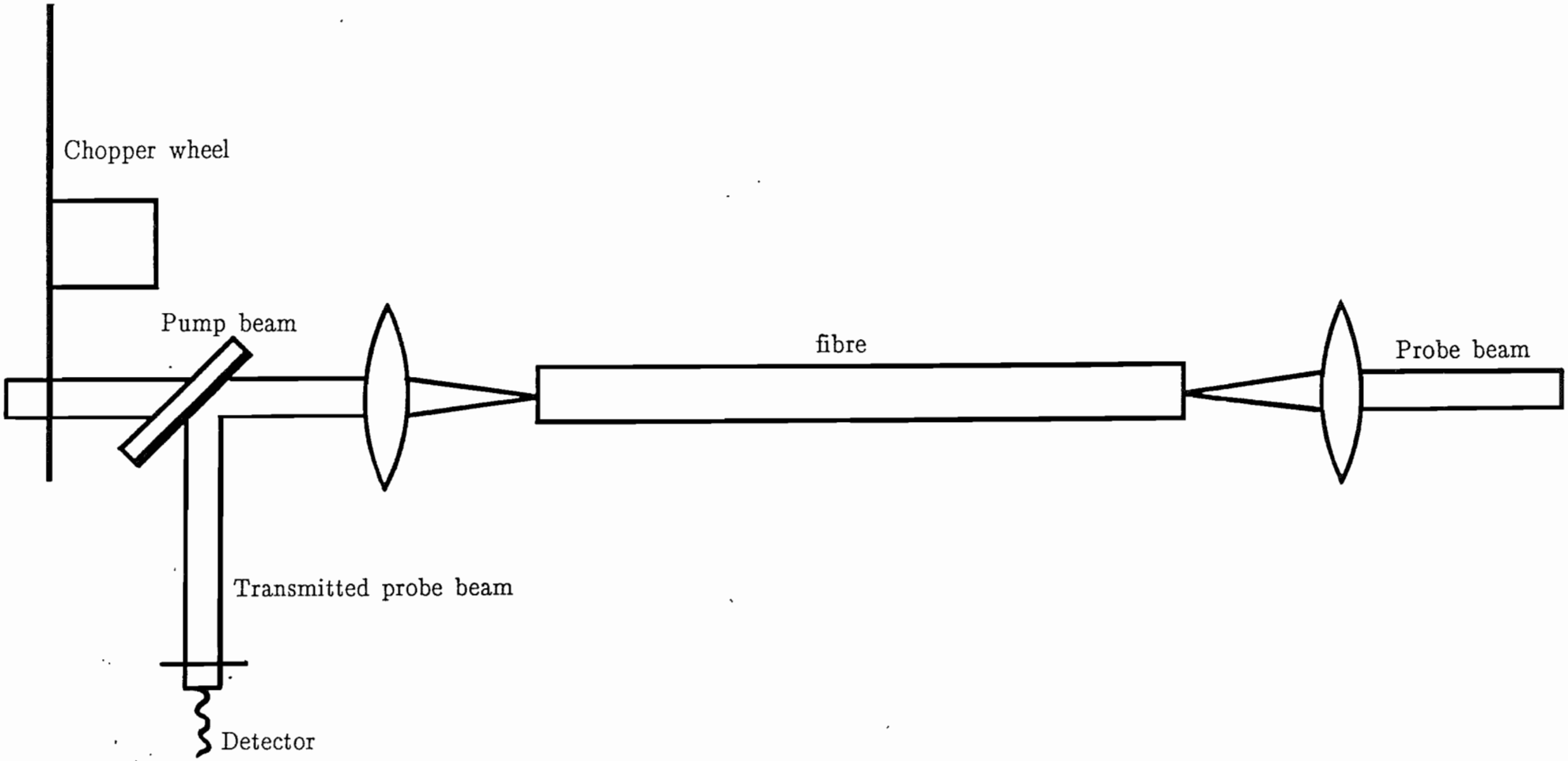

Figure 3.6

Pump and probe configuration

Figure 3.7

Rare earth free ion energy levels. (From Ref. 22)

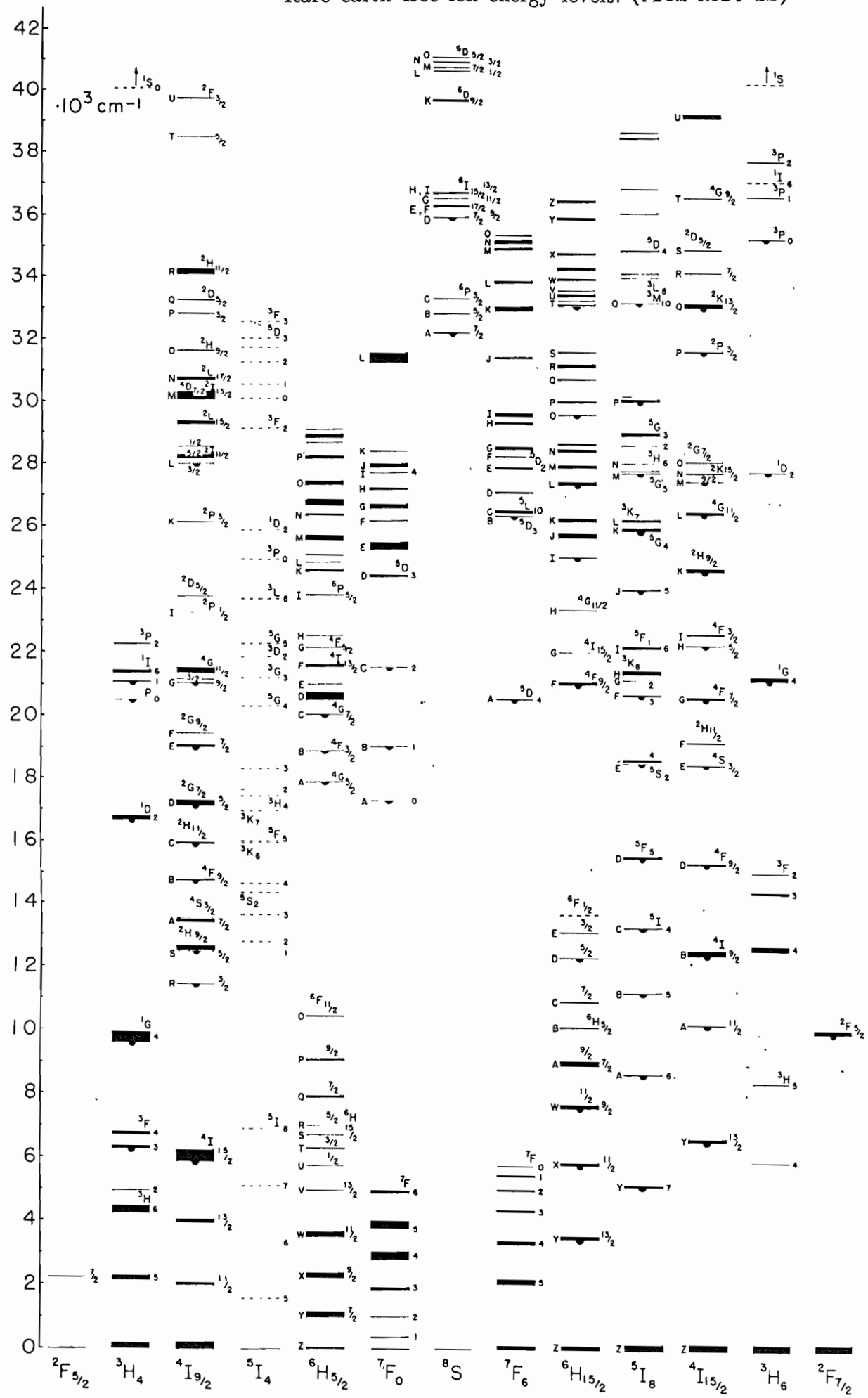

Since the absorption appears to be decreasing with longer wavelengths whilst the fluorescence intensity is increasing (figure 2.9) it is possible that net gain may be experienced at the long wavelength end of the fluorescence band. However, no suitable probe sources were available to do the measurement with.

3.5 Tunable, c.w. Fibre Lasers

Many experiments, such as those outlined in section 2.4, require a narrow linewidth and tunable source. The broad emission lines of the Nd^{3+} impurity ion in the glass host offer the potential of widely tunable sources and suggest that fibre lasers may prove to be an important class of tunable laser. The main advantages of such systems are that they do not suffer from poor photochemical stability, unlike many near infra–red dyes, nor do they require low temperature operation, a feature of some near infra–red colour centre and vibronic lasers. In view of the different mechanisms responsible for broadening the laser transitions of ions in glass hosts, the efficiency under narrow linewidth operation has been investigated. This section describes the type of cavity used and the results obtained.

3.5.1 Experimental Configuration

The laser cavity was similar to that used in the previous experiments except that frequency selective components were inserted between the intra–cavity microscope objective and output coupler (figure 3.8). Initially it was found that a weak etalon was formed between the microscope objective and fibre end causing strong spectral modulation on the laser output. In order to overcome this problem a x10 objective, with a longer working distance of 8mm, was used instead of the previously used x20. The longer working distance of the objective ensures that the rapidly diverging beam is much larger if it is reflected off the objective and back onto the fibre face (figure 3.9).

Although a grating had been previously used [5] as the frequency selective component for a fibre laser, a birefringent filter mounted at Brewsters angle (as used in Coherent dye lasers) was chosen. This type of filter has the advantage over a grating in that it has a very low insertion loss when linearly polarised light is incident upon it.

Because the fibre was non–polarisation preserving then the elliptically polarised output had to be converted into linearly polarised light. This was achieved by two quartz quarter–wave plates which could be rotated independently. The orientation of the wave–plates was initially set up by rotating them until the light reflected off the Brewster angled filter was minimised whilst maximising the output power. It was found that as the laser was tuned it was necessary to make small adjustments to the quarter–wave plates in order to maintain maximum output power. If a polarisation preserving fibre had been available then the need for readjustment of the polarisation would have been eliminated.

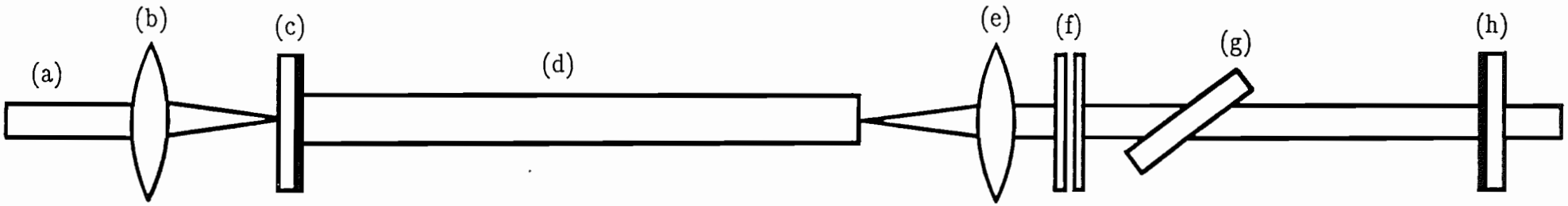

(a) Pump beam

(b) Focusing lens

(c) High reflector

(d) Fibre

(e) Intra–cavity microscope objective

(f) Quartz quarter–wave plates

(g) Brewster angled Birefringent filter

(h) Output coupler

Figure 3.8

Tunable fibre laser cavity

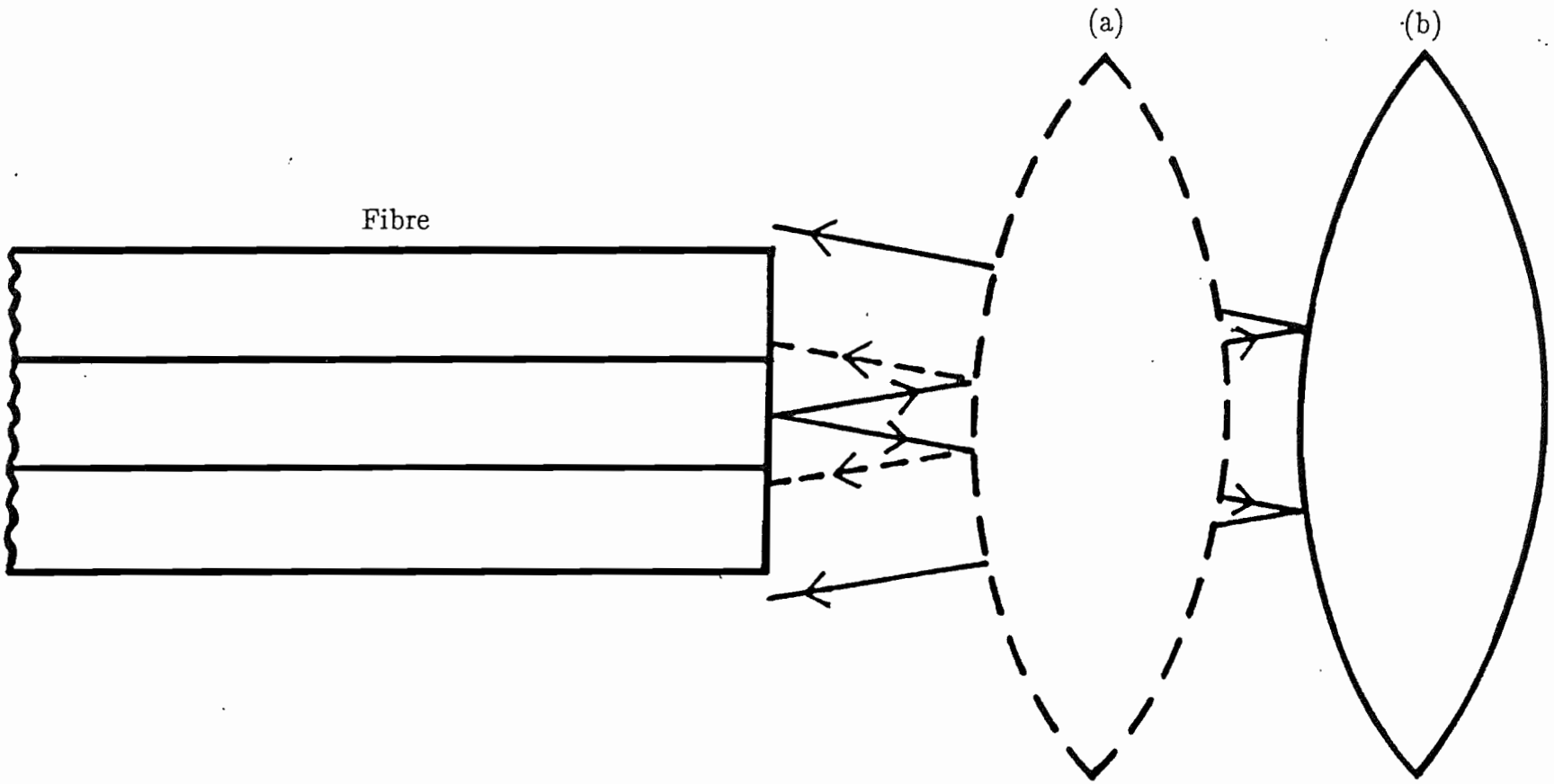

Figure 3.9

Longer working distance of lens (b) ensures that the beam reflected back onto the fibre is larger.

3.5.2 (a) $^4F_{3/2} - {}^4I_{9/2}$ Tunable Operation

The cavity parameters are summarised in table 3.4. As in the broadband case, mirror reflectivities were chosen to help suppress lasing on the $^4F_{3/2} - {}^4I_{11/2}$ transition. The 1m length of fibre gave a reasonable compromise between good pump absorption and a reduction of reabsorption losses.

A continuous tuning range from 900nm to 945nm was achieved as shown in figure 3.10. The tuning range achieved was probably limited by self–absorption at the short wavelength end. If a shorter fibre had been used then it is possible that, providing there was sufficient gain to overcome the losses, the tuning range may have been extended. However, the output at the longer wavelengths, where reabsorption is less of a problem, would have been reduced on account of the reduction of absorbed pump power. Therefore, particular regions of the tuning curve can be optimised by tailoring the fibre length (a similar situation exists in dye lasers where the dye concentration can be altered to enhance the short or long wavelength ends of the curve).

Adding the birefringent filter to the cavity reduced the laser bandwidth to 20GHz from 350GHz without a noticeable change in output power.

Table 3.4

Summary of parameters for the tunable fibre laser operating on the $^4F_{3/2} - {}^4I_{9/2}$ transition.

R_1 @ 934 nm	0.98
R_2 @ 934 nm	0.70
absorbed pump power (mW)	53
fibre length (m)	1.0

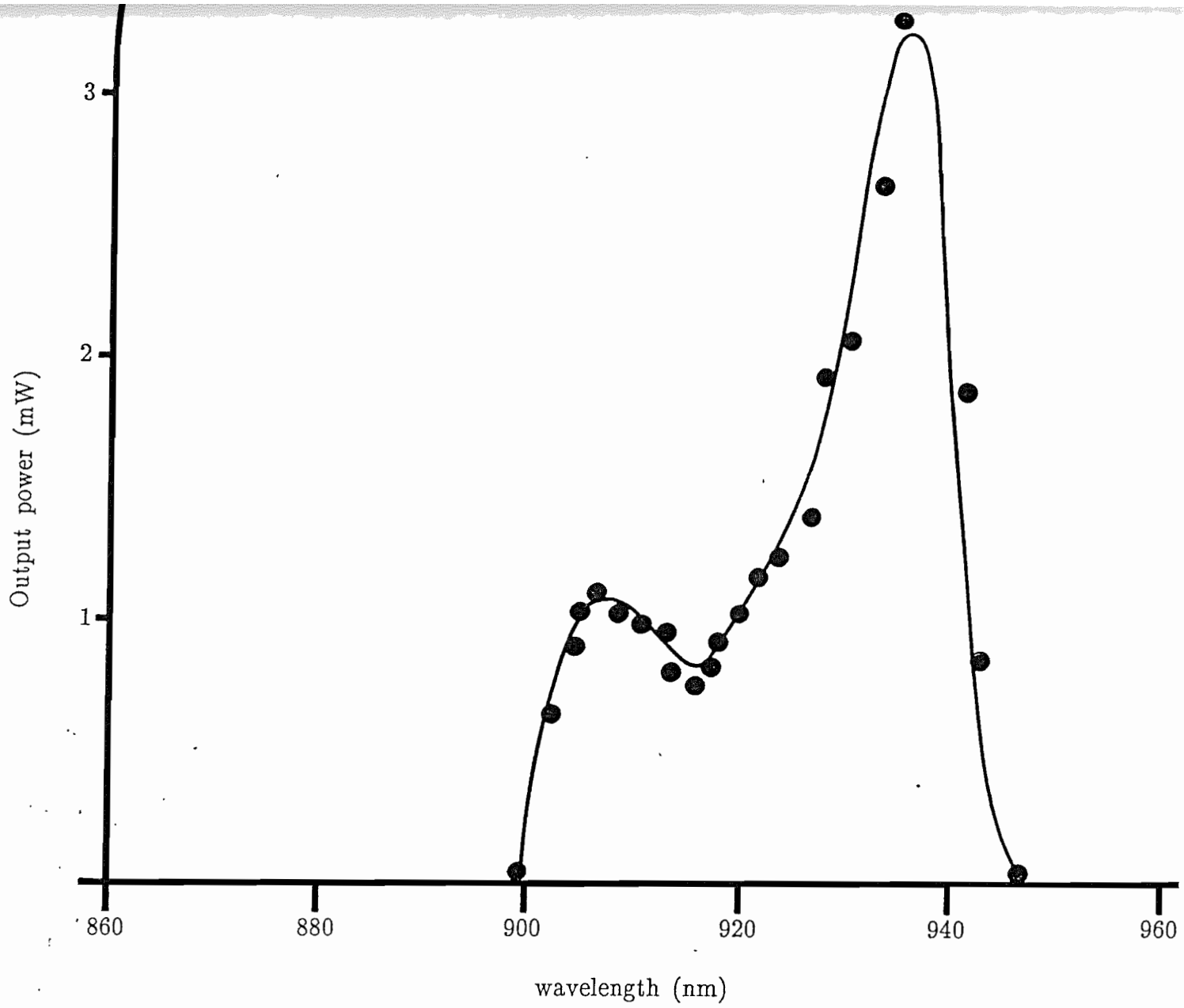

Figure 3.10

Tuning curve for Nd^{3+} doped silica fibre operating on $^4F_{3/2} - {}^4I_{9/2}$ transition

3.5.2 (b) $^4F_{3/2} - {}^4I_{11/2}$ Tunable Operation

For this transition the population in the lower laser level is very small and so a longer length of fibre could be used. The mirror reflectivities etc are summarised in table 3.5 and were optimised for the peak of the tuning curve.

The continuous tuning range obtained was from 1.070 μm to 1.135 μm (figure 3.11). The tuning range achieved with the birefringent filter was limited by inadequate suppression of satellite transmission peaks of the filter so that at the extremes of the tuning range, the wavelength would jump back to near the peak. The previously tuned fibre laser using a grating [5] had a slightly greater tuning range of 70nm since it was not limited by wavelength hopping. However, the efficiency of the system was almost an order of magnitude worse.

An improved tuning range should therefore be possible with a birefringent filter which has better suppression of the satellite peaks. Also an output coupler whose reflectivity increases towards the edges of the tuning curve, where the gain is less, would be a benefit.

Adding the birefringent filter reduced the free running bandwidth from 1THz to 25GHz, F.W.H.M., without a change in output power. The similar efficiency for narrow and broadband operation on both transitions suggests that there is a strong homogeneous component in the line broadening mechanism. This is in agreement with the conclusions reached in chapter 2. From these observations it is anticipated that single longitudinal mode operation should be achievable without a significant change in the efficiency obtained.

Table 3.5

Summary of parameters for the tunable fibre laser operating on the $^4F_{3/2} - {}^4I_{11/2}$ transition.

R_1	0.98
R_2	0.70
absorbed pump power (mW)	35
fibre length (m)	1.8

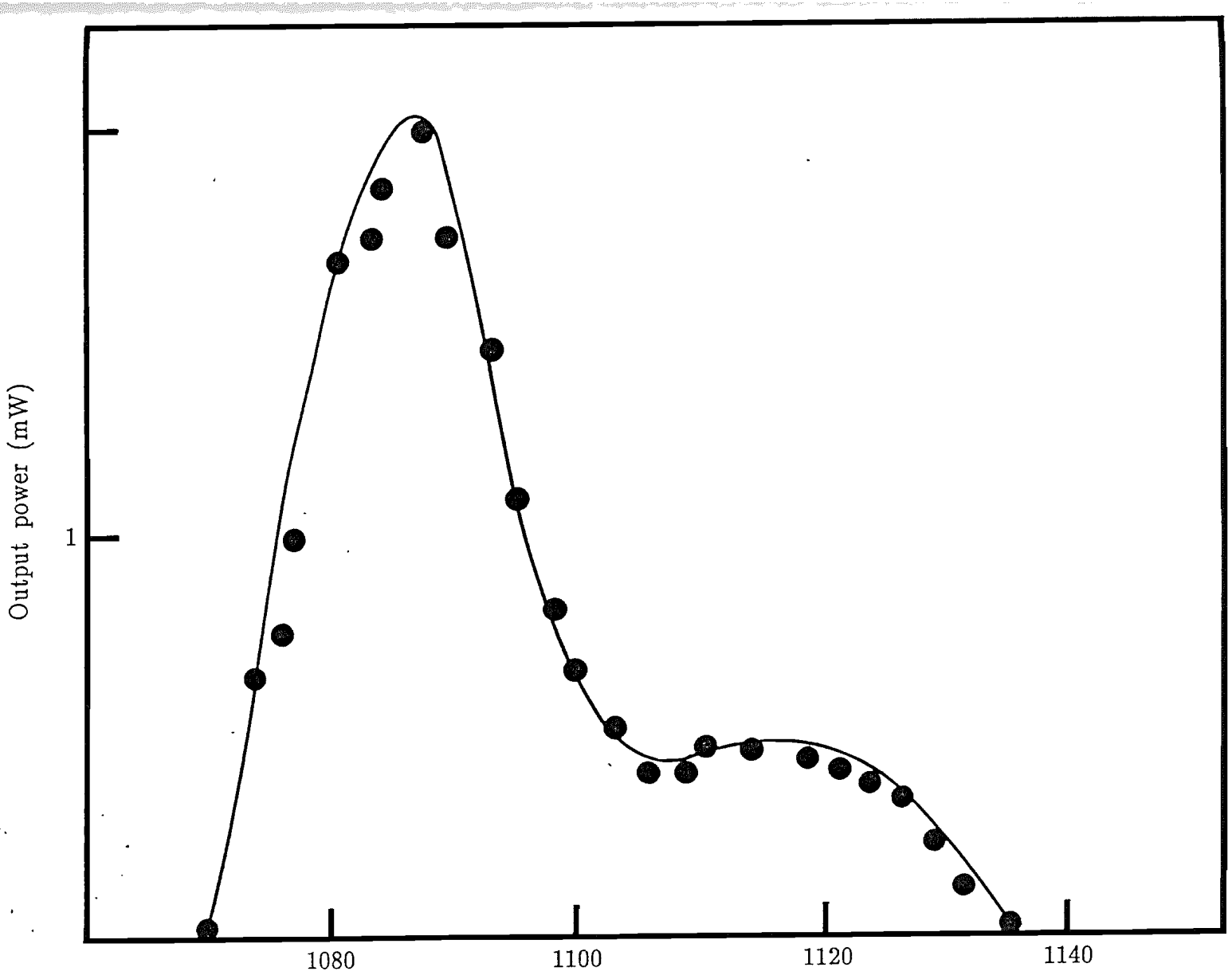

Figure 3.11

Tuning curve for Nd^{3+} doped silica fibre laser operating on $^4F_{3/2} - {}^4I_{11/2}$ transition

CHAPTER 4

4. Pulsed Fibre Lasers

In the schemes described in the previous chapter, the laser output is emitted continuously. There are, however, circumstances when a pulsed output is required, either to increase the peak power of the output or to provide short pulses. Various methods of realising this mode of operation have been developed for conventional systems. Some of these methods have been applied to fibre lasers and the results are presented in this chapter.

4.1 Q–switching

Q–switching allows short, high power pulses to be produced by varying the cavity losses. The technique can be pictured by imagining a shutter placed in the cavity. If the shutter is closed and prevents feedback off one of the mirrors then the inversion can build up above the threshold value without lasing action taking place. When the shutter is opened the system will have a gain which is far in excess of the losses and stimulated emission will rapidly build up producing a short intense pulse.

4.1.1 Theory

The behaviour of the laser output has been investigated by Wagner [46] who found numerical solutions to the coupled rate equations. A simplified analysis by Carlson [47] allows analytical solutions to be found provided that the rate of change of the photon number is small compared to the photon number divided by the cavity lifetime, ie the cavity lifetime is small compared to the pulse duration. Within the framework of this approximation the normalised photon number is given by [47].

$$q = \frac{q_m}{\cosh^2\left\{\frac{q_m}{2\tau_c \tau_l}(t - t_o)^2\right\}^{1/2}} \qquad (4.1)$$

where τ_l is the lifetime for spontaneous emission into the laser transition

t_o is the time at which the peak output occurs

q_m is the peak photon number given by

$$q_m = \frac{\tau_l}{\tau_c}(x - 1 - \ln x) \qquad (4.2)$$

From (4.1) and (4.2) the peak power and pulse duration can be calculated.

$$P_{max} = h\nu\ p\ q_m \frac{c\delta_2}{L} \qquad (4.3)$$

$$\Delta t_p = \frac{2.48\ \tau_c}{(x - 1 - \ln x)^{1/2}} \qquad (4.4)$$

δ_2 is the fractional loss through the output coupler

$$p = 8\pi^2 n^3 \nu^2 \frac{V\,\Delta\nu}{c^3} \qquad (4.5)$$

n is the refractive index

V is the volume of the cavity

$\Delta\nu$ is the linewidth of the laser transition

The time delay between reducing the cavity losses and the pulse peak occurring can be estimated by considering the time taken for the photon number to grow from its value prior to Q–switching to the maximum value using expression (4.1).

The normalised photon number prior to Q–switching can be deduced from [47].

$$q_i = \frac{1}{p}\,\eta\,\frac{\tau'_c}{\tau}\,D \qquad (4.6)$$

τ'_c is the cavity lifetime for the low Q condition

n is the limiting inversion which can be estimated

D is the fraction of emitted photons which are travelling in the correct direction

$$D \approx \frac{(N.A.)^2}{4n_{co}^2} \qquad (4.7)$$

4.1.2 Experimental Configuration

The laser cavity was similar to that described in section3.2(a) except that a modulator was placed in between the intra–cavity microscope objective and output coupler (figure 4.1). This allowed the cavity loss to be modulated whilst retaining a constant pump rate.

The type of device chosen to modulate the cavity losses, ie act as the shutter, was an acousto–optic modulator. When r.f. power was applied to the transducer on the modulator crystal an acoustic travelling wave was set up. This produced a refractive index grating in the crystal [42] and caused Bragg diffraction of incident light. By switching the r.f. power on and off, the grating and hence the loss could be made time dependent.

Alignment of the modulator was critical to get optimum results and the crystal was therefore mounted in a gimbal mount with height adjustment. A short cavity with the modulator outside it, allowed the single pass modulation to be measured. The modulation was found to be 40% and held the laser below threshold when it was inside the cavity in its low 'Q' state.

The cavity lifetime could be measured using a chopper to modulate the pump, and drive relaxation oscillations, as in section 3.3.

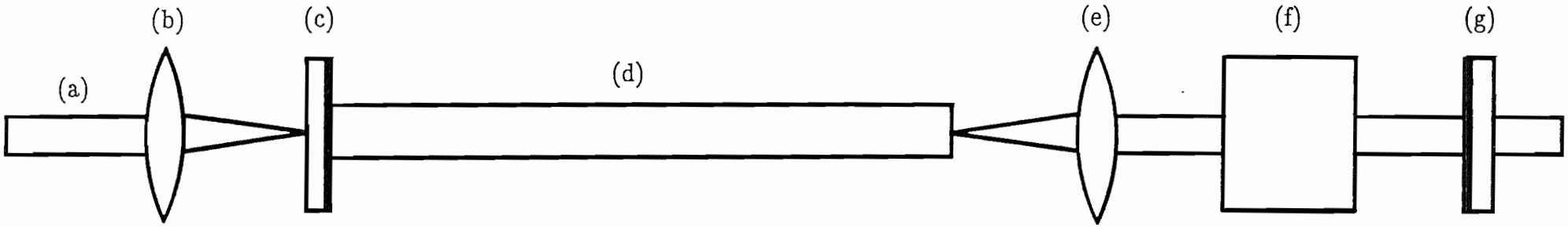

(a) Pump beam

(b) Focusing lens

(c) High reflector

(d) Fibre

(e) Intra–cavity microscope objective

(f) Q–switch

(g) Output coupler

Figure 4.1

Q–switched Fibre laser cavity

4.1.3 (a) Q–switched Operation on the $^4F_{3/2} - {}^4I_{11/2}$ Transition

The mirror reflectivities and other cavity parameters are given in table 4.1. When square–wave modulated r.f. power was applied to the 'Q' switch the laser output during the high 'Q' cycle consisted of a large pulse followed by several smaller spikes and continuous–wave action. By altering the duty cycle so that the high 'Q' period was shortened with respect to the low 'Q' period all emission after the initial spike could be suppressed with a small gain in peak power. Figure 4.2 shows a typical output pulse obtained at 100Hz repetition rate with a high 'Q' period of 5 μs. The repetition rate could be increased up to 1KHz without a noticeable drop in peak power.

The peak power pulse duration and pulse delay were calculated using expressions (4.2)–(4.7), the Wagner tables [46] and the contents of table 4.1. There was good agreement between the calculated and measured values as can be seen from table 4.1. Also it is obvious that the cavity lifetime was small compared to the pulse duration thereby demonstrating the validity of the approximations made.

The addition of the acousto–optic modulator used for Q–switching invariably increased the cavity losses. It was also difficult to align the modulator to achieve a good modulation depth. Therefore, a simple and cheaper means of Q–switching the laser was sought.

An optical chopper wheel placed close to the output coupler was used to block and unblock the beam. By keeping the wheel close to the output coupler, where the laser beam is smallest, the switch on time was kept to a minimum. Although the pulses (figure 4.3) were not as short as those obtained with the acousto–optic modulator, the low cost and simplicity makes the technique

Table 4.1

Summary of parameters and results for the Q-switched fibre laser operating at $\lambda = 1.08\,\mu m$.

τ_{rel} (μs)	27
x	1.9
L_{opt} (m)	3.49
τ (μs)	480
τ_1 (ns)	1.02
δ_2	0.4
ν (THz)	276
A(m^2)	$9.08 \cdot 10^{-12}$
$\Delta\nu$ (THz)	9
τ_c' (ns)	19.6
N.A.	0.21

Calculated and measured peak powers, pulse-widths and pulse delays.

	calculated		
	Carlson	Wagner	Measured
P_{max} (W)	9.17	9.17	8.8
Δt_p (ns)	171	170	180
t_d (μs)	1.79	0.9	1.6

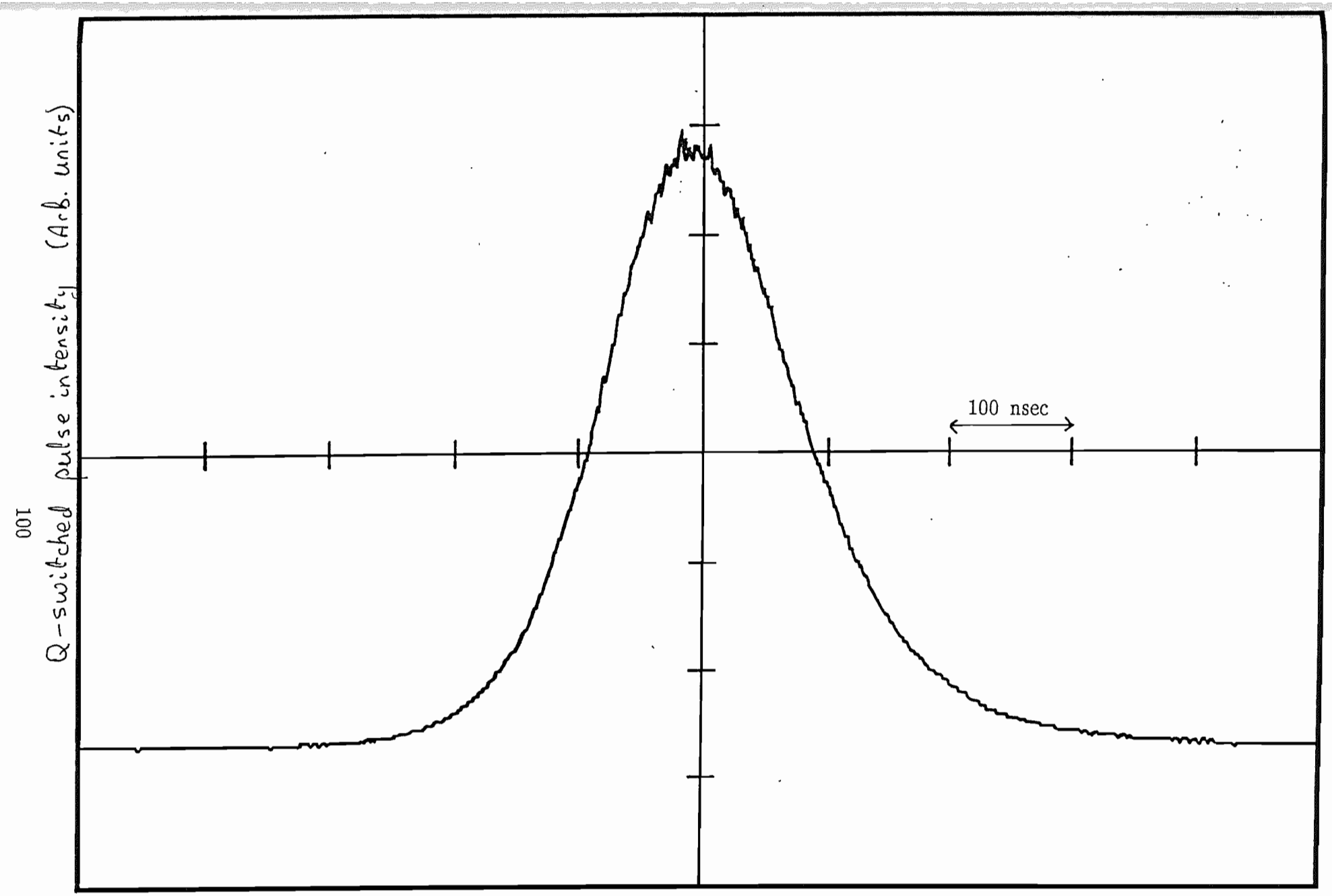

Figure 4.2

Q–switched pulse ($\lambda = 1.08 \mu m$)

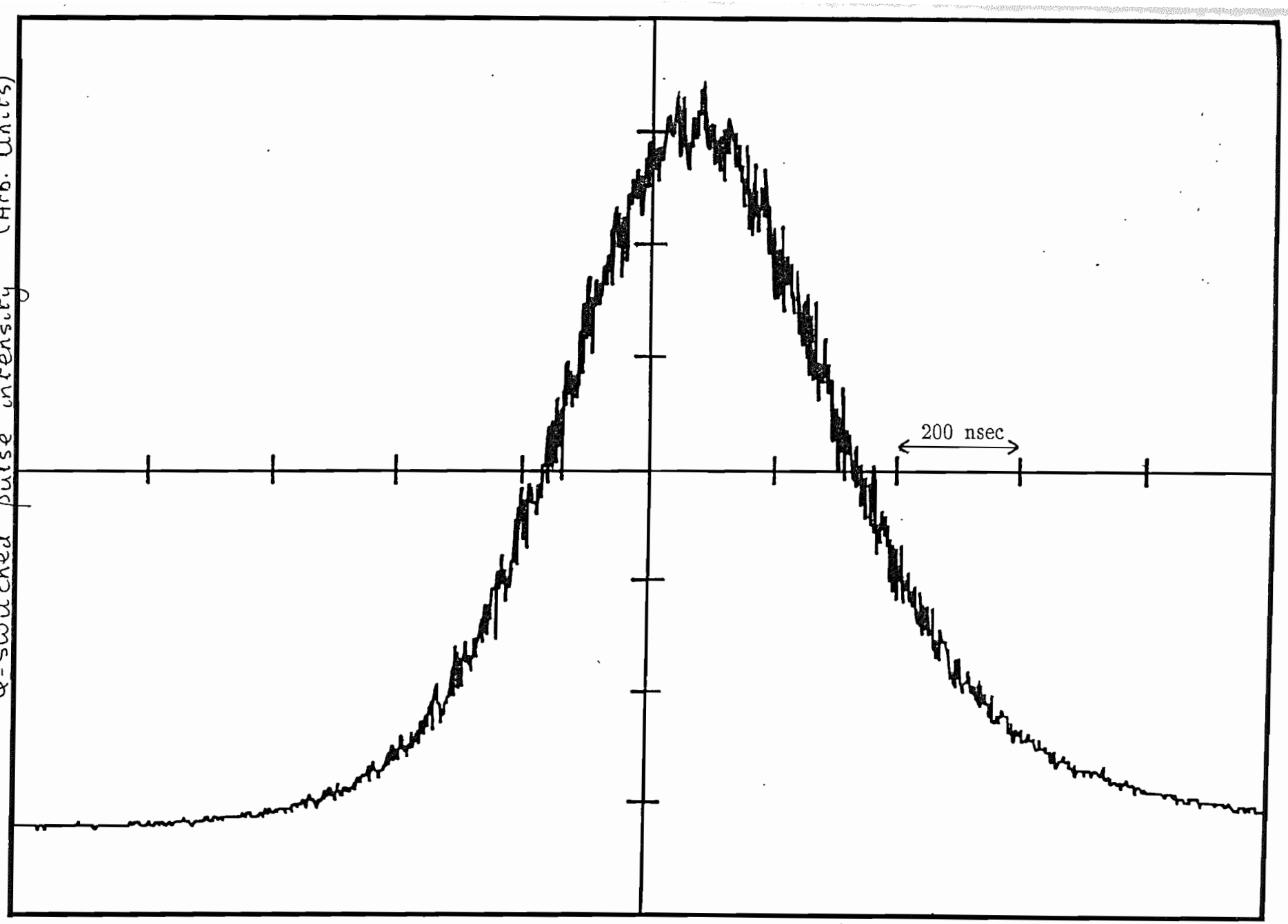

Figure 4.3

Q–switched pulse using chopper ($\lambda = 1.08 \mu m$)

appealing.

If shorter pulses are required (either using a chopper wheel or a modulator) then one needs to increase x or reduce the cavity lifetime, τ_c (see expression (4.4)). Increasing x will only have a small effect on the pulse width. Reducing the cavity lifetime will have a larger effect and this can be brought about by making the cavity more lossy or shorter. Obviously the former is not desirable but making the cavity shorter by using short lengths of highly doped fibres would be a good way of reducing pulse widths.

4.1.3 (b) Q–switched Operation on the $^4F_{3/2} - {}^4I_{9/2}$ Transition

The cavity was the same as that used for operation on the $^4F_{3/2} - {}^4I_{11/2}$ transition except that the fibre length and mirror reflectivities differed (see table 4.2). The shorter fibre length helped to reduce reabsorption losses.

A typical output pulse of 74ns F.W.H.M. and 5.4W peak power is shown in figure 4.4. This was achieved at 100Hz repetition rate and a high Q period of 5 μs. If the expressions relevant to three level systems are used, there is poor agreement between the calculated and measured values. Also an asymmetric pulse (figure 4.4) is observed which is different to the predicted symmetrical profile. The cause of the discrepancy is believed to be due to the dynamics neglected in the theory.

When the laser is in the low 'Q' state, the inversion is very large. Conversely, the ground state population is small on account of the bleaching of the population due to the pump, and so reabsorption losses will be small. As soon as the cavity 'Q' is increased and stimulated emission builds up, the ground state population and hence reabsorption losses increase. This means that there will be a time dependent loss in addition to that provided by the modulator which has not been considered in the theory. A detailed analysis including all the dynamics would require numerical solutions to the time dependent coupled rate equations in Appendix A and is not presented.

Table 4.2

Summary of parameters and results for the Q-switched fibre laser operating at $\lambda = 934$ nm.

x	1.6
L_{opt} (m)	1.89
τ (μs)	480
τ_1 (ms)	1.09
δ_2	0.3
ν (THz)	331
A (m^2)	$9.08 \cdot 10^{-12}$
$\Delta\nu$ (THz)	7.3
τ_c (ns)	15
N.A.	0.21
τ_c' (ns)	9.3

Calculated and measured peak powers, pulse widths and pulse delays.

	calculated		
	Carlson	Wagner	Measured
P_{max} (W)	6.04	6.04	6.3
Δt_p (ns)	103	110	74
t_d (μs)	0.55	0.46	1.6

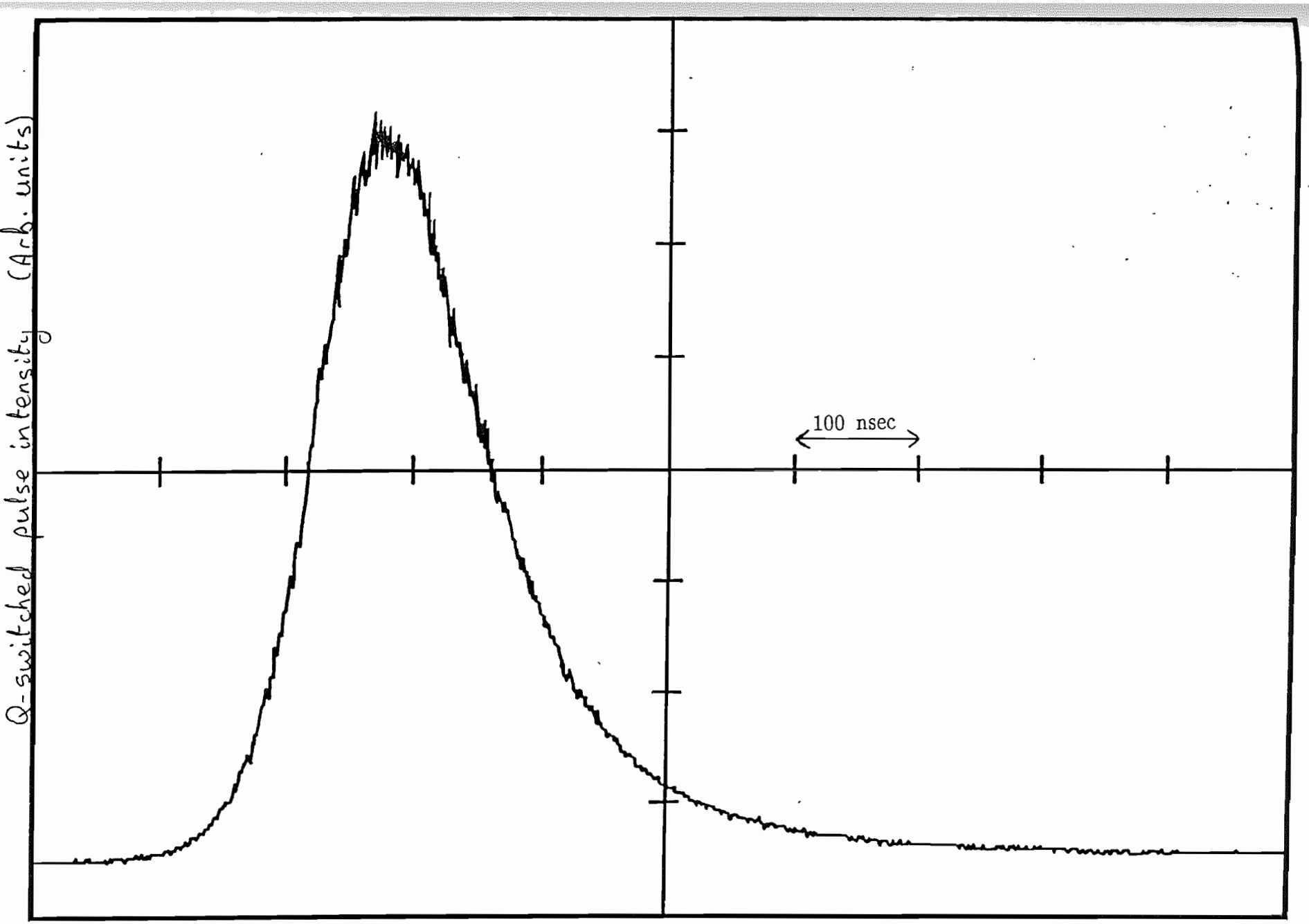

Figure 4.4

Q-switched output pulse ($\lambda = 934$ nm)

4.2 Mode–locking

Another method of obtaining a pulsed output is mode–locking. Generally, when a laser is operating on several longitudinal modes their relative phases vary which causes random fluctuations in the output intensity to take place because of interference between the modes. This is not always desirable and a method of increasing the coherence of the laser output is to force the phases to maintain their relative values, ie mode–lock. This has the result of producing a periodic train of short, coherent pulses which are separated by a time equal to the inverse of the longitudinal mode spacing. The width of the pulses is inversely proportional to the laser bandwidth. The production of short, coherent pulses is useful for spectroscopic studies in the time domain, study of non–linear effects and optical communications.

The broad optical linewidths of doped ions in glass hosts potentially offer large lasing bandwidths and their ability to generate short pulses has been successfully demonstrated both in guided [48] and unguided [49, 50] configurations. However, the dispersion introduced by the long length of active medium in the fibre lasers discussed in the preceding chapters could be an obstacle to any attempts of producing short pulses. Also the small mode sizes lead to high intensities which greatly enhance non–linear effects. With this in mind, mode–locking of a fibre laser was attempted for the first time in order to see if there are any limitations on its performance and if so, to understand the underlying physics.

There are several ways in which the laser output can be mode–locked and the method chosen was active mode–locking by amplitude modulation. An intra–cavity modulator varies the cavity losses and hence produces an amplitude modulation on the laser intensity at the same frequency as the

intermode spacing. This results in the A.M. sidebands coupling with adjacent cavity modes and the modes becoming locked together in a fixed phase relationship.

4.2.1 Theory

The theory of active mode–locking by amplitude modulation has been investigated by several authors. Kuizenga and Siegman [51–54] have presented a self–consistent approach in the time domain rather than the coupled mode or frequency domain approach [55–56] previously used. This treatment has resulted in simple expressions which characterised mode–locked Nd^{3+}:YAG and Nd^{3+}:Glass systems [51], with good agreement between the predicted and experimentally found parameters.

Their theory essentially assumes the existence of a short pulse in the cavity and follows its progress through the modulator and gain medium as it completes one round trip of the cavity. A self–consistent solution is then found.

The pulse width is given by [51]

$$\tau_{po} = \sqrt{\frac{2 \ln 2}{\theta_m f_m}} \frac{1}{\pi} \left[\frac{g}{\Delta f}\right]^{1/4} \qquad (4.8)$$

f_m is the driving frequency of the modulator

θ_m is the depth of modulation produced by the modulator

g is the round trip amplitude gain at the line centre

Δf is the linewidth of the transition

The presence of the dispersive media can be accounted for by considering the addition phase terms as contributing to an effective gain which is then treated as the true gain of the medium [51].

If the phase shift due to the dispersion is assumed to vary slowly with frequency then it can be expanded about a central frequency ω_L [57].

$$\phi(\omega) = \phi(\omega_L) + \left[\frac{d\phi}{d\omega}\right]_{\omega_L} (\omega - \omega_L) + \frac{1}{2}\left[\frac{d^2\phi}{d\omega^2}\right]_{\omega_L} (\omega - \omega_L)^2 \qquad (4.9)$$

Since the phase shift is given by

$$\phi(\omega) = \frac{n(\omega)l\omega}{c} \qquad (4.10)$$

one can calculate the additional terms due to dispersion and insert them into the Kuizenga analysis.

The pulse then becomes

$$\tau_{po} = \sqrt{\frac{2\sqrt{2}\ln 2}{\theta_m f_m}} \frac{1}{\pi} \left[\frac{g(1 + a^2)^{1/2}}{\Delta f^2}\right]^{1/4} \qquad (4.11)$$

ie it is broader than that produced without dispersion by a factor of

$$\left[2(1 + a^2)^{1/2}\right]^{1/4}$$

where $$a = \frac{\pi l}{2} \frac{\lambda^3}{c^2 g} \Delta f^2 . \frac{d^2 n}{d\lambda^2} \qquad (4.12)$$

If a Sellmeier relationship [58] is used to describe the change of refractive index with wavelength, the broadening can be calculated from a knowledge of the cavity and material parameters.

Typically a Nd^{3+} doped fibre laser operating on the $^4F_{3/2} - {}^4I_{11/2}$ transition at 1.08 μm might have the following characteristics for a 2.3m length of fibre.

$$g = 0.3$$

$$\Delta f = 9 \text{ THz}$$

$$\theta_m = 0.24$$

$$f_m = 20.723 \text{ MHz}$$

$$\frac{d^2n}{d\lambda^2} = 7.32\times10^9 \text{ m}^{-2} \text{ (for quartz at 1.08 } \mu\text{m)}$$

This would give pulses approximately 41.5×10^{-12}s wide without dispersion and 156×10^{-12}s taking into account the dispersion of the active medium.

If the fibre were 100m long, then with f_m = 500 kHz one would expect pulse durations of approximately 270×10^{-12}s without dispersion and 2.58×10^{-9}s with dispersion.

One can see that the broadening is only moderate even for long lengths of fibre, a factor of 10 for 100m of fibre. Therefore, the presence of dispersion should not be too detrimental in any attempts to mode-lock fibre lasers.

4.2.2 Experimental Configuration

The laser cavity was similar to that used for the tunable lasers except that the birefringent filter was replaced by a Brewster angled, quartz acousto–optic modulator. The quarter–wave plates helped to ensure that vertically polarised radiation was incident on the mode–locker and that reflection losses off the Brewster surfaces were minimised (figure 4.5). They also ensured that the laser polarisation was normal to the direction of the acoustic wave in the modulator, thereby allowing the largest modulation depth of the laser to be achieved.

The mode of operation of the modulator was different to that used for Q–switching in that when R.F. power was applied to the transducer, bonded to the modulator, a standing rather than travelling acoustic wave was set up. This had the effect of creating a time dependent refractive index grating and hence produced cavity loss modulation.

Because the resonances of the high 'Q' transducer were sharp and highly temperature dependent, it was necessary to mount the mode–locker in a temperature stabilised enclosure. The enclosure was then held in a gimbal mount which aided the alignment required to achieve the maximum depth of modulation. This was placed close to the output coupler so that the state of the modulator was unchanged when the reflected laser pulse went back through it. The output coupler was mounted on a translation stage so that the cavity length could be adjusted to match the drive frequency of the mode–locker.

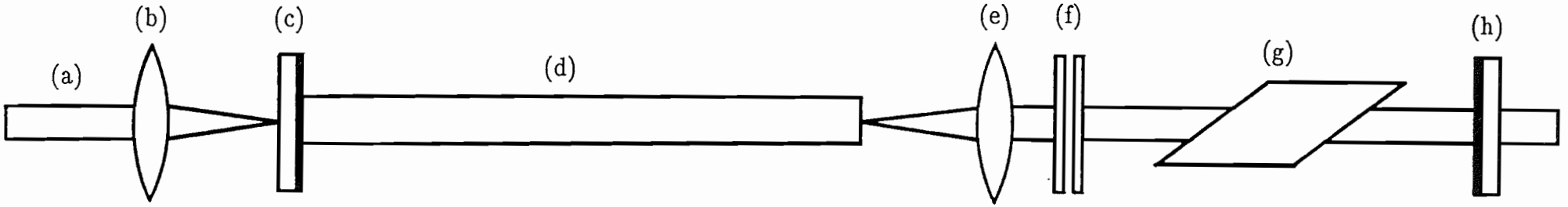

(a) Pump beam

(b) Focusing lens

(c) High reflector

(d) Fibre

(e) Intra–cavity microscope objective

(f) Quartz quarter–wave plates

(g) Brewster angled mode–locker

(h) Output coupler

Figure 4.5

Mode–locked fibre laser cavity

Initially a short cavity was set up with the mode–locker outside the cavity and the transmitted beam was detected with a Germanium photodiode and oscilloscope. When the alignment of the mode–locker had been adjusted to give maximum modulation depth, the output coupler was moved to the position required for mode–locking; the aligned mode–locker was then inside the cavity. An approximate position for the output coupler was found by monitoring the amplified signal from the Germanium detector on a Tektronix 7L14 R.F. spectrum analyser. With no R.F. power applied to the mode–locker, the laser output contained weak longitudinal cavity mode beats (figure 4.6) and the cavity length was adjusted until these roughly matched the drive frequency.

When R.F. power at 20.723MHz was applied to the mode–locker and the cavity length adjusted further, the beats became stronger and narrower (figure 4.6). Eventually higher harmonics appeared and dramatically increased as the R.F. power was increased and the cavity length fine tuned. The R.F. spectrum (figure 4.6) shows a comb of modes obtained with 250mW of R.F. power applied to the mode–locker. The high frequency roll off is due to the bandwidth of the amplifier and detector.

Once the cavity length was fairly well adjusted, the output was studied in the time domain using a fast detector (R.C.A. CA309709E, F.W.H.M. resolution of approximately 60ps) and oscilloscope (Tektronix 7A19 amplifier in a 7904 mainframe with a combined bandwidth of approximately 400MHz). The trace on the oscilloscope showed an envelope containing relatively sharp pulses which merged into each other. These satellite pulses could occur if the laser was operating on several different frequencies within the gain bandwidth and the pulses produced by each region were slightly displaced in time because of dispersion.

Figure 4.6

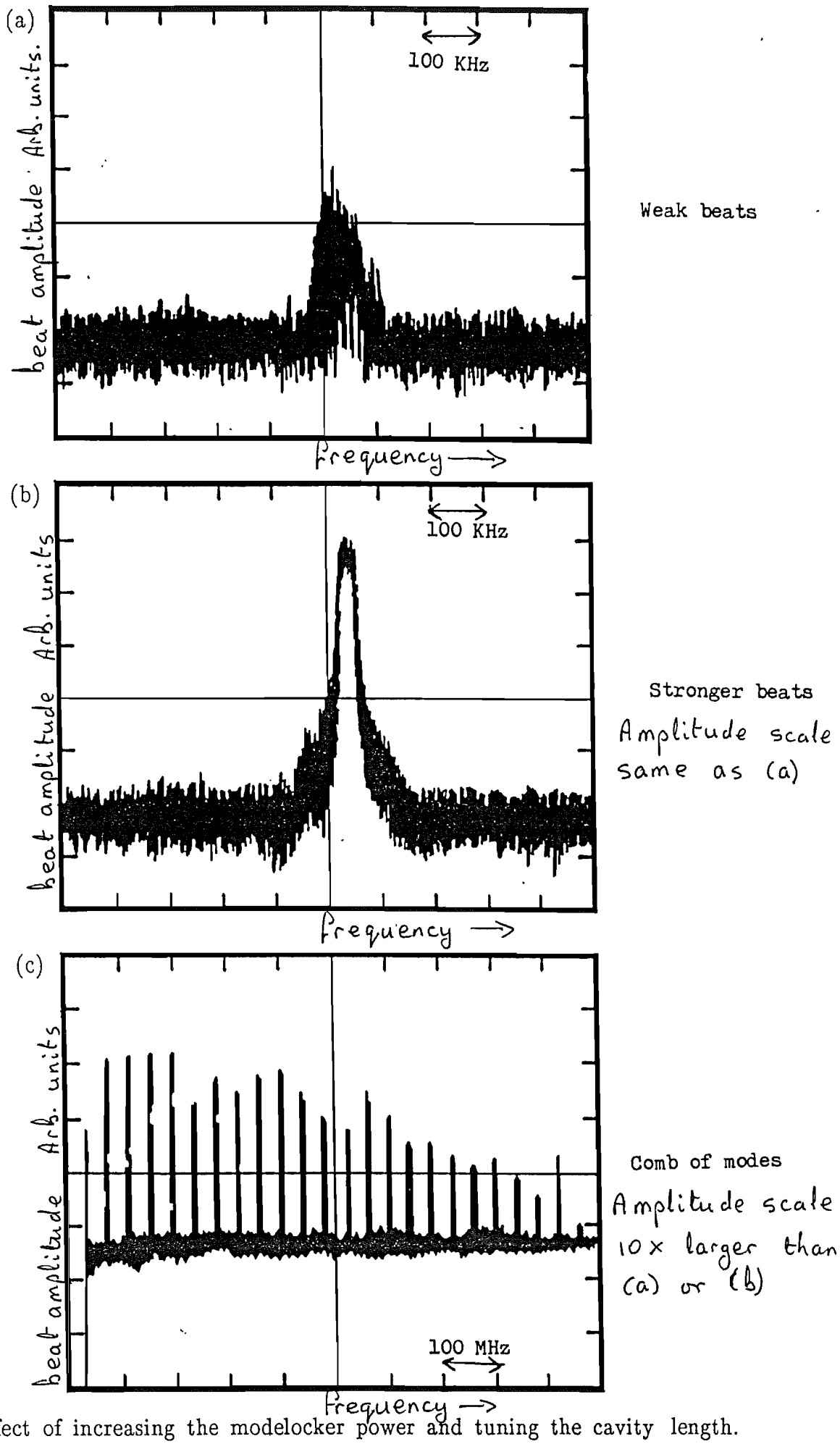

The effect of increasing the modelocker power and tuning the cavity length.

This type of behaviour would occur when etalons within the cavity caused spectral modulation of the output and had been seen in the experiments on tunable lasers. The intra–cavity x10 microscope objective which had been chosen for its long working distance was replaced by a high quality singlet (15mm focal length) but virtually no difference in the trace was seen.

It was observed that when there was no R.F. power applied to the mode–locker, modulation was occasionally present on the laser output, with a time period of approximately 1.8ns. The associated beat frequency of approximately 0.5GHz could also be observed using the R.F. spectrum analyser. This corresponded to beats between the cavity formed by the two mirrors and a sub–cavity between the output coupler and fibre face, verified by moving the output coupler position and noting the change in beat frequency.

A 250 μm thick (free spectral range 600GHz) uncoated quartz etalon was inserted into the cavity to provide a small degree of frequency selection and force the laser to operate on one of the parasitic etalon modes (figure 4.7). This was fairly successful and produced the pulse shown in figure 4.8 although some structure around the pulse was still evident. The measured width was limited by the bandwidth of the oscilloscope and a deconvolved pulse width of 450ps F.W.H.M. was calculated from a measurement of the instrumental broadening using a known source. The bandwidth of the output was less than 8GHz, the measurement being limited by the resolution of the monochromator used.

With the laser mechanically Q–switched using a chopper wheel, the output consisted of a train of pulses whose F.W.H.M. was less than 3ns inside a

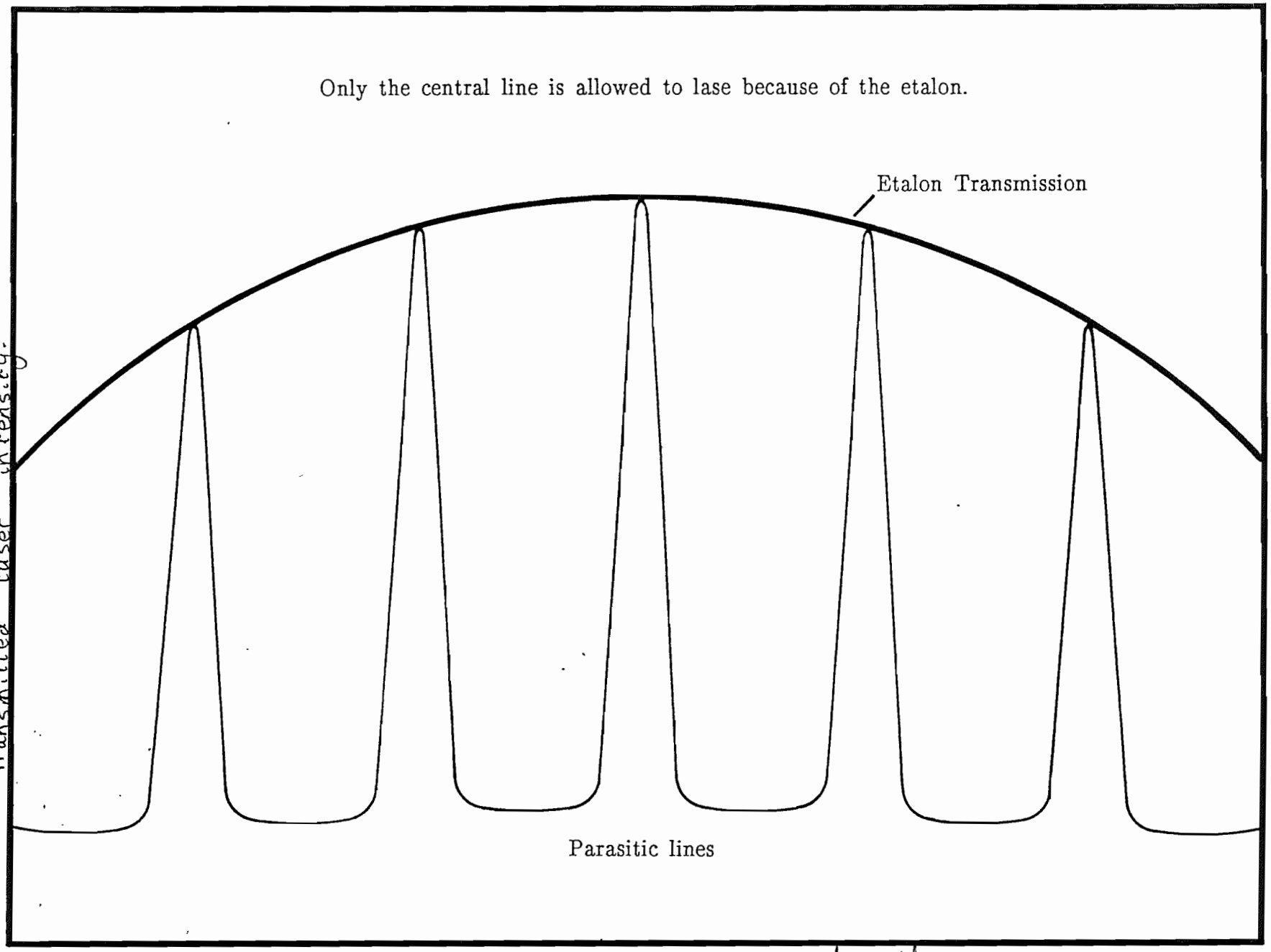

Figure 4.7

Etalon selecting one parasitic line

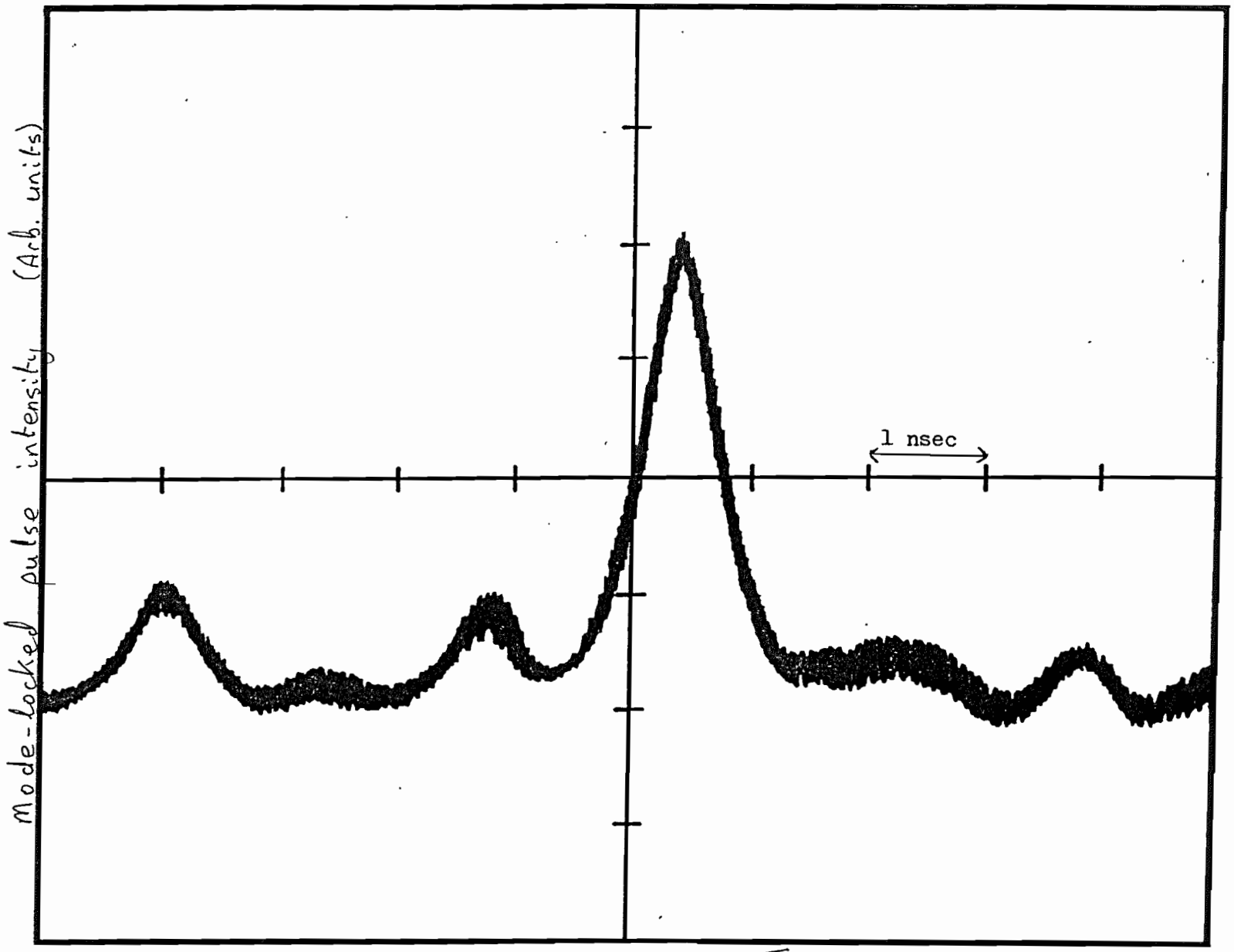

Figure 4.8

Mode–locked output pulse Deconvolved FWHM = 450 ps

690ns envelope (figure 4.9). Once again some structure was seen on the mode–locked pulses.

The addition of the uncoated etalon modifies the pulse width expression to

$$\tau_{po} = \sqrt{\frac{2\ln 2}{\theta_m f_m}} \frac{1}{\pi} \left[\frac{g}{\Delta f^2} + \frac{1}{\Delta f_e^2}\right]^{1/4} \left[2(1 + a^2)\right]^{1/4} \quad (4.13)$$

$$\text{where} \quad a = \frac{\pi l}{2c^2} \lambda^3 \frac{}{\left[\frac{g}{\Delta f^2} + \frac{1}{\Delta f_e^2}\right]} \frac{d^2 n}{d\lambda^2} \quad (4.14)$$

and Δf_e is the effective bandwidth of the etalon [51].

The cavity parameters in table 4.3 and expressions (4.13), (4.14) allow a pulse duration of 247ps to be calculated for the c.w. mode–locking case.

The situation is somewhat different for the Q–switching and mode–locking experiments because the Q–switch build up time of approximately 5μs was not long enough for a steady state to be reached. For this regime one must use the transient expressions derived by Kuizenga et al [52].

$$\tau_p = \sqrt{\frac{\ln 2}{2}} \frac{1}{\pi} \frac{1}{\theta_m f_m} \frac{1}{\sqrt{m}} \quad (4.15)$$

m is the number of trips performed before emission occurs.

This expression together with the contents of table 4.3 enable a pulse duration of 2.9ns to be calculated.

Figure 4.9

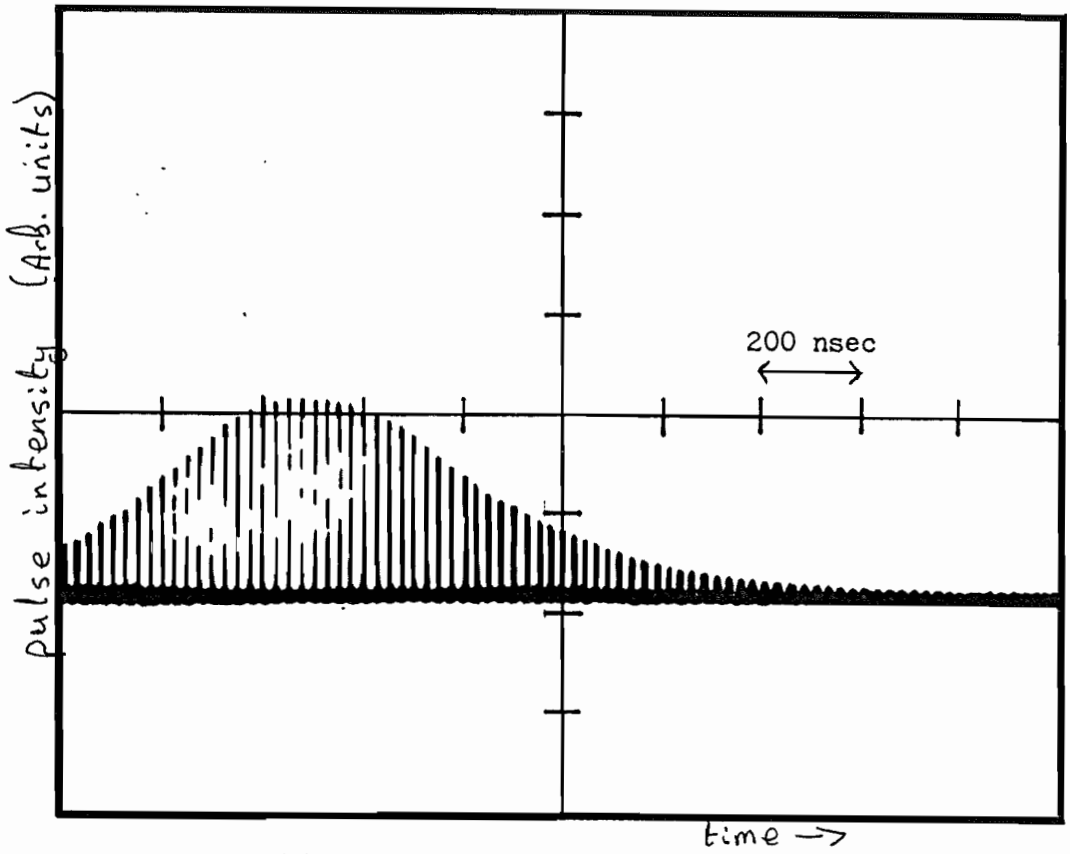

(a) Q-switched and mode-locked pulse

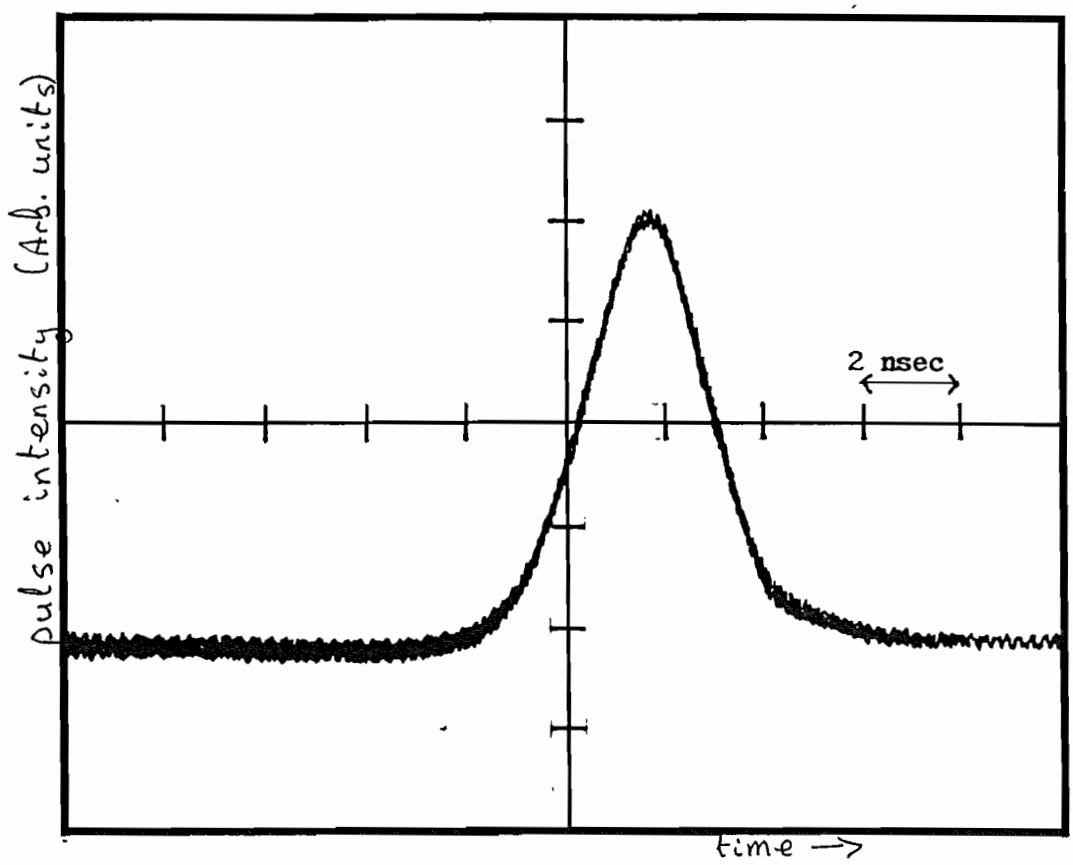

(b) Mode-locked pulse inside the Q-switched envelope

Table 4.3

Parameters and results for the c.w. mode-locked laser operating at $\lambda = 1.08\mu m$

	c.w. mode–locking
θ_m	0.24
f_m (MHz)	20.723
g	0.4
Δf (THz)	9.0
Δf_e (GHz)	700
l (m)	2.3
λ (μm)	1.088
$\frac{d^2n}{d\lambda^2}$ (m^{-2})	$7.32 \cdot 10^9$
a	0.185
τ_{po} (ps) calculated	247
τ_{po} (ps) measured	450

Parameters and results for the Q-switched and mode-locked laser operating at $\lambda = 1.08\mu m$.

	Q–switching and mode–locking
θ_m	0.24
f_m (MHz)	20.723
τ_c (ns)	29
Buildup time (μs)	4.9
m	169
τ_{po} (ns) calculated	2.9
τ_{po} (ns) measured	3.0

The discrepancy between the calculated and measured pulse durations for the c.w. mode–locking is due to the omission of the effects of the subcavity. The spectral narrowing due to the subcavity is difficult to model using the approximations made in the Kuizenga approach because of the addition terms involved. Physically the difficulty arises because some of the photons do not pass through the modulator or gain medium the same number of times for every trip around the cavity.

In the case of Q–switching and mode–locking, the short prelase period means that the gain medium and etalons do not have time to greatly influence the pulse shape and so the transient expression adequately describes the laser behaviour.

Although the reflection back off the fibre face was small, probably only a few percent, the presence of gain in the fibre would effectively increase the reflectivity. Therefore, methods of reducing the feedback to a very small amount were sought.

In a simple model, wedging the face of the fibre at an angle greater than the acceptance angle of the fibre, any reflected rays would no longer undergo total internal reflection and remain bound in the core (figure 4.10). However, the wedge angle must not be so great that total internal reflection occurs at the wedged face and nothing exits out of the fibre (figure 4.10). Polishing an angle on the fibre was considered difficult so an adaption of the idea was tried.

If a wedged blank was optically butted to the fibre end, it should achieve the same result and be easier to fabricate. There are additional advantages in that the beam would rapidly diverge as it emerged from the fibre core and

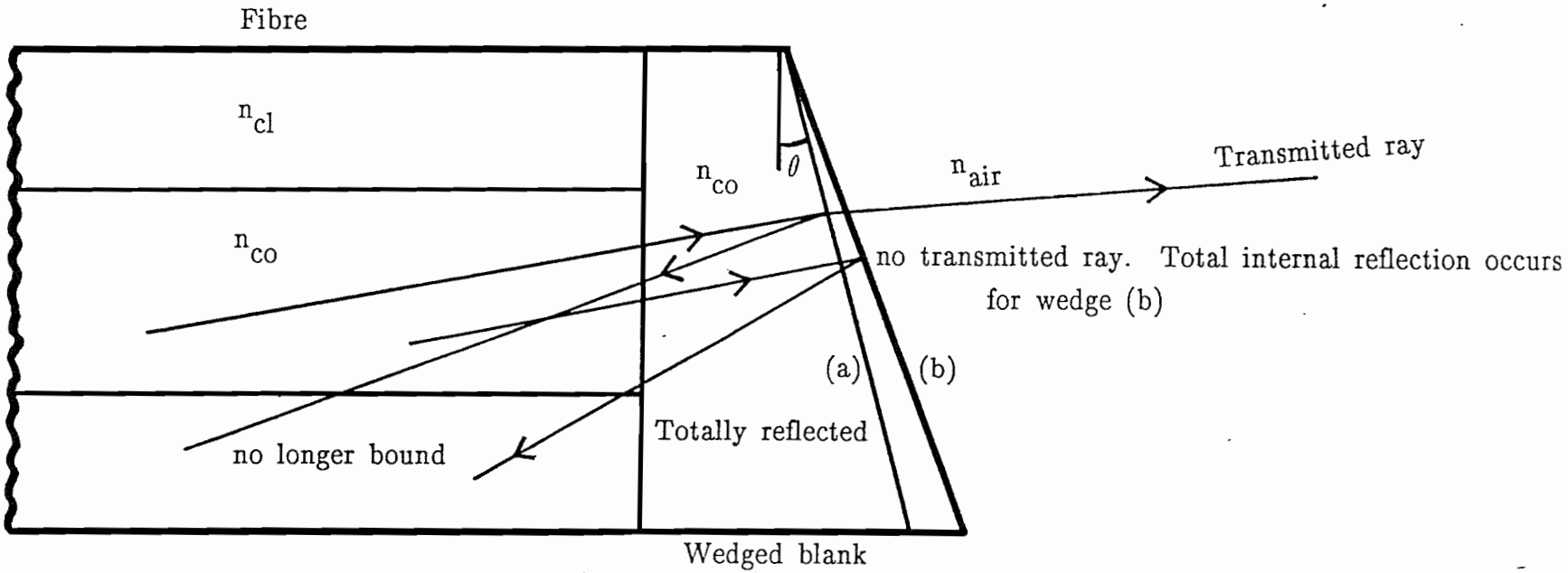

To prevent reflected rays remaining bound in the fibre or total internal reflection off the wedged face

$$\frac{1}{2}\cdot\cos^{-1}\left[\frac{n_{cl}}{n_{co}}\right] < \theta < \sin^{-1}\left[\frac{n_{air}}{n_{co}}\right] - \cos^{-1}\left[\frac{n_{cl}}{n_{co}}\right]$$

Figure 4.10

The effect of butting a wedged blank to the fibre end.

result in a large spot being reflected back. Also only the outer region of the beam, which is of much lower intensity than the centre, would be incident on the fibre face on account of the tilting caused by the reflection off the wedged surface. Both of these factors should help to reduce the feedback further.

With a 15° wedged, quartz blank butted up to the fibre end the modulation was reduced but not eradicated. Although the improvement in mode–locking was moderate, the cavity losses significantly went up because of the increased reflection losses and no correction was made for the astigmatism introduced by the wedged surface [59, 60]. The technique did not work as well as expected because of either a non–perfect match between the refractive index of the quartz blank and fibre core or the wedge angle was not large enough. Similar problems were encountered when trying to mode–lock the $^4F_{3/2} - {}^4I_{9/2}$ transition. Ideally either a polarisation maintaining fibre wedged at the internal Brewster angle or an all fibre modulator and output coupler would have been used to remove the feedback.

Until the unwanted modulation is completely suppressed or controlled,the role of non–linear effects such as self–phase modulation or Raman scattering cannot be fully investigated. The problems highlighted on mode–locking fibre lasers are now the subject of study for a continuing project.

4.3 Modulated Pump Experiments

Other methods of obtaining a pulsed output rely on pumping the laser with a modulated source.

Before the problems associated with actively mode–locking the laser with the mode–locker were fully appreciated, an attempt to synchronously pump the fibre laser was tried.

4.3.1 Synchronous Pumping

A Spectra–Physics c.w. mode–locked, frequency doubled Nd^{3+}:YAG laser was used to pump the fibre laser. Although weak lasing action was observed, the pulses were very broad, tens of ns wide. It is likely that dispersion plays an important role in this case because the pump and laser photons will have different group velocities and drift out of synchronism as they propagate down the fibre.

Assuming a pump source at 532nm (group velocity $\approx$ 1.886 x 10^8 ms^{-1} for silica) and laser at 1.088 μm (group velocity = 1.987 x 10^8 ms^{-1}) it is clear that the laser pulse will try to lead the pump. Therefore, only the trailing edge of the laser will see gain as the pulses separate in time until after travelling, for example, 35cm when the time separation is 100 ps, the pulses may no longer overlap at all or the laser pulse is stretched backwards making it broader.

4.3.2 Resonant driving of relaxation oscilllations

Danielmeyer et al [61] devised an alternative modulated pump scheme which resonantly drove the relaxation oscillations present of the output of a Nd^{3+}:YAG laser. They observed enhanced, undamped pulses using small pump modulations when on resonance. As this appears to be a simple means of providing high power output pulses, it was tried on a fibre laser. The laser cavity was identical to that used in section 3.4(a). and the acousto–optic modulator from section 4.1.2 was used to modulate the dye laser pump. The zero order spot was used since it allowed the pump to be modulated about the threshold pump power.

When the modulation frequency was far from resonance the normal damped oscillations were observed. As the frequency was increased the oscillations slowly became larger and less damped until the pulses shown in figure 4.11 were obtained when on resonance. Increasing the frequency further causes the pulses to become smaller again. This behaviour, as well as the phase between the pump and laser output is shown in figure 4.12. There is a rapid transition about the resonant frequency when the pump and laser become out of phase. This behaviour is the same as that observed by Danielmeyer [61].

During these experiments, other effects were observed. The sequence of figures 4.13 to 4.16 show the change in output behaviour as the alignment of the output coupler was altered. The undamped oscillations in 4.16 were present even when the pump was not modulated. Figure 4.17 shows that the periodicity of these undamped oscillations is essentially the same as that of the normal damped relaxation oscillations. In all cases the behaviour could be reproducibly changed from one state to another by moving the output coupler. It was thought that the behaviour was due to the combination of pump power

and cavity loss resulting in an unstable solution to the rate equations of Appendix A. However, the effect persisted as the pump power was slowly reduced to the threshold value. Further studies on fibre lasers pumped by modulated sources [43] have revealed other phenomena, such as optical bistability, unstable spiking, which have been attributed to deterministic optical chaos. It is likely that the effects described in this section have a similar origin to those reported by Phillips et al [43].

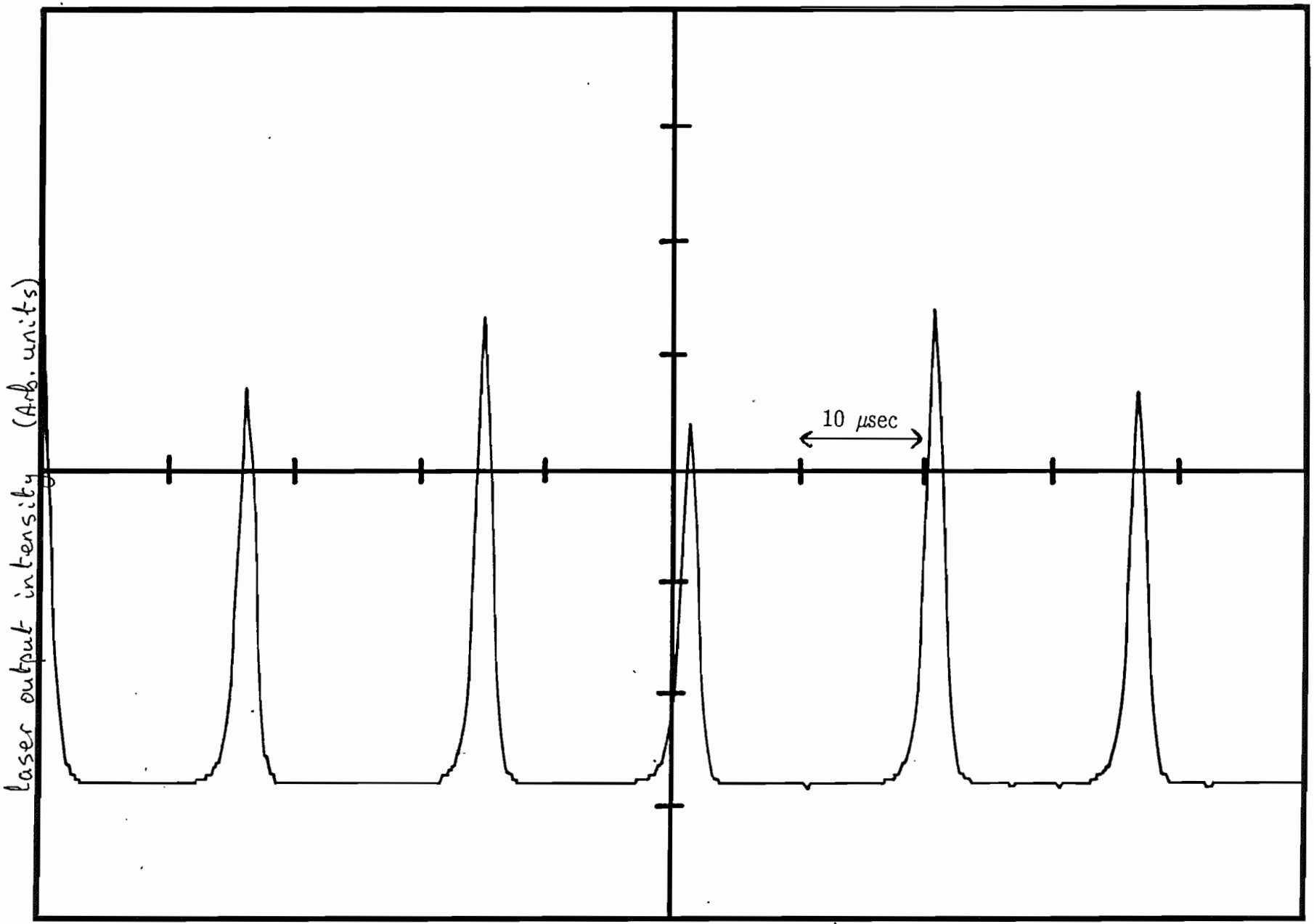

Figure 4.11

Resonantly pumped relaxation oscillations

Figure 4.12

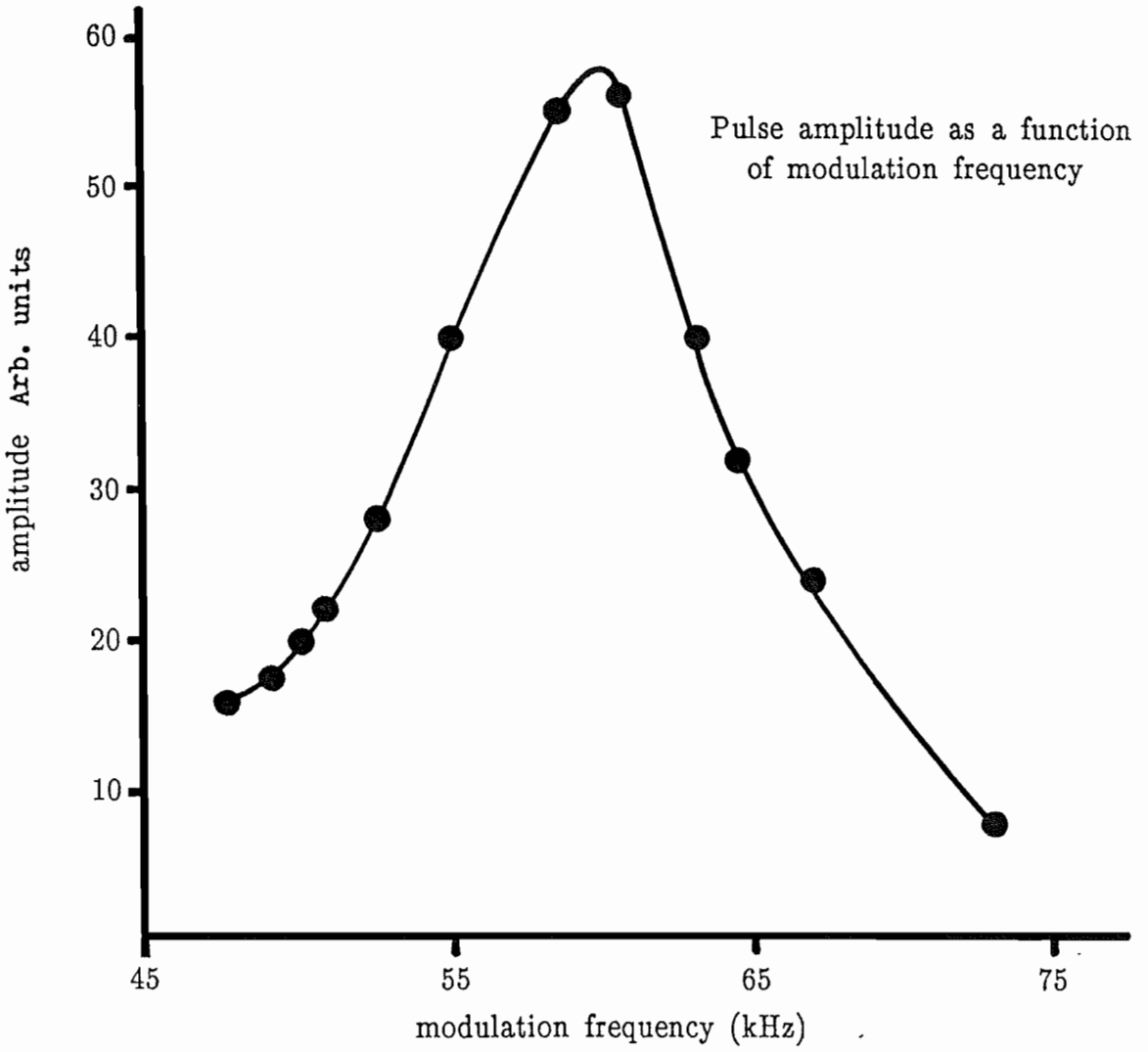
60
50
40
30
20
10
amplitude Arb. units
Pulse amplitude as a function of modulation frequency
45
55
65
75
modulation frequency (kHz)

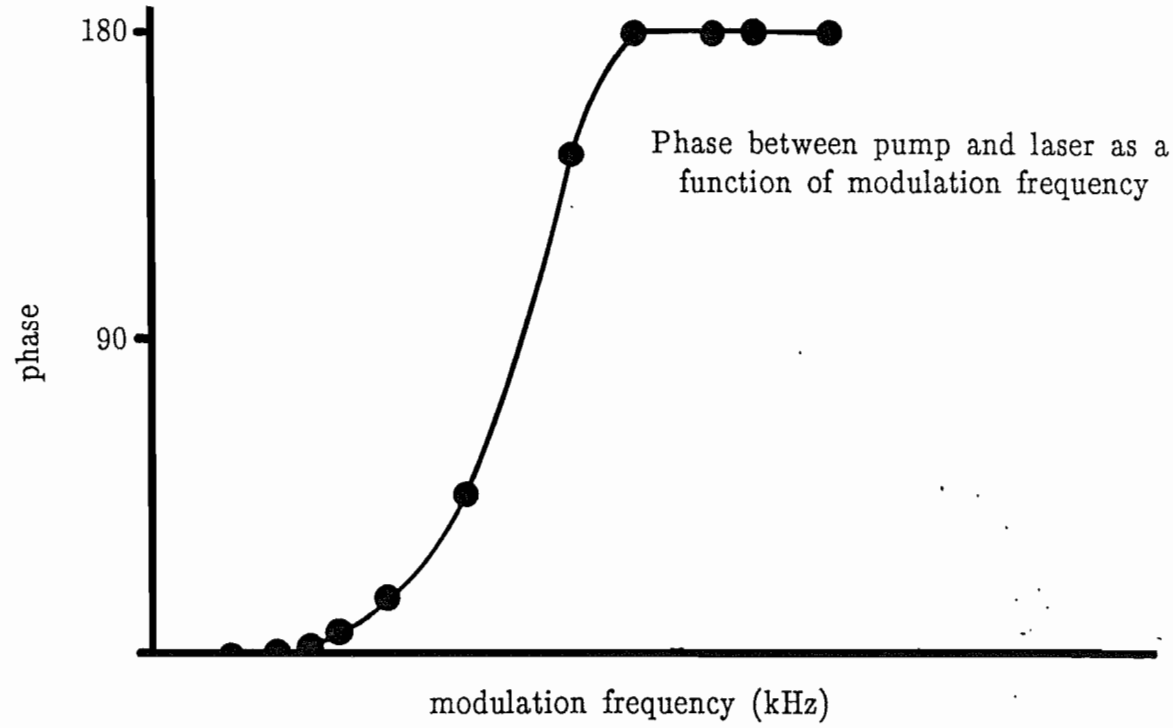
180
90
phase
Phase between pump and laser as a function of modulation frequency
modulation frequency (kHz)

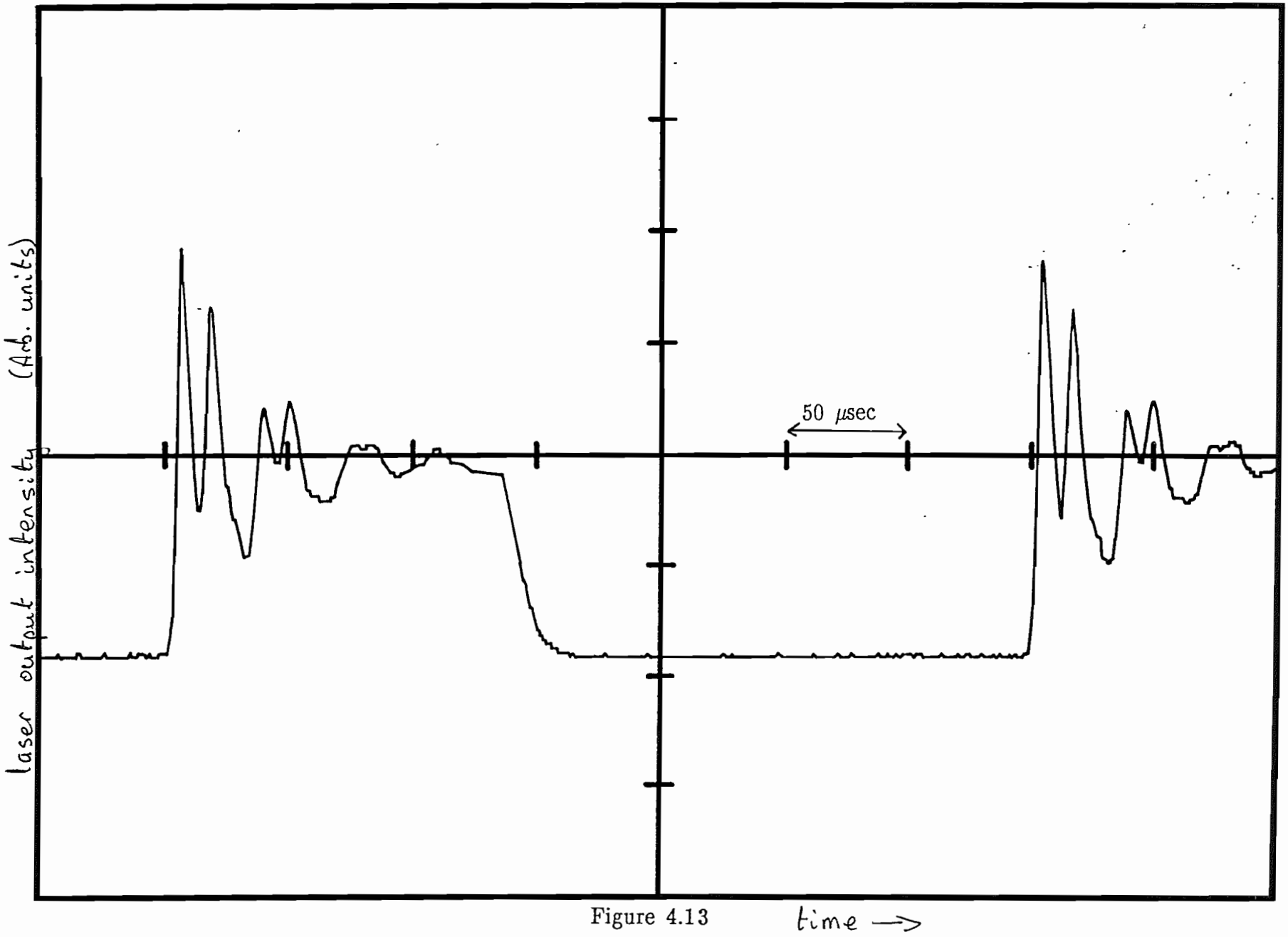

Figure 4.13

Temporal behaviour of fibre laser output for an unmodulated pump.

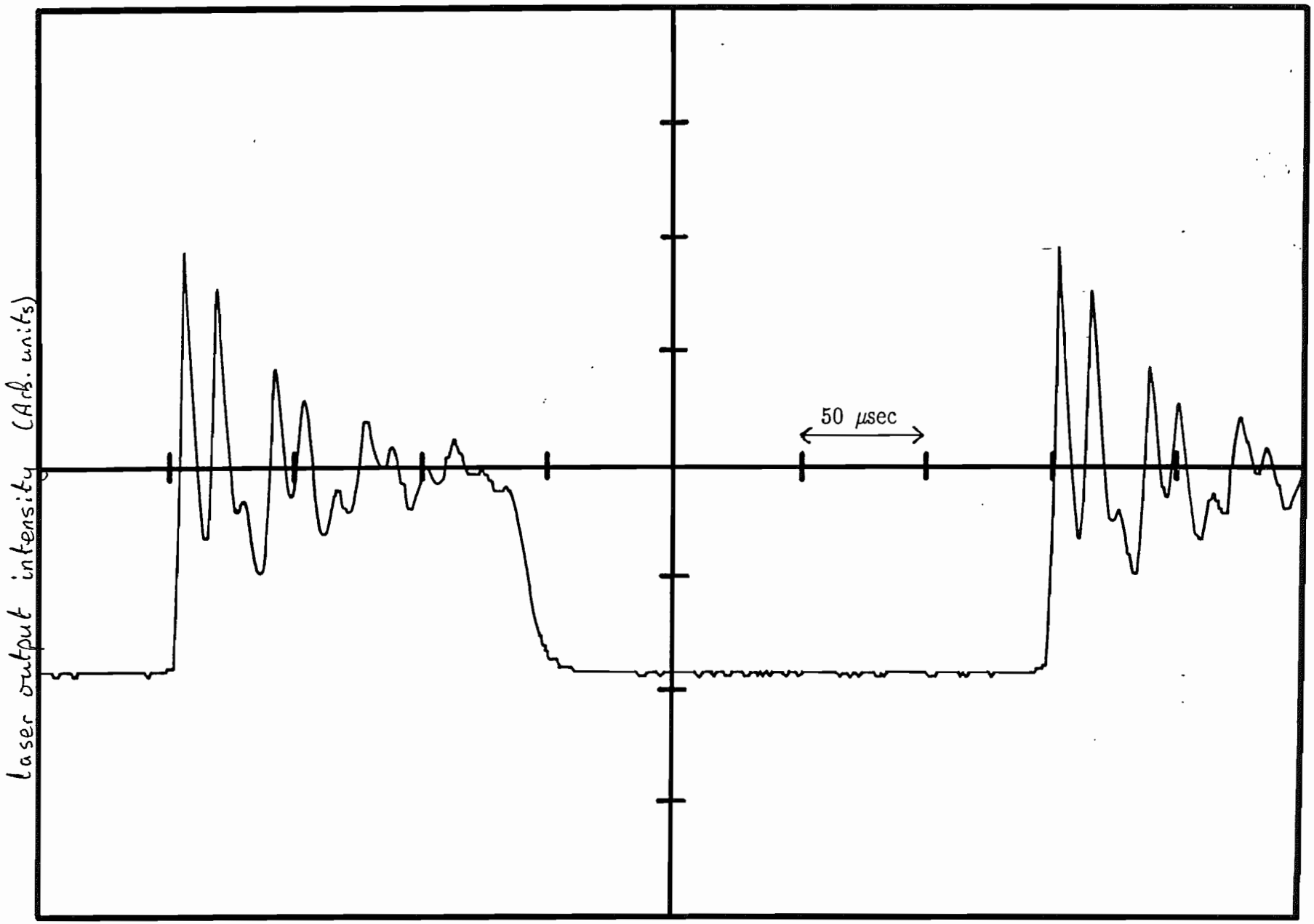

Figure 4.14

Temporal behaviour of fibre laser output for an unmodulated pump.

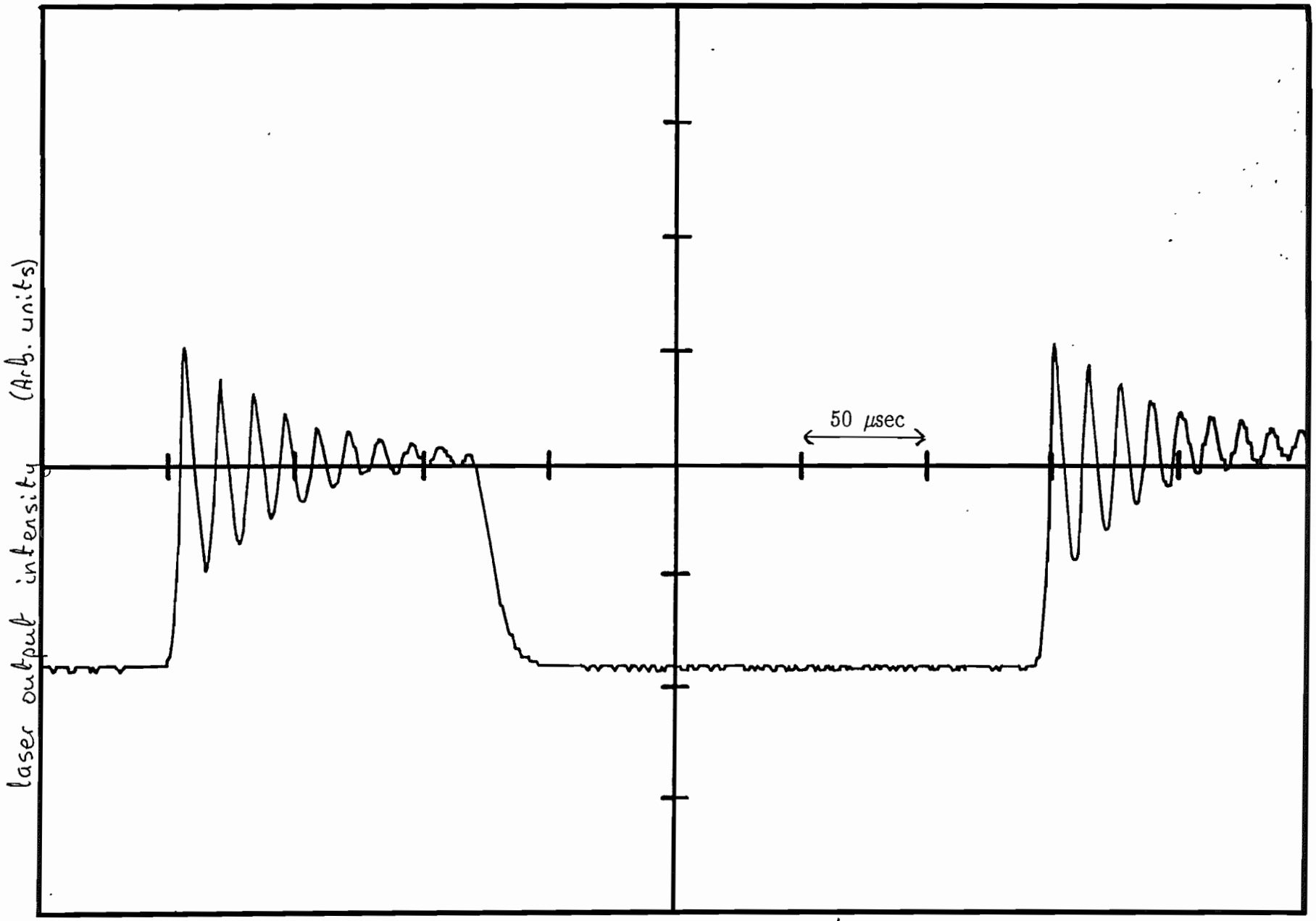

Figure 4.15

Temporal behaviour of fibre laser output for an unmodulated pump.

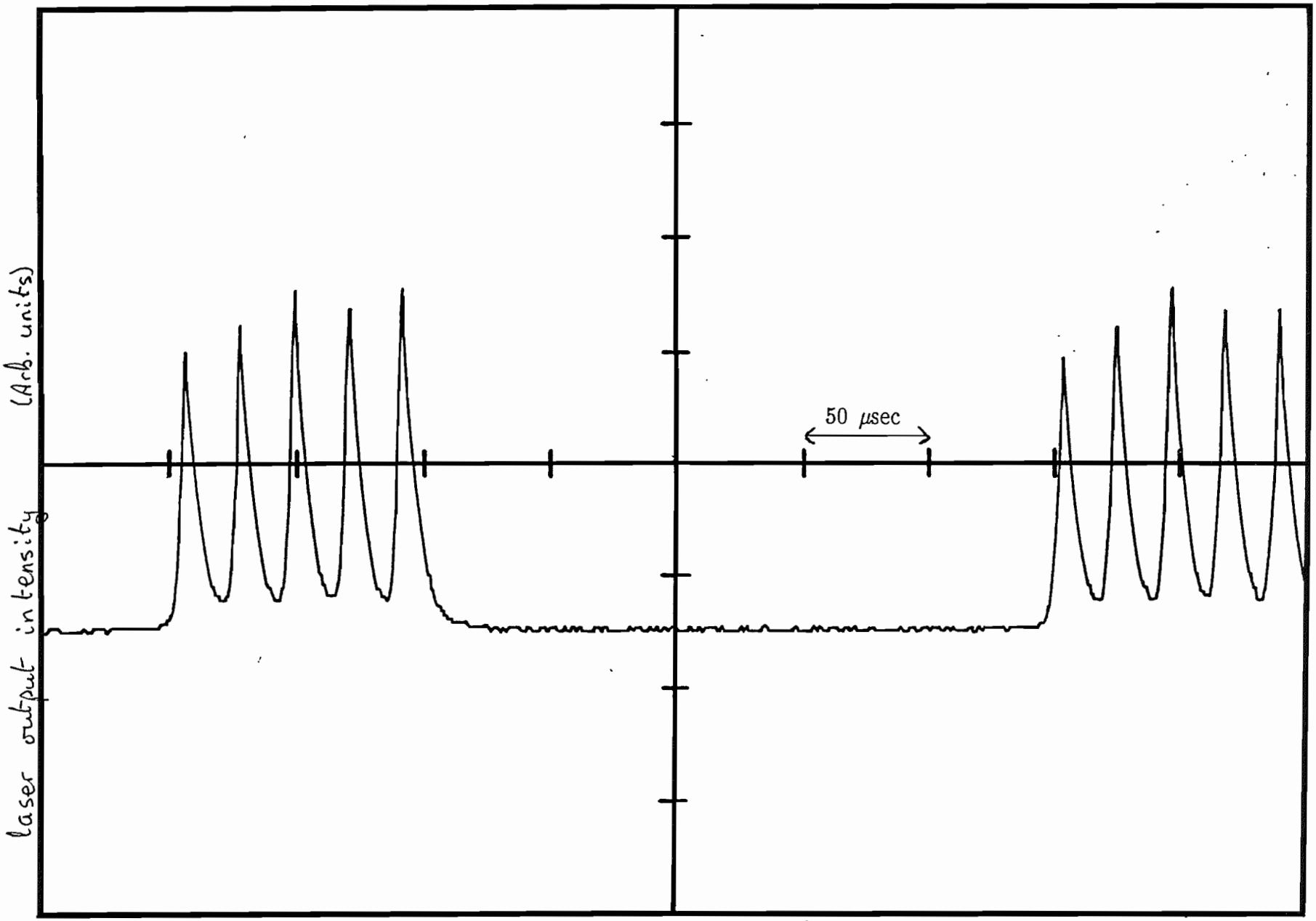

Figure 4.16

Undamped relaxation oscillations with an unmodulated pump.

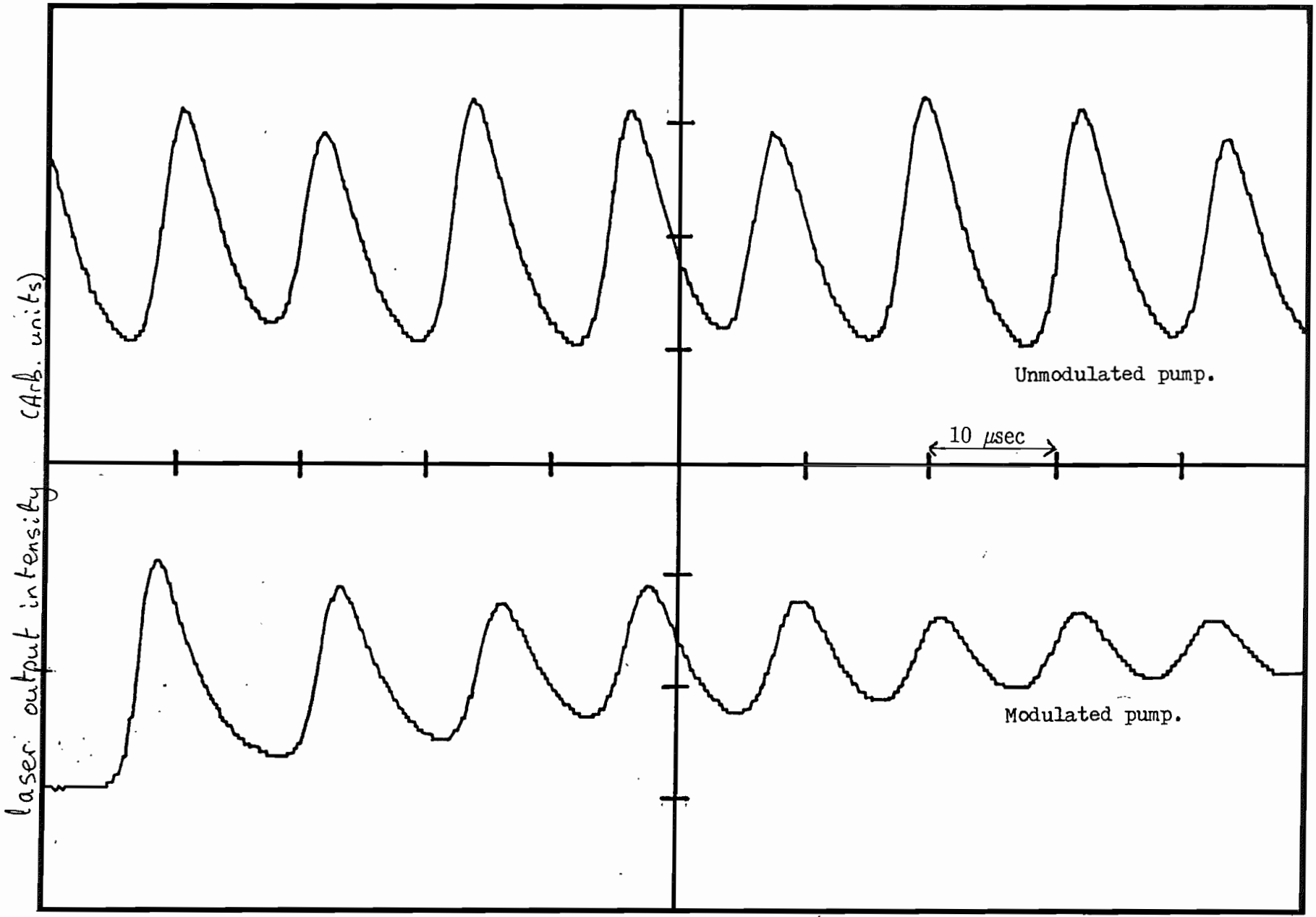

Figure 4.17

Comparison of oscillations with and without a modulated pump.

CHAPTER 5

Conclusions and Suggestions for further work

The lifetime and line narrowed experiments carried out in chapter 2 suggest that the dominant broadening process at 298K in the doped fibre is homogeneous in nature. This infers that fibre lasers should not have their efficiency impaired when operating under narrow bandwidth conditions, as is borne out by the results of studies described in chapter 3. These results are very encouraging since operation on a single longitudinal mode should also be as efficient. However, this has yet to be verified experimentally.

The line narrowed peak observed at 77K has a F.W.H.M. which is broader than that associated with the lifetime of the levels and indicates the existence of rapid dephasing. It is, therefore, important that the homogeneous linewidth measurements are extended to other temperatures since the dynamical behaviour of the glass matrix can be deduced. In view of the difficulties experienced with Optical Hole Burning, perhaps one ought to consider temporal techniques such as Photon Echoes [28, 35].

Other neodymium doped glasses tend to have their spectral features occurring at shorter wavelengths than doped fused silica [10, 38, 39]. Therefore, by altering the glass composition one may be able to move the spectral bands around and extend the range covered by neodymium doped glass lasers or tune them to suit particular applications. An example of this would be to "pull" the $^4F_{3/2}$ - $^4I_{11/2}$ transition to 1.064 μm and allow amplification of a Nd^{3+}: YAG laser. Another example would be to reduce the energy splitting between the ground state components so that any thermally induced population variation would be greater for a given temperature change. This

would have the benefit of improving the sensitivity of the temperature sensor reported by [8]. Alternatively one could do the opposite and then make lasers with more "4 level" type behaviour. Changing the glass composition may also prevent ESA, which has definitely been observed at 1.34 μm and possibly at 590 nm.

Other dopants such as Er^{3+}, Pr^{3+}, Eu^{3+} should be tried as these could greatly extend the spectral regions covered, possibly even into the visible region. Co–doping offers exciting possibilities since emission bands from different dopant ions may overlap and allow tuning over vast ranges. Also energy transfer from one dopant ion to another could allow lasers to be pumped in regions where there would normally be no absorption or allow up–conversion so that visible lasers could be pumped by infra–red sources.

Although the performance of the lasers described may not be exceptional it should be appreciated that they have allowed potential pitfalls and areas for improvement to be highlighted and direct comparison to be made between different modes of operation. Considerable improvements in the efficiency and threshold powers have subsequently been demonstrated by using different pump sources eg. semi–conductor diode lasers (with the exception of three level systems) and having the output coupler directly on the fibre [2, 43, 44]. However, some flexibility is sacrificed until tuning elements, modulators etc can be readily fabricated from fibre components.

The wide tuning ranges and ability to operate with a narrow linewidth without impaired efficiency are encouraging as applications such as spectroscopic and ranging sources are made possible. Two examples immediately apparent for the neodymium doped silica fibre are compatibility with a Nd^{3+}: YAG line at 946 nm and a spectroscopic requirement for

radiation around 1.08 μm. The former could result in amplification of miniature single longitudinal mode Nd^{3+}: YAG lasers or enable the spectral noise characteristics of fibre amplifiers to be assessed. The latter could be used for nuclear polarisation experiments carried out on ^3He by a group from Laboratoire de Spectroscopie Hertzienne de L'ENS, in France. Both wavelengths could be used for aerial inshore depth gauging where pulsed fundamental and second harmonic beams are projected co–axially. The fundamental (infra–red) will reflect off the sea–surface and back to a detector while the second harmonic (blue or green) will be transmitted through the water and reflected off the sea bed. By measuring the time delay between receiving the fundamental and second harmonic pulses one can deduce the sea depth. Since the sources would be tunable then it would be possible to tune to the edge of any atmospheric or water absorption bands.

Q–switching of the fibre laser, both with acousto–optic modulators and mechanical choppers, produced good results and achieved reasonably short pulses. Shorter pulses could easily be generated by using shorter lengths of more highly doped fibre, and hence shorter cavities. The enhanced performance of these shorter, more compact systems would only be realised if the luminescence efficiency is unaltered by higher dopant concentrations and this is obviously an area that should be investigated further.

Shorter lengths of fibre would also be a great advantage for synchronously pumping a mode–locked fibre laser since the effects of material dispersion would be virtually eliminated. Alternatively one could try to propagate the pump in a higher order mode and rely on modal dispersion to correct for material dispersion. However, it is quite probable that even if the temporal overlap of the pump and laser was good, the spatial overlap would not be as good and the efficiency would suffer.

Active mode–locking of the fibre laser was the most problematical and is likely to remain so until modulators can be directly spliced onto the doped fibre. Even when the spurious etalons have been eliminated it is likely that some bandwidth control will be required, otherwise unstable behaviour could result if the stringent requirements on the match between the intermode spacing and modulation frequency are not met (c.f. active mode–locking of dye lasers). The degree of matching required can be estimated from expression (4.15), eg. to produce pulses 4×10^{-12} s wide with $f_m = 20.7$ MHz and $\theta_m = 0.24$ one requires approximately 8×10^{7} round trips which will take 4 seconds. This implies that the circulating pulse and modulation frequency must remain in step for this period of time, which requires that the modulation frequency and laser are stable to and can be set to within $1{:}10^{8}$. To achieve this would be extremely difficult and so some bandwidth control to generate more modest pulse widths should be considered. Passive mode–locking or synchronous pumping are likely to be the best approach for generating very short pulses.

At no time during the experiments performed were any non–linear effects observed. However, as peak powers get higher and pulses become shorter these effects will manifest themselves. This raises the intriguing possibility of generating short mode–locked pulses at 1.5 μm with an Er^{3+} doped fibre and getting pulse compensation with the same piece of fibre. Also a Nd^{3+} doped fibre laser operating at 1.08 μm would have its first Stokes shift inside the Nd^{3+} gain curve and some interesting dynamics may occur as the Stokes depletes the gain, reducing the laser intensity, thereby reducing the Stokes and hence allowing gain to build up once more.

The main conclusion from this study is that fibre lasers can realise many of their potential benefits and they ought to be considered as useful sources. Their flexibility and ability to perform similar modes of operation of existing systems has been demonstrated. Once fibre modulators, tuning elements etc can be easily fabricated then the fibre laser should prove a very useful tool.

Appendix A

Four level laser rate equations for longitudinal pumping

The assumptions made are that level 3 is rapidly depopulated and so is level 1 (see figure A.1), ie the population of levels 1 and 3 is assumed to be zero. Therefore, to conserve the total population one can write

$$\frac{dN_2(z)}{dt} = \eta W_{03}(z)N_0(z) - \frac{N_2(z)}{\tau} - B_{21}N_2(z)\rho(\nu,z) \qquad (A1)$$

$N_0(z)$ = population density at a point z in the medium

η = fraction of excited ions which end up in level 2

τ = flourescent lifetime of level 2

B_{21} = stimulated emission rate

$W_{03}(z)$ = pump rate at point z

$\rho(\nu,z)$ = radiation energy density of frequency ν at a point z

The pump rate can be expressed as

$$W_{03}(z) = \frac{I_p(z)\sigma_p}{h\nu_p} \qquad (A2)$$

$I_p(z)$ = pump intensity at point z

σ_p = absorbtion coefficient

ν_p = pump frequency

If the stimulated emission terms are neglected whilst below threshold then for a steady state $\frac{dN_2(z)}{dt} = 0$, (A.1) reduces to

Figure A.1

Energy levels for the laser.

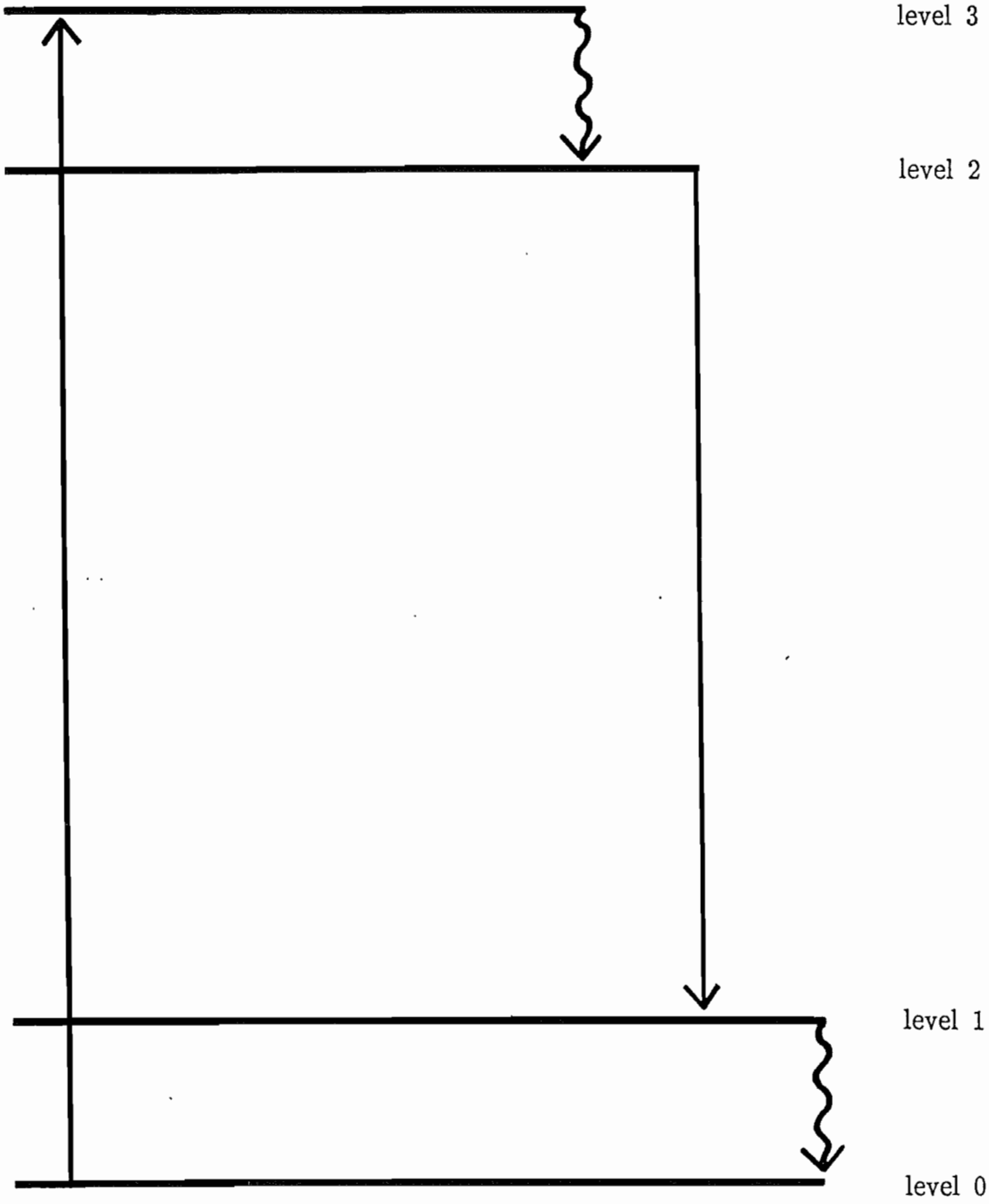

$$N_2(z) = \frac{\eta I_p(z)}{h\nu_p}\,\sigma_p \tau N_0(z) \qquad \text{(A3)}$$

Now the total density of ions is fixed at N_t so

$$N_0(z) = N_t - N_2(z) \qquad \text{(A4)}$$

from which one can write, with (A.3),

$$N_0(z) = \frac{N_t}{1+\eta I_p(z)\left[\frac{\sigma_p \tau}{h\nu_p}\right]} \qquad \text{(A5)}$$

The inversion density is given by

$$n(z) = N_2(z) - \frac{g_2}{g_1}N_1(z) = N_2(z)$$
$$= \frac{N_t}{\left[1+\frac{\eta I_p(z)}{I_{sp}}\right]}\left[\frac{\eta I_p(z)}{I_{sp}}\right] \qquad \text{(A6)}$$

The pump intensity will vary as

$$\frac{dI_p(z)}{dz} = -N_0(z)\sigma_p I_p(z)$$

$$= \frac{-N_t \sigma_p I_p(z)}{1+\eta\frac{I_p(z)}{I_{sp}}} \qquad \text{(A7)}$$

where $\frac{h\nu_p}{\sigma_p \tau} = I_{sp}$

The solution to (A7) is

$$\ln \frac{I_p(o)}{I_p(l)} + \eta \frac{\left[I_p(o)-I_p(l)\right]}{I_s} = N_t \sigma_p l \qquad \text{(A8)}$$

By integrating (A6) over the length of the fibre one can calculate the total inversion/unit area. The integration is made easier by changing the variable and integrating with respect to $dI_p(z)$ using (A7). This gives

$$n_{total} = \frac{\eta}{\sigma_p I_{sp}} \left[I_p(o)-I_p(l)\right] \qquad \text{(A9)}$$

and a total gain of

$$\text{gain} = n_{total}\ \sigma_e$$

$$= \frac{\eta \sigma_e}{h\nu_p} \tau \left[I_p(o)-I_p(l)\right] \qquad \text{(A10)}$$

Since the gain equals the loss, γ, at threshold then the criterion to reach threshold is

$$I_p(o)-I_p(l) = \frac{h\nu_p \gamma}{\sigma_e \tau \eta} \qquad \text{(A11)}$$

As soon as threshold is reached stimulated emission builds up and so this term must now be included. (A5) now becomes

$$N_0(z) = \frac{N_t\left[1+B_{21}\tau\rho(\nu,z)\right]}{1+B_{21}\tau\rho(\nu,z)+\eta\frac{I_p(z)}{I_{sp}}} \tag{A12}$$

and (A6) becomes

$$n(z) = \frac{\eta I_p(z)\frac{N_t}{I_{sp}}}{1+B_{21}\tau\rho(\nu,z)+\eta\frac{I_p(z)}{I_{sp}}} \tag{A13}$$

If one writes

$$B_{21}\rho(\nu,z) = \frac{I(z)\sigma_e}{h\nu} = \frac{I(z)}{I_s\tau}$$

then we have

$$n(z) = \frac{\eta I_p(z)\frac{N_t}{I_{sp}}}{1+\frac{I(z)}{I_s}+\eta\frac{I_p}{I_{sp}}(z)} \tag{A14}$$

$$N_0(z) = \frac{N_t\left[1+\frac{I(z)}{I_s}\right]}{1+\frac{I(z)}{I_s}+\eta\frac{I_p(z)}{I_{sp}}} \tag{A15}$$

The pump and laser intensities are now described by the coupled rate equations

$$\frac{dI(z)}{dz} = n(z)\sigma_e I(z) \tag{A16}$$

$$\frac{dI_p(z)}{dz} = - N_0(z)\sigma_p I_p(z) \qquad \text{(A17)}$$

A laser oscillator can be thought as consisting of two mirrors and two counter–propagating beams [41] (see figure A.2). For this case one can write

$$\frac{dI_1(z)}{dz} = n(z)\sigma_e I_1(z) \qquad \text{(A18)}$$

and

$$\frac{dI_2(z)}{dz} = n(z)\sigma_e I_2(z) \qquad \text{(A19)}$$

Multiplying (A18) by $I_2(z)$, (A19) by $I_1(z)$, and adding the two expressions together shows that the geometric mean intensity in the cavity is constant

$$\left[I_1(z)I_2(z)\right]^{\frac{1}{2}} = I = \text{constant} \qquad \text{(A20)}$$

It is also apparent that the output intensity is given by

$$I_{out} = I_2(l)-I_1(l)$$

$$= \frac{\left[1-R_2\right]}{R_2^{\frac{1}{2}}} \qquad \text{(A21)}$$

By substituting the geometric mean intensity in expressions (A14), (A15), (A16), (A17) the total inversion per unit area and hence gain can be calculated. This is once again easier if the variable is changed from dz to $dI_p(z)$

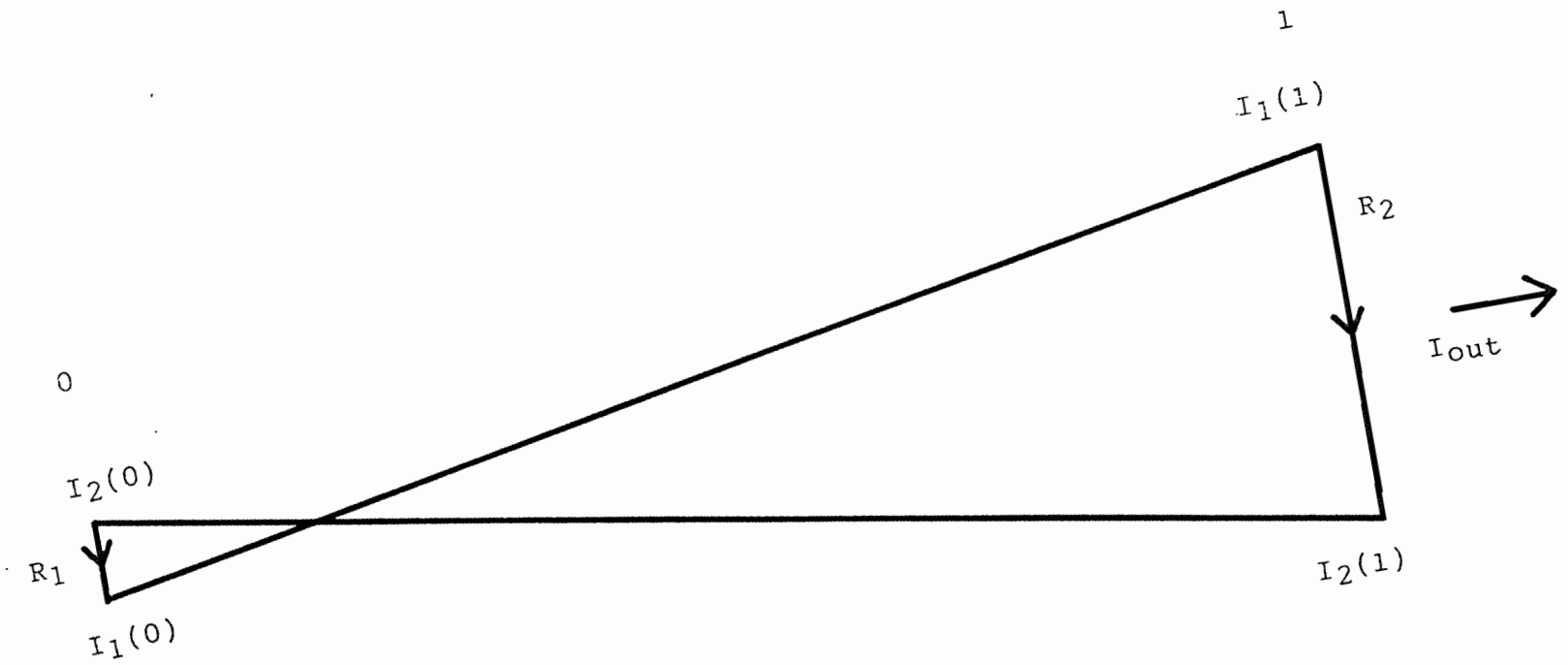

Figure A.2

Beams circulating in a laser cavity.

$$\text{gain} = n_{\text{total}}\,\sigma_e$$

$$= \frac{\sigma_e \eta}{\sigma_p\left[1+\frac{I}{I_s}\right]} \frac{\left[I_p(o)-I_p(l)\right]}{I_{sp}} \qquad \text{(A22)}$$

The gain is pinned at the threshold value ie it equals the cavity losses γ. From this and (A21) the output intensity and hence output power can be found.

$$P_{out} = \frac{I_s\left[1-R_2\right]}{R_2^{1/2}} A(x-1) \qquad \text{(A23)}$$

where $$x = \frac{I_p(o)-I_p(l)}{\frac{h\nu_p \gamma}{\sigma_e \tau \eta}}$$

$$= \frac{I_p(o)-I_p(l)}{I_p(o)-I_p(l)\Big|_{\text{threshold}}} \qquad \text{(A24)}$$

For a laser amplifier the reflected signal $I_2(z)$ is quite small and so (A16), (A17) describe the behaviour. In this case numerical solutions are required to find the gain and output intensity.

Rate equations for longitudinal pumping systems in which the terminal laser level is populated

The analysis is similar to that for four level systems except that the population of level 1 is no longer zero, so

$$\frac{dN_2(z)}{dz} = \eta W_{03}(z)N_0(z) - \frac{N_2(z)}{\tau} - B_{21}\rho(\nu,z)\left[N_2(z) - \frac{g_2}{g_1}N_1(z)\right] \qquad (A25)$$

Now one has

$$N_1(z) = e^{-\frac{\Delta E}{kT}} N_0(z) \qquad (A26)$$

and $$n(z) = N_2(z) - \frac{g_2}{g_1}N_1(z)$$

$$= \frac{N_t}{\left[1 + \eta\frac{I_p(z)}{I_{sp}}\right]}\left[\eta\frac{I_p(Z)}{I_{sp}} - \frac{g_2}{g_1}\cdot e^{-\frac{\Delta E}{kT}}\right] \qquad (A27)$$

assuming that level 1 is thermally populated and the system is below threshold.

Following similar steps as before, the criterion to reach threshold can be written as

$$I_p(o) - I_p(l) = \frac{I_{sp}}{\eta}\left\{\frac{g_2}{g_1}e^{-\frac{\Delta E}{kT}} \ln\left[\frac{I_p(o)}{I_p(l)}\right] + \frac{\sigma_p}{\sigma_e}\gamma\right\} \qquad (A28)$$

It is obvious from (A27) that the maximum total inversion occurs when

$$I_p(1) = \frac{I_{sp}}{\eta} \frac{g_2}{g_1} e^{-\frac{\Delta E}{kT}} \qquad \text{(A29)}$$

because a smaller value of $I_p(1)$ will result in the inversion becoming negative, ie absorption will take place.

When the system is above threshold similar arguments as before allow the output power to be found

$$P_{out} = \frac{\left[1-R_2\right]}{R_2^{1/2}} I_s A\,(x-1) \qquad \text{(A30)}$$

$$\text{where } x = \frac{\frac{\eta}{I_{sp}}\left[I_p(o) - I_p(1)\right] - \frac{g_2}{g_1} e^{-\frac{\Delta E}{kT}} \ln\left[\frac{I_p(o)}{I_p(1)}\right]}{\frac{\sigma_p \gamma}{\sigma_e}}$$

$$= \frac{\frac{\eta}{I_{sp}}\left[I_p(o) - I_p(1)\right] - \frac{g_2}{g_1} e^{-\frac{\Delta E}{kT}} \ln\left[\frac{I_p(o)}{I_p(1)}\right]}{\left.\frac{\eta}{I_{sp}}\left[I_p(o) - I_p(1)\right] - \frac{g_2}{g_1} e^{-\frac{\Delta E}{kT}} \ln\left[\frac{I_p(o)}{I_p(1)}\right]\right|_{threshold}} \qquad \text{(A31)}$$

An amplifier the behaviour is described by

$$\frac{dI(z)}{dz} = n(z)\sigma_e I(z)$$

$$= \frac{N_t\sigma_e \left[\eta\frac{I_p(z)}{I_{sp}} - \frac{g_2}{g_1}e^{-\frac{\Delta E}{kT}}\right]}{1 + \eta\frac{I_p(z)}{I_{sp}} + \frac{I(z)}{I_s}\left[1 + \frac{g_2}{g_1}e^{-\frac{\Delta E}{kT}}\right]} \qquad \text{(A32)}$$

and $$\frac{dI_p(z)}{dz} = -N_0(z)\sigma_p I_p(z)$$

$$= \frac{-N_t\sigma_p \left[\frac{I(z)}{I_s} + 1\right] I_p(z)}{1 + \eta\frac{I_p(z)}{I_{sp}} + \frac{I(z)}{I_s}\left[1 + \frac{g_2}{g_1}e^{-\frac{\Delta E}{kT}}\right]} \qquad \text{(A33)}$$

data source. Each equaliser had 15 forward taps and 3 feedback taps.

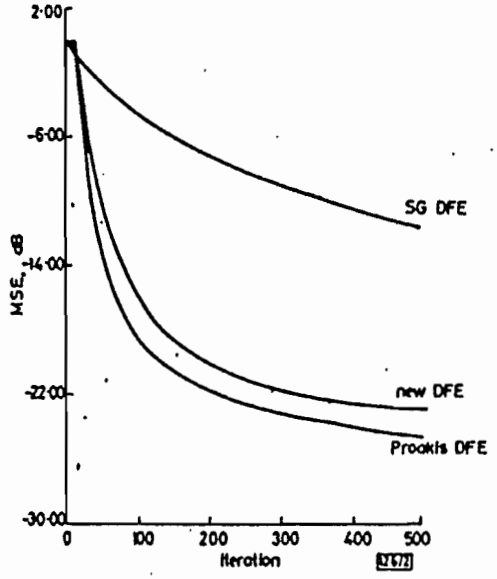

Fig. 2 *Speed of convergence on a time-invariant channel*

Speed of convergence: The new algorithm converges slightly less quickly than those in Reference 1. The improvement over the SG algorithm is substantial (Fig. 2). The sensitivity of the new algorithm to synchronisation errors was found to be lowest.

Steady-state behaviour: Its error-rate/SNR characteristics measured on a fading channel are comparable to the exact LS algorithm and superior to the SG algorithm (Fig. 3).

Conclusions: In spite of a slight degradation in performance, the new algorithm is very worthwhile, owing to the substantial reduction in algorithm complexity.

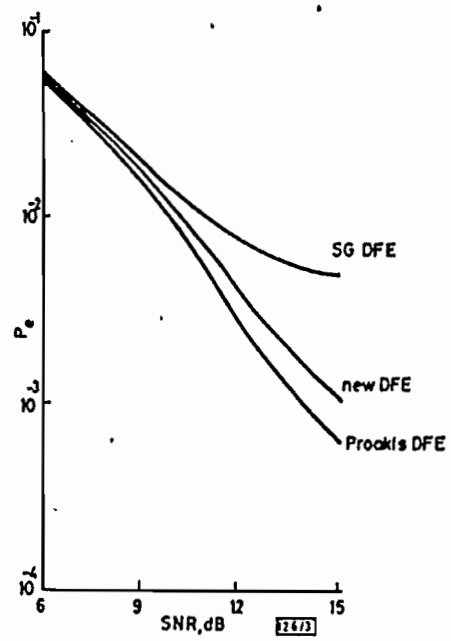

Fig. 3 *Probability of bit error on a Rayleigh fading channel*

Acknowledgment: This work is sponsored by Digital Equipment International B.V. (Clonmel).

A. D. FAGAN
N. M. O'HIGGINS

Department of Electronic Engineering
University College Dublin
Dublin 2, Republic of Ireland

21st November 1985

References

1 PROAKIS, J. G., and LING, F.: 'Lattice decision feedback equalisers and their application to fading dispersive channels'. Proceedings of international conference on communication, Boston, 1983, pp. C8.2.1–5

2 TAMBURELLI, G.: 'Digital receiver with distributed and integrated decision feedback and feedforward (to overcome the Nyquist barrier)', *CSELT Rapp. Tec.*, 1976, 4, pp. 199–209

Q-SWITCHED OPERATION OF A NEODYMIUM-DOPED MONOMODE FIBRE LASER

Indexing terms: Lasers and laser applications, Doping

Q-switched operation of a neodymium-doped monomode fibre laser at 1·08 μm has been demonstrated. An intracavity acousto-optic modulator was used to switch pulses of 200 ns duration and 8·8 W peak power at a repetition rate of 100 Hz.

Introduction: There has recently been considerable interest in the use of rare-earth-doped single-mode fibres in high-gain laser systems.[1,2] The devices reported so far have been continuous-wave, typically producing a few milliwatts of continuous-wave laser light. For many applications, such as frequency conversion of the output light by nonlinear optical processes, this power level is insufficient. In this letter we report the first demonstration of Q-switching of a fibre laser, and have shown that an enhancement of some[3–4] orders of magnitude in the peak power output can be readily obtained.

Design: The laser system was designed to allow the insertion of a Q-switched into the cavity while maintaining low cavity losses and efficient pumping. This resulted in the arrangement shown in Fig. 1.

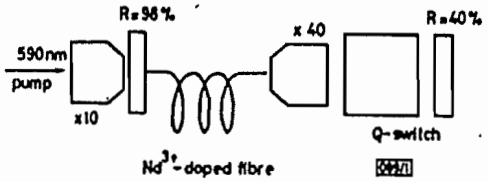

Fig. 1 *Experimental arrangement used to demonstrate Q-switched operation of an Nd^{3+}-doped fibre laser*

The active medium was an Nd^{3+}-doped single-mode optical fibre of length 2·3 m over which the continuous-wave dye laser pump light at 590 nm was totally absorbed. The high reflector ($R \simeq 98\%$) was butted against the cleaved fibre end, and launching of the pump laser into the fibre was achieved through this reflector using a ×10 microscope objective. The very low optical losses incurred with this configuration allowed an output coupler of 40% transmission to be used with an intracavity microscope objective (×40) to provide a collimated beam at the output mirror. The Q-switch, an Isomet 1205C-1 acousto-optic modulator, was inserted into the cavity between the microscope objective and output coupler, an arrangement in which the pumping rate is not affected by the Q-switch losses. The monomode fibre ensured that the output beam was a pure TEM_{00} mode.

Performance: The RF power was applied to the modulator in the form of a square wave, producing an estimated 40% modulation in the single-pass transmission. The laser output in each low-loss half-cycle consisted of a large spike followed by several smaller spikes and then continuous-wave action. During the low Q cycle of the modulator the laser was below threshold. By altering the duty cycle to shorten the high Q period relative to the low Q period, all laser output after the initial large spike in each cycle could be suppressed, with a corresponding increase in peak power. Fig. 2 shows a typical

output pulse obtained for a 100 Hz repetition rate and a high Q period of 5 μs. A peak power of approximately 8·8 W was achieved in a pulse of 200 ns duration. This pulse duration is in good agreement with the calculated value. The fibre laser

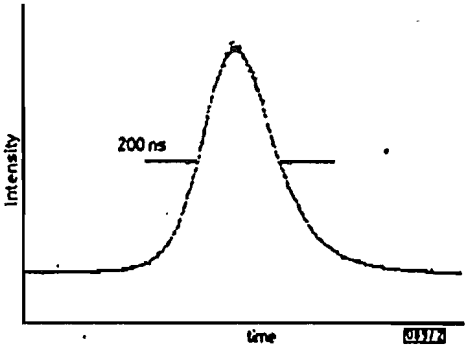

Fig. 2 *Profile of 1·08 μm pulse obtained in Q-switched operation*

operated in Q-switched mode for a day or more continuously with negligible long-term variation of the pulse shape.

We also investigated the effect of replacing the modulator in the cavity by an ordinary optical chopper wheel. Remarkably, we found that, in spite of the slow switch-on time of the chopper, which was 10 μs or a few hundred cavity round-trip times, peak powers approaching half those given by the acousto-optic modulator, whose switch-on time was a few nanoseconds, could be achieved. Fig. 3 shows a typical pulse

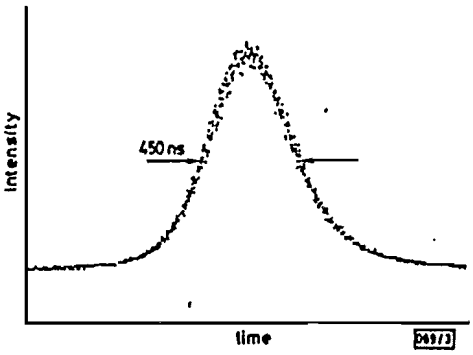

Fig. 3 *Profile of 1·08 μm pulse obtained by Q-switching with optical chopper*

of 4 W peak power and 450 ns duration obtained in this way. Multiple subsidiary pulses followed the initial pulse and could not readily be eliminated, but the experimental simplicity of this technique, which has no associated problems of alignment and cavity loss, makes it attractive.

Conclusion: We have demonstrated that Q-switching allows an Nd^{3+}-doped monomode fibre laser to produce high peak powers. If the dye laser pump source was replaced by a semiconductor diode laser as in Reference 1, then a compact high-power source could be envisaged. The same Q-switching techniques described here should also prove suitable for fibre lasers based on other dopant ions. In particular, the ability to use a simple mechanical chopper, with the advantage of low cost and ease of use, looks encouraging.

Acknowledgments: This work has been supported by a grant from the UK SERC and also in part under a JOERS programme. The authors are grateful to S. Poole and other members of the Fibre Optics Group in the Department of Electronics & Information Engineering, Southampton University, for kindly providing the doped fibre. One of us (I. P. Alcock) acknowledges the support of an SERC studentship.

I. P. ALCOCK
A. C. TROPPER
A. I. FERGUSON
D. C. HANNA

Department of Physics
University of Southampton
Southampton SO9 5NH, United Kingdom

12th November 1985

References

1 POOLE, S. B., PAYNE, D. N., and FERMANN, M. E.: 'Fabrication of low-loss optical fibres containing rare-earth ions', *Electron. Lett.*, 1985, 21, pp. 737–738

2 MEARS, R. J., REEKIE, L., POOLE, S. B., PAYNE, D. N.: 'Neodymium-doped silica single-mode fibre lasers', *ibid.*, 1985, 21, pp. 738–740

IMPROVED SYSTOLIC ARRAY FOR LINEAR DISCRIMINANT FUNCTION CLASSIFIER

Indexing term: Signal processing

A word-level systolic array with 100% efficiency is described for the linear discriminant function classifier. When compared with two previous word-level linear classifier arrays, it not only saves about C inner product step cells, where C is the number of weighted vectors used, but also simplifies the chip's I/O design.

Introduction: The linear discriminant function classifier is widely used in statistical pattern recognition, such as the Euclidean minimum distance classification[1] and voiced/unvoiced classification[2] etc. Let $X = [x^1 x^2 \dots x^n]$ be a feature vector and $W_i = [w_i^1 w_i^2 \dots w_i^n w_i^{n+1}]$ be the ith weighted vector, where $i = 1, 2, \dots, C$. Then the ith class linear discriminant function is defined as

$$g_i(X) = x^1 w_i^1 + x^2 w_i^2 + \cdots + x^n w_i^n + w_i^{n+1} \quad (1)$$

$$= X' W_i^T \quad (2)$$

$$= w_i^{n+1} + X W_i'^T \quad (3)$$

where $X' = [x^1 x^2 \dots x^n]$ and $W_i' = [w_i^1 w_i^2 \dots w_i^n]$. Following the method used by Urquhart,[3] operations of the linear discrimint function classifier can be partitioned into: (i) computing $g_i(X)$ for $i = 1, 2, \dots, C$, and (ii) finding the class label l_i for which $g_i(X)$ is maximum.

To perform the above operations fast, several linear classifier arrays whose computations are based on eqn. 2 have been described in References 3 and 4. Those with contraflow possess only 50% efficiency and those with static weighted vectors possess 100% efficiency. However, updating the weighted vectors is much easier to achieve in the former than in the latter. Besides, using eqn. 2, which is an $(n + 1)$-dimensional inner product computation, to compute the linear discriminant function is not efficient enough in terms of both hardware and computation time, owing to the fact that the last multiplication operation in eqn. 2 is unnecessary. In this letter an improved word-level systolic array with both contraflow and 100% efficiency is proposed for the linear discriminant function classifier to remove the redundancy and the tradeoff. Moreover, for ease of both constructing a large array from smaller unit chips and interfacing with memory, a byte-serial grouped I/O scheme is described for the chip.

Systolic system: In the proposed array shown in Fig. 1, which is in fact a module for constructing larger arrays, each linear discriminant function is computed from eqn. 3 instead of eqn. 2, i.e. each $g_i(X)$ is obtained by performing one n-dimensional inner product initialised by some proper value. The leftmost column of C delay elements is used to properly provide the initial values. The subarray composed of $C \times n$ inner product step cells is used for the computations. The column of C classification cells is used for performing the classification. The rightmost column of C delay elements is used to properly provide the class labels for each current discriminant function. When compared with the two word-level arrays in Reference 3, the proposed one requires an additional

Conclusion: These experiments show that a sapphire resonator can be excited by the thermal effect. The vibration of a bar in a flexural mode, described here, was generated by heating a thin layer vapour-deposited on one side of the bar. The mechanical displacement was detected by an optical method. A Q-factor of 800 000 has been measured for the bar vibrating at a resonance frequency of 20 262 Hz in an environmental pressure of about 0·2 torr. This figure shows that sapphire crystals can, as expected, compete with quartz crystals with regard to the Q-factor. Further experiments are necessary to examine the operation of different modes of vibration, the practical range of frequencies and the influence of the temperature. It should also be interesting to study other possible techniques of excitation[2] and detection.[3,4]

Acknowledgments: The authors are grateful to H. Duchaussoy of DRET, J. P. Aubry of CEPE and Y. Shui of Nanjing University for their helpful assistance in this project, and to L. Michel and P. Kou of CEPE, Thomson CSF (Argenteuil) for technical assistance. This work has been carried out with the support of DRET (Paris).

E. DIEULESAINT *13th January 1986*
D. ROYER
X. SERVAJAN

Laboratoire d'Acoustoélectricité
de l'Université Pierre et Marie Curie
10 rue Vauquelin, 75231 Paris Cedex 05, France

References

1 DIEULESAINT, E., and ROYER, D.: 'Elastic waves in solids—applications to signal processing' (Wiley, 1980), p. 428
2 DIEULESAINT, E., ROYER, D., and RAKOUTH, H.: 'Optical excitation of quartz resonators', *Electron. Lett.*, 1982, **18**, pp. 381–382
3 DE LA RUE, R. M., HUMPHRYES, R. F., MASON, I. M., and ASH, E. A.: 'Acoustic surface wave amplitude and phase measurements using laser probes', *Proc. IEE*, 1972, **119**, pp. 117–126
4 ROYER, D., DIEULESAINT, E., and MARTIN, Y.: 'Improved version of a polarised beam heterodyne interferometer'. IEEE ultrasonics symposium proceedings, 1985 (in press)

MODE-LOCKING OF A NEODYMIUM-DOPED MONOMODE FIBRE LASER

Indexing terms: Lasers and laser applications, Doping

A neodymium-doped monomode fibre laser operating at 1·08 μm has been actively mode-locked using intracavity acousto-optic loss modulation. The mode-locked laser output consisted of a train of pulses of less than 1 ns FWHM with an energy of ~17 pJ at a repetition rate of 41·45 MHz. When the laser was simultaneously Q-switched the peak power of the mode-locked pulses inside the 690 ns-wide envelope was enhanced by more than three orders of magnitude.

Introduction: Rare-earth-doped monomode fibre lasers have previously been demonstrated to operate continuously.[1] It has also been demonstrated that these lasers can be Q-switched by acousto-optic switching or mechanical chopping and produce peak powers of several watts.[2] In this letter we report the first demonstration of mode-locking in a fibre laser.

Experiment: The laser cavity (Fig. 1) is similar to that described by Alcock *et al.*[3] The active medium was a 2 m length of Nd^{3+}-doped low-loss fibre (which was monomode at about 1 μm).[3] The pump laser was a continuous-wave rhodamine 6 G dye laser operating at 590 nm which was launched through a butted high reflector ($R \simeq 98{\cdot}5\%$ at 1·08 μm). An acousto-optic rhomb mode-locker (Crystal Technology) with Brewster-angled surfaces was inserted between the intracavity x 10 microscope objective and output coupler ($R \simeq 70\%$). Since the fibre was not polarisation-

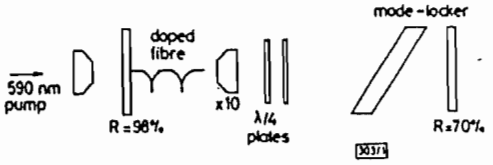

Fig. 1 *Cavity arrangement*

preserving, two $\lambda/4$ plates were used to convert the elliptically polarised output from the fibre into vertically polarised radiation and so reduce the reflection loss off the Brewster surfaces.

When radio-frequency power was applied to the transducer on the mode-locker, an acoustic standing wave was set up in the rhomb. This produced a time-varying refractive index grating and caused Bragg diffraction of the incident 1·08 μm laser beam, thereby effecting cavity loss modulation. Since the resonances of the high-Q transducer were highly temperature-dependent, it was found necessary to mount the mode-locker in a temperature-stabilised enclosure.

The output coupler was mounted on a translation stage so that the frequency difference between longitudinal cavity mode beats could be matched to the loss modulation frequency. Simultaneous Q-switching and mode-locking was achieved by also inserting a mechanical chopper wheel between the modulator and intracavity microscope objective.

The laser output was detected by a Ge photodiode and the amplified photocurrent fed into a Tektronix 7L14 RF spectrum analyser. With no RF power applied to the mode-locker the laser output cintained weak longitudinal cavity mode beats. When RF at 20·723 MHz was applied to the mode-locker and the cavity length was adjusted to match the loss modulation frequency, the beats became stronger and narrower. Eventually higher harmonics appeared and dramatically increased in intensity as the RF power was increased. The RF spectrum (Fig. 2) shows the comb of modes obtained with

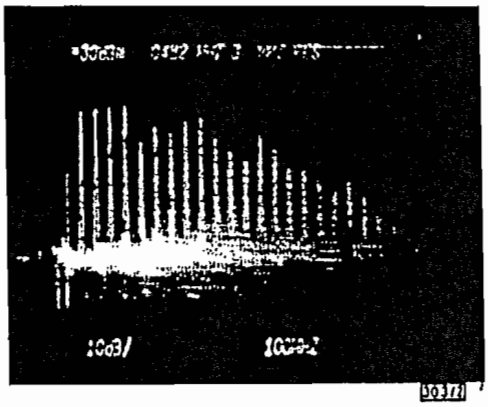

Fig. 2 *Comb of modes*

250 mW of RF power applied to the mode-locker. The high-frequency roll-off is due to the bandwidth of the amplifier and detector.

The laser output was then studied in the time domain using a fast detector (RCA CA309709E, FWHM resolution of ~60 ps) and oscilloscope (Tektronix 7A19 amplifier in a 7904 mainframe). The laser output consisted of a train of short pulses with a repetition rate corresponding to the cavity round-trip time. The pulse shown in Fig. 3 has an FWHM of less than 1 ns, limited by the 400 MHz bandwidth of the oscilloscope, and an energy of ~17 pJ. The structure around the pulse is believed to be due to etalon effects in the cavity.

With the laser mechanically Q-switched the output consisted of a train of pulses whose FWHM was less than 3 ns, inside a 690 ns envelope (Fig. 4). The energy of the largest pulse in the envelope was ~20 nJ. Structure was seen on the mode-locked pulses and is again believed to be due to etalon

effects in the cavity. In addition, the build-up time for the Q-switching was not long enough for a steady state to be reached, and so the pulses would be longer than the CW case.

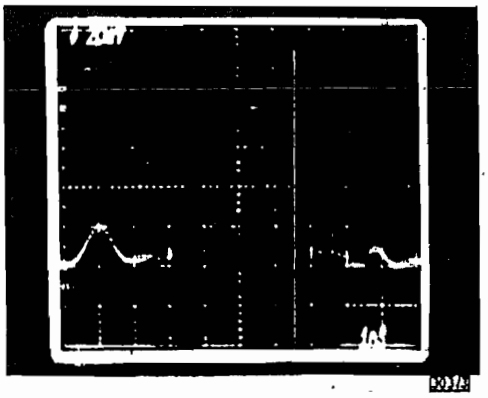

Fig. 3 *Mode-locked pulse*

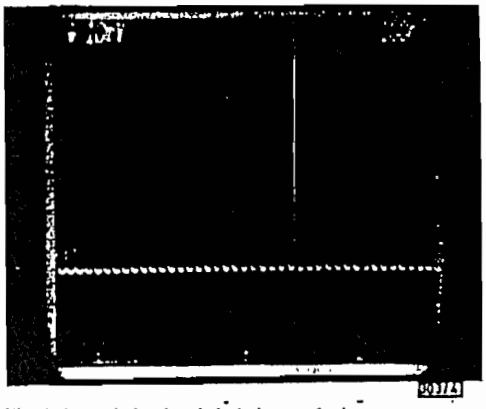

Fig. 4 *Q-switched and mode-locked train of pulses*

Discussion: Although the laser gain bandwidth of the broad rare-earth transition in glass fibres offers the potential of the generation of very short mode-locked pulses, there are a number of possible limitations which need to be eliminated before the shortest pulse duration can be achieved.

We have observed that the lasing bandwidth is influenced by etalon effects in the cavity, and have therefore attempted to eliminate these effects where possible, for example by using a long focal length intracavity microscope objective and Brewster-angled surfaces on the mode-locker. However, some etalon effects still remain. Since the output endface of the fibre was neither wedged nor antireflection-coated, immersion in index-matching liquid may provide a solution to this problem.

Since the length of the active medium is significantly greater than in conventional laser systems, and the small mode size (a few micrometres) leads to high intensities, the frequency chirp produced by second-order dispersion and self-phase modulation could have an important influence on pulse duration when these systems are mode-locked. The higher peak power available when the system is Q-switched greatly increases the degree of self-phase modulation and is approaching the level at which other nonlinear effects such as stimulated Raman scattering can be expected to occur.

However, the presence of self-phase modulation also provides scope for obtaining pulse compression in fibre lasers operating in the negative group-velocity dispersion region, such as 1·5 μm operation in Er^{3+}-doped fibres,* with soliton propagation in the laser medium itself as an interesting possibility.

In conclusion, we have demonstrated mode-locking and simultaneous mode-locking and Q-switching of a fibre laser. Further analysis of the etalon effects and nonlinear effects is in progress, aimed at achieving shorter pulse durations. A prelase scheme is also being examined which would allow the pulse duration to approach the steady-state value under conditions of simultaneous Q-switching and mode-locking.

* REEKIE, L., MEARS, R. J., POOLE, S. B., and PAYNE, D. N.: 'Tuneable single-mode fibre lasers' (to be published in *IEEE J. Lightwave Technol.*)

Acknowledgments: This work has been supported by a grant from the UK SERC and also in part under a JOERS programme. The authors are grateful to S. Poole and other members of the Fibre Optics Group in the Department of Electronics & Information Engineering, Southampton University, for kindly providing the doped fibre. The authors would also like to thank D. A. Humphreys of the National Physical Laboratory for the loan of a fast detector and mount. One of us (I. P. Alcock) acknowledges the support of an SERC studentship.

I. P. ALCOCK
A. I. FERGUSON
D. C. HANNA
A. C. TROPPER

Physics Department
University of Southampton
Southampton SO9 5NH, United Kingdom

15th January 1986

References

1 MEARS, R. J., REEKIE, L., POOLE, S. B., and PAYNE, D. N.: 'Neodymium-doped silica single-mode fibre lasers', *Electron. Lett.*, 1985, 21, pp. 738–740

2 ALCOCK, I. P., TROPPER, A. C., FERGUSON, A. I., and HANNA, D. C.: 'Q-switched operation of a neodymium-doped monomode fibre laser', *ibid.*, 1986, 22, pp. 84–85

3 POOLE, S. B., PAYNE, D. N., and FERMANN, M. E.: 'Fabrication of low-loss optical fibres containing rare-earth ions', *ibid.*, 1985, 21, pp. 737–738

ERROR-CORRECTING CODING FOR BANKING DOCUMENT BAR CODES

Indexing terms: Codes, Reed–Solomon codes, Bar codes, Error-correction codes

Bar codes, used for the automatic processing of financial payment records, may be protected by extended Reed–Solomon codes over prime field alphabets. New decoding methods which handle both random and erasure errors are presented.

Introduction: Bar codes are currently being used as a means of enhancing the processing of financial documents such as bank cheques. In one implementation, cheques are routed automatically through the banking system's return paths by means of bar codes printed on the back of each item. As each document passes through a high-speed sorter, a bar code reader senses the records printed by previous processing institutions and optionally applies additional records for further processing by other institutions.

Several formats have been proposed[1] for the bar code symbols and for the record structures, and the most popular and technically promising ones are likely to be based on decimal or hexadecimal alphabets, i.e. 10 or 16 information symbols. However, most formats are designed to accommodate relatively short records which can be printed at various decision points in the documents' processing paths. An additional synchronisation symbol is usually included in the alphabet, giving either 11 or 17 symbols. However, these values correspond with prime finite fields for which powerful extended Reed–Solomon codes exist. The emphasis in the following discussions is on the decimal format because the hexadecimal scheme is a straightforward extension of these techniques.

Extended Reed–Solomon code over prime finite field, GF(p): A standard Reed–Solomon code can be extended by adding two more check digits, increasing the minimum distance by two.[2,3]

Volume 58, number 6 OPTICS COMMUNICATIONS 15 July 1986

CONTINUOUS-WAVE OSCILLATION OF A MONOMODE NEODYMIUM-DOPED FIBRE LASER AT 0.9 μm ON THE $^4F_{3/2} \rightarrow {}^4I_{9/2}$ TRANSITION

I.P. ALCOCK, A.I. FERGUSON, D.C. HANNA and A.C. TROPPER

Department of Physics, University of Southampton, Highfield, Southampton SO9 5NH, UK

Received 19 February 1986

A monomode silica fibre doped with Nd has allowed the first demonstration of cw laser action on the $^4F_{3/2} \rightarrow {}^4I_{9/2}$ transition of Nd in a glass host, with tuning over the range 900–945 nm.

Recent experiments have demonstrated the possibility of incorporating high concentrations of impurity ions onto a monomode fibre structure [1,2] and the achievement of laser action in such fibres [3–5]. Initial experiments have studied the $^4F_{3/2}-{}^4I_{11/2}$ transition in Nd doped fibre, operating at 1.08 μm, with demonstrated performance on this transition so far including pumping with a CW dye laser [3,5], an Ar ion laser [4], a GaAs diode laser [3] and both Q-switched [5] and actively mode-locked operation [6] of the fibre laser.

End pumping of the fibre by a laser source allows very efficient pumping and, by virtue of the small core size, very intense pumping. The small transverse dimensions of the fibre also means that the thermal effects which plague bulk glass lasers are reduced to a negligible level. Given this ability to achieve and to withstand intense pumping, and the ability to incorporate a wide variety of dopant ions [2], one now has greatly extended prospects for lasing from impurities in a glass host. For example it should be possible to achieve lasing on transitions which have not hitherto only shown pulsed operation. An example of the latter is the first demonstration of CW laser action on the 1.54 μm line in a Er^{3+} doped fibre [4]. In this letter we report a further example – the first demonstration of CW operation of the $^4F_{3/2}-{}^4I_{9/2}$ transition of Nd in glass around 0.9 μm.

A brief summary of the laser performance is given here and a more detailed description of its performance, which includes Q-switched operation, and mode-locked operation over a wide tuning range, from 0.90 μm to 0.945 μm, will be given in a later paper. First however we give some indication of the extent by which the gain in a fibre laser can exceed the typical gains achievable in bulk glass pumped by thermal light sources. We also provide some estimates of the limitations on gain imposed by fibre stress, heating and pump saturation.

When a conventional cylindrical glass laser rod is pumped by a flash lamp or arc lamp the limit on average pump power input to the rod is imposed by stress resulting from the radial thermal gradient and its associated differential expansion. A glass host is much more seriously limited by this compared to crystalline hosts, such as YAG since the thermal conductivity of glass is typically an order of magnitude smaller. In addition, the threshold pump power for a glass laser is typically more than an order of magnitude greater than for the same transition in a crystal host since the transition linewidth in glass is much greater. These two characteristics of glass lasers have made CW operation difficult to achieve. However the thermal gradient can be reduced by using a rod of smaller radius. In fact, for the same pump density in the rod, hence the same heat dissipated per unit volume, and the same population inversion density produced, the thermal gradient is proportional to the radius of the rod and the maximum stress is proportional to the square of the radius [7]. This implies that the maximum population in-

0 030-4018/86/$03.50

version density, and hence gain, that can be sustained continuously without incurring fracture, is inversely proportional to the square of the rod radius. This feature was exploited by Young [8] in the first demonstration of a CW glass laser, with the medium in the form of a short length (few cm) of multimode cladded glass fibre. The same principle, of using a small rod diameter, was used by Uchida et al. [9] who demonstrated CW oscillation in a SELFOC Nd glass rod of 1.5 mm diameter, pumped by a Kr arc lamp. An alternative approach, which achieves the same end, is to use a laser to end pump a glass rod [10]. Since the pump beam spot size can be kept small, a high inversion density can be achieved for a small heat load, and furthermore the thermally induced birefringence is small over the narrow cross section of the pump beam.

In this way Kishida et al. [10] achieved the first CW oscillation in Nd phosphate glass. The laser-pumped monomode fibre laser takes this approach to the limit where the pump beam is confined by waveguiding in a doped core of few microns diameter and the small diameter of the cladding ensures a small radial temperature gradient.

An analysis of the temperature distribution and associated stress distribution in the fibre, assuming uniform heat deposition in the core (radius R_1) yields a maximum stress σ_{max}, which occurs at the outer surface of the cladding (radius R_2), given by

$$\sigma_{max} = \frac{2^{1/2}\alpha E P_a}{8k(1-\nu)}\,[2-(R_1/R_2)^2]$$

where k is the thermal conductivity, α the thermal expansion coefficient, E is Young's Modulus, ν is Poisson's ratio and P_a is the heat deposition per unit length of fibre. Thus, as far as the fracture limit is concerned the fibre laser can operate at a gain which is $\sim\frac{1}{2}(R_2/R_1)^2$ greater than possible in a uniformly doped rod of radius R_2 subject to uniform heat deposition of the same value P_a i.e. it appears that a much higher gain can be achieved in the fibre. However, for single mode fibre, where R_1 may be only a few microns, the maximum value of P_a, and hence the gain, will be limited in practice neither by the fracture limit nor, as estimates show, by stress-induced birefringence effects. Instead, in the case of a lightly doped single mode fibre such as we have used the maximum achievable P_a will be limited by saturation of the pump transition. In the case of non-saturating fibre (e.g. heavily doped or having a large diameter core) the maximum allowable P_a will be limited by the overall temperature rise that can be tolerated. A rough estimate of the maximum permissible heat deposition in a fibre of cladding diameter ~100 μm, cooled by unforced convection in air, indicates 1 W/m (for ~100°C temperature rise) whereas the fracture limit would be much higher, ~100 W/m. Our estimate below indicates that for the Nd doped fibre we have used (core diameter ~6 μm, Nd^{3+} concentration ~300 ppm the pump absorption saturates at ~100 mW absorbed power per metre length.

An estimate of the absorbed pump power P (photon energy $h\nu$) which produces saturation when absorbed in a length L of core (radius R_1) is given by

$$N\pi R_1^2 L/2\tau = P/h\nu, \qquad (2)$$

where N is the total impurity concentration, and τ is the decay time of the upper laser level. Eq. (2) expresses the condition for the pump to maintain half the dopant population in the upper laser level, and thus also indicates the threshold pump power for three level laser operation to be achieved. For four-level laser operation the gain exponent for an upper laser level population of $N/2$ where σ_e is the emission cross-section, and using (2) thus becomes

$$N\sigma_e L/2 = P\tau\sigma_e/h\nu\pi R_1^2. \qquad (3)$$

Inserting typical figures for the 1.08 μm, $^4F_{3/2} \rightarrow {}^4I_{11/2}$ transition in Nd^{3+} for a 6 μm core diameter yields a gain per unit length, $N\sigma_e/2$ of ~6 m^{-1} for an absorbed power per unit length, P/L of 0.1 W m^{-1}. By using a length of several metres, a very high gain can be achieved under these conditions (say e^{30} for 5 m length). By contrast a typical lamp-pumped Nd glass rod (under pulsed conditions) would provide a gain exponent of 2–3. These simple estimates illustrate the much higher gain achievable in a fibre laser. They also confirm the possibility of CW 3-level operation on the $^4F_{3/2} \rightarrow {}^4I_{9/2}$ transition in Nd^{3+}. Assuming σ_e for this transition to be comparable to that for the $^4F_{3/2}-{}^4I_{11/2}$ transition (indicated by the similar branching ratios in other glasses [11]), and allowing for the fact that the upper levels of the $^4I_{9/2}$ manifold are significantly less populated than the lower levels (see [12] for example) threshold pump powers

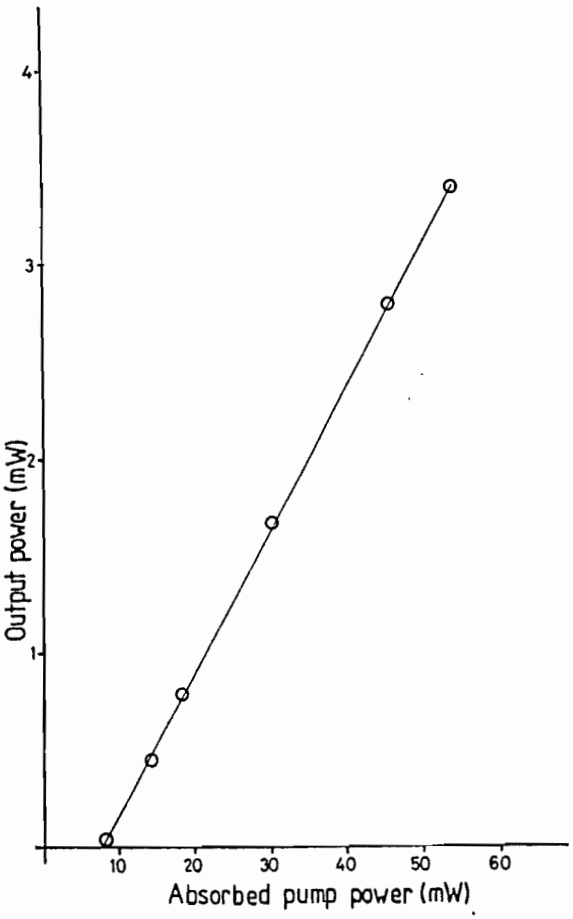

Fig. 1. Schematic of fibre laser resonator with provision for insertion of intracavity control devices such as Q-switch, mode-locker or birefringent filter.

of ~10 mW absorbed in a 1 m length are indicated.

The arrangement used to achieve oscillation on the $^4F_{3/2} \rightarrow {}^4I_{11/2}$ transition is shown in fig. 1. The cw dye laser used to pump the Nd ions was tuned to the strong absorption at ~590 nm. The pump beam was launched into the fibre core (~6 μm diameter) using a X10 microscope objective. The fibre laser mirror at this input end was butted against the fibre end face to minimise coupling losses for the fibre resonator. The output mirror was located away from the fibre output face, to allow insertion of intracavity control devices, and a microscope objective was used to collimate the beam in this section of the resonator.

The input mirror, chosen to suppress lasing on the 1.08 μm line, had a low reflectivity at 1.08 μm and

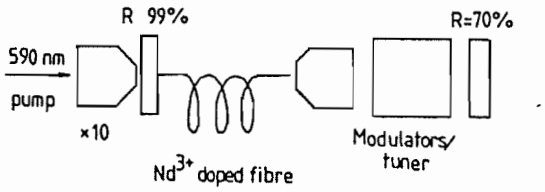

Fig. 2. Output power versus absorbed pump power for the resonator of fig. 1 without tuner or modulator.

high reflectivity (~99%) in the range 900–945 nm. The output mirror transmission was ~30%. With these mirrors and using a 1 m length of fibre with 300 ppm Nd^{3+} concentration it was found that the threshold for oscillation for the resonator without tuning element or modulator present corresponded to an absorbed pump power of 8 mW. Fig. 2 shows a plot of output power versus input power, with an output of 3.4 mW for the maximum available absorbed pump power of 53 mW. At this maximum pump level only a few milliwatts of pump emerged from the output end of the fibre, indicating that saturation was not significant.

The optimum length of fibre has not been determined experimentally. It depends on a compromise between the need to avoid excessive absorption loss at the laser frequency due to the unpumped fibre. The significance of this absorption loss was shown by the observation that while oscillation readily occurred in the 1 m fibre, it was not possible to achieve oscillation in a 2 m length At 1.08 μm such reabsorption losses are not significant. With the 1 m fibre sufficient gain could be achieved to demonstrate mode-locking and Q-switching with acousto-optic modulators and tuned operation using a two-plate birefringent filter. Q-switched operation produced pulses of 75 ns duration. Tuned operation was achieved continuously over the range 900 nm to 945 nm, covering most of the range of the fluorescence spectrum. A detailed description of the tuning, mode-locking and Q-switching results is being prepared for a further publication, but these results already suggest that this fibre laser shows promise as a convenient source of coherent radiation in the near infrared.

This work has been supported by the SERC under the JOERS scheme and I.P. Alcock holds an SERC Research Studentship. We are grateful to the Optical Fibre Group in the Department of Electronics and Information Engineering for supplying us with the fibre.

References

[1] S.B. Poole, D.N. Payne and M.E. Fermann, Electron. Lett. 21 (1985) 737.
[2] S.B. Poole, D.N. Payne, R.J. Mears and M. Fermann, to appear in Journal of Light Wave Technology.
[3] R.J. Mears, L. Reekie, S.B. Poole and D.N. Payne, Electron. Lett. 21 (1985) 738.
[4] R.J. Mears, L. Reekie, S.B. Poole and D.N. Payne, Electron. Lett. 22 (1986) 159.
[5] I.P. Alcock, A.C. Tropper, A.I. Ferguson and D.C. Hanna, to appear in Electron. Lett.
[6] I.P. Alcock, A.I. Ferguson, D.C. Hanna and A.C. Tropper, submitted to Electron. Lett.
[7] W. Koechner, Solid State Laser Engineering, Vol. 1 Springer Series in Optical Sciences (Springer-Verlag, 1976).
[8] C.G. Young, Appl. Phys. Letts. 2 (1963) 126.
[9] T. Uchida, S. Yoshikawa, K. Washio, R. Tatsumi, K. Tsushima, I. Kitano, K. Koisumi and Y. Ikeda, Jap. J.A.P. 12 (1973) 126.
[10] S. Kishida, K. Washio and S. Yoshikawa, Appl. Phys. Lett. 34 (1979) 273.
[11] M.J. Weber, D.C. Zeigler and C.A. Angell, J. Appl. Phys. 53 (1982) 4344.
[12] M.M. Maun and L.G. De Shazer, J. Appl. Phys. 41 (1970) 2951.

Tunable Solid-State Lasers II

Proceedings of the OSA Topical Meeting,
Rippling River Resort, Zigzag, Oregon,
June 4–6, 1986

Editors:
A.B. Budgor, L. Esterowitz, and
L.G. DeShazer

With 285 Figures

Springer-Verlag Berlin Heidelberg New York
London Paris Tokyo

Monomode Neodymium-Doped Fibre Laser: Tunable Continuous-Wave Oscillation at 0.9 μm

I.P. Alcock, A.I. Ferguson, D.C. Hanna, and A.C. Tropper

Physics Department, University of Southampton,
Southampton, SO9 5MH, UK

Recent experiments have shown that monomode silica fibre which has rare earth impurity ions incorporated into the core region can exhibit laser action with low threshold and high efficiency when end pumped by an external laser source [1,2]. Initial studies featuring the $^4F_{3/2} - {}^4I_{11/2}$ transition around 1.08 μm of Nd^{3+} ions in monomode silica fibre investigated this sytem under conditions of Q-switching [3] and active modelocking [4] and demonstrated tuning over the range 1.07 μm - 1.14 μm [2]. A number of different sources have been used to pump fibre lasers including a cw dye laser [1,3,4], and GaAs diode laser [1], and an Ar^+ ion laser [2].

In this paper, we describe the first demonstration of cw operation of the $^4F_{3/2} - {}^4I_{9/2}$ transition of Nd^{3+} ions in glass around 0.9 μm using an end pumped monomode fibre laser of this type. The configuration of the fibre laser cavity is shown in Fig. 1. Five hundred and eighty (580) nm wavelength light from a R6G dye laser is launched into the fibre through a high reflector optically contacted to the cleaved end of a Nd^{3+}-doped fibre (core diameter ~6 μm). An intracavity microscope objective (x10) produced a collimated beam at the output coupler. Tuning of the laser output is accomplished by a 2-plate birefringent filter of the type used in cw dye lasers. The insertion loss of such a filter is negligible when used at Brewster's angle with appropriately polarized light. However since the

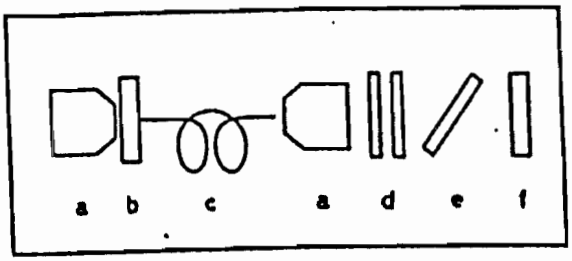

Fig.1. Fibre laser cavity: a) x 10 microscope objective; b) high reflector; c) doped fibre; d) λ/4 plates; e) birefringent filter; f) output coupler

fibre does not preserve polarization, it is necessary to insert two $\lambda/4$ plates into the cavity between the fibre and filter to convert elliptically polarized output of the fibre into the correct linear polarization.

For the $^4F_{3/2} - {}^4I_{11/2}$ Nd^{3+} 4-level laser transition, the fibre length is chosen simply to ensure that the available pump power is absorbed. For the $^4F_{3/2} - {}^4I_{9/2}$ Nd^{3+} transition, the situation is complicated by ground state reabsorption of the laser radiation, and, in general, shorter lengths of fibre must be used. The data presented here were obtained using a 1.2 m length of fibre which absorbed ~53 mW out of the available pump power of 130 mW.

Without any tuning elements in the cavity, the laser could be operated either at 906 nm or at 935 nm--wavelengths corresponding to the two peaks in the fluorescence curve (Fig. 2). Either peak could be selected by a small focusing adjustment (~5 μm) of the intracavity microscope objective. The linewidth at 935 nm was 1 nm in this configuration. With the birefringent filter and $\lambda/4$ plates in place, the laser output could be tuned smoothly from 900 nm to 945 nm. The variation of power output with wavelength is shown in Fig. 2.

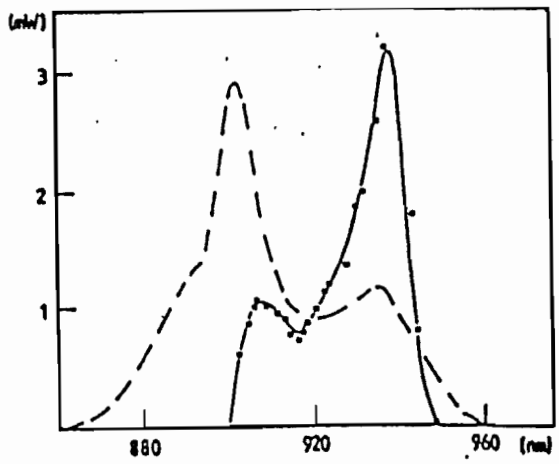

Fig.2. $^4F_{3/2}$ $^4I_{9/2}$ tuning curve (solid line) and fluorescence spectrum (broken line, arbitrary units)

Small rotations of the $\lambda/4$ plates were needed to maintain the correct polarization over the entire tuning range. With the tuning elements in the cavity, the laser linewidth is 0.06 nm. A cw output power of 3.2 mw was measured at the peak of the gain curve.

In conclusion, we have observed cw laser operation on the $^4F_{3/2} - {}^4I_{9/2}$ Nd^{3+} transition which has hitherto only been shown to lase in pulsed mode in glass. This illustrates an essential property of glass lasers in fibre form: that confinement of the pump radiation field within a core of small transverse dimensions produces intense pumping without associated thermal problems [5]. Another instance has been provided by the first

demonstration of cw laser operation on the 1.54 μm line in an Er^{3+}-doped fibre [2]. We anticipate that it should be possible to achieve lasing on other transitions which have not hitherto exhibited laser action in a glass host. The special technique used to fabricate these doped fibres can be adapted to a very wide range of impurity types [6]. In addition we have applied a simple technique for tuning fibre lasers which has the merit of producing polarized laser output from a polarization non-preserving fibre [7].

This work has been supported by a grant from the UK SERC and also under a JOERS program. The authors are grateful to the Optical Fibre Group in the Department of Electronics and Information Engineering for supplying us with the fibre.

References

1. R. J. Mears, L. Reekie, S. B. Poole, and D. N. Payne, Electron. Lett. 21, 738 (1985).

2. L. Reekie, R. J. Mears, S. B. Poole, and D. N. Payne: Journal of Lightwave Technology 4 956 (1986).

3. I. P. Alcock, A. C. Tropper, A. I. Ferguson, and D. C. Hanna, Electron. Lett. 22, 85 (1986).

4. I. P. Alcock, A. I. Ferguson, D. C. Hanna, and A. C. Tropper, Electron. Lett. 22, 268 (1986).

5. I. P. Alcock, A. I. Ferguson, D. C. Hanna, and A. C. Tropper, Opt. Comm., in press.

6. S. B. Poole, D. N. Payne, and M. E. Fermann, Electron. Lett. 21, 737 (1985).

7. I. P. Alcock, A. I. Ferguson, D. C. Hanna, and A. C. Tropper, Opt. Lett. in press.

November 1986 / Vol. 11, No. 11 / OPTICS LETTERS 709

Tunable, continuous-wave neodymium-doped monomode-fiber laser operating at 0.900–0.945 and 1.070–1.135 μm

I. P. Alcock, A. I. Ferguson, D. C. Hanna, and A. C. Tropper

Department of Physics, Southampton University, Southampton SO9 5NH, UK

Received May 30, 1986; accepted August 27, 1986

A tunable Nd^{3+}-doped monomode-fiber laser has been constructed that operates continuously at room temperature. The tuning range covered is 0.900–0.945 and 1.070–1.135 μm. Output powers of 3 mW for 53 mW of absorbed pump and 2 mW for 35 mW of absorbed pump, respectively, were achieved for the two ranges from pumping by a dye laser operating at 590 nm.

Efficient continuous-wave and pulsed fiber lasers[1–4] were recently developed by doping rare-earth ions into low-loss, monomode silica fibers using a modified chemical-vapor-deposition technique.[5] The small transverse dimensions of the fiber permit effective conduction of heat from the fiber, so that the thermal fracture and birefringence problems encountered in bulk glass lasers are eliminated. This has permitted continuous-wave operation, even on three-level laser transitions such as $^4I_{13/2}$–$^4I_{15/2}$ in Er^{3+}-doped glass[2] and $^4F_{3/2}$–$^4I_{9/2}$ in Nd^{3+}-doped glass,[6] which have hitherto not shown cw operation. The broad emission lines of impurity ions in glass offer the possibility of a wide tuning range, suggesting that fiber lasers may prove to be an important new class of tunable laser. They do not suffer the disadvantage of poor photochemical stability shown by many near-infrared dyes, nor do they need low-temperature operation, a feature of near-infrared color-center lasers and vibronic lasers. To assess their potential as tunable lasers, we have investigated their tuning behavior and, in view of the inhomogeneous broadening of the laser transitions, we have investigated the efficiency that can be obtained under narrow-linewidth operation. In this Letter we report the results of these investigations for Nd^{3+}-doped fiber. We have observed tuning ranges of 0.900 to 0.945 μm ($^4F_{3/2}$–$^4I_{9/2}$ transition) and 1.070 to 1.135 μm ($^4F_{3/2}$–$^4I_{11/2}$ transition) with conversion efficiency from the pump laser of up to 6% for an output linewidth of 0.06 nm. Attempts were also made to achieve operation at ~1.3 μm on the $^4F_{3/2}$–$^4I_{13/2}$ transition, without success. Evidence points to an excited-state absorption preventing laser operation.

The general cavity arrangement of the tunable-fiber laser is shown in Fig. 1. A cw dye laser operating in the region of 590 nm was used as the pump source. This laser was launched through a high-reflectivity mirror of 3-mm thickness, which was butted against the cleaved end of a Nd^{3+}-doped monomode fiber of numerical aperture 0.2 and Nd^{3+} concentration of 300 parts in 10^6. The length of fiber used was chosen to optimize the performance at the operating wavelength and ranged from 1 to 2 m. Launch efficiency into the fiber was estimated to be ~40%. Better launch efficiency could probably be achieved if a thinner mirror substrate was used, thus reducing the spherical aberration. The output of the fiber passed through a 10× microscope objective and propagated, in a collimated beam, to the plane output coupler. Étalon effects between the fiber end face and the objective were much in evidence. A long-working-distance objective (8 mm) reduced this effect. The distance between the collimating objective and the output coupler was typically 30 cm, thus permitting the insertion of frequency-selective elements into the cavity.

Tuning of a fiber laser was previously achieved by using a grating as the frequency selector.[2] For this work we have used two- and three-plate birefringent filters as supplied for a cw dye laser (Coherent). The birefringent filter has the advantage over a grating of a small insertion loss. The fiber used in these experiments was nonpolarization preserving, and hence the output from the fiber was, in general, elliptically polarized. To obtain a low insertion loss for the birefringent filter requires a linearly polarized beam incident upon the filter. This was achieved by using two quartz quarter-wave plates, which could be rotated independently. With this arrangement any elliptical polarization can be converted to a given linear polarization. It was found that as the laser was tuned it was necessary to make small adjustments of the quarter-wave plates to maintain maximum output. A polarization-maintaining fiber would remove the need for this readjustment of polarization.

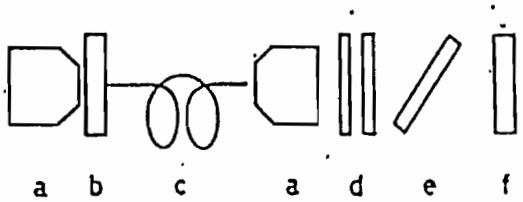

Fig. 1. Schematic diagram of the fiber-laser cavity: a's, microscope objectives; b, high reflector; c, doped fiber; d, quarter-wave plates; e, birefringent filter; f, output coupler.

0146-9592/86/110709-03$2.00/0

The first report of continuous-wave operation on the $^4F_{3/2}$–$^4I_{9/2}$ transition in a glass host was made recently.[6] Here we report the first observation to our knowledge of tunable operation on this transition. Unlike the $^4F_{3/2}$–$^4I_{11/2}$ transition, which has four-level lasing behavior, the $^4F_{3/2}$–$^4I_{9/2}$ transition involves a significant population in the lower laser level. Lasing on the $^4F_{3/2}$–$^4I_{9/2}$ transition can therefore be suppressed as a result of reabsorption loss if too long a fiber is used. Careful optimization of the fiber length was not attempted, but a 1-m length was found to give a reasonable compromise between the need to ensure essentially complete pump absorption and the need to minimize reabsorption loss.

The input mirror was chosen to have a reflectivity of approximately 99.5% at 900 nm and 15% at 1.08 μm, which gave sufficient discrimination to suppress lasing on the $^4F_{3/2}$–$^4I_{11/2}$ transition. The output coupler had a reflectivity of approximately 70% at 900 nm. In the absence of a tuning element in the cavity it was found that the laser would operate at either 906 or 935 nm, corresponding to the two peaks in the fluorescence curve (Fig. 2). It was found that changes in the objective-to-fiber-end distance of approximately 5 μm were sufficient to cause the wavelength to jump between these values. A possible explanation for this behavior is that the different mode size in the fiber for these two wavelengths requires different mode-matching conditions and hence a different location of the microscope objective. However, when a two-plate birefringent filter was placed in the cavity, continuous tuning from 900 to 945 nm was achieved, as shown in Fig. 2, and the free-running linewidth was reduced from 1 to 0.06 nm, FWHM. At threshold the absorbed pump power was 8 mW (unchanged from the value without the birefringent filter), and the output power was 3.2 mW at the peak of the tuning curve for an absorbed pump power of 53 mW.

For operation on the $^4F_{3/2}$–$^4J_{11/2}$ transition the input

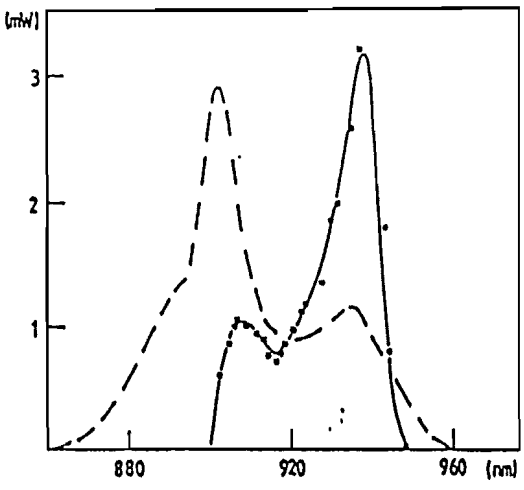

Fig. 2. Photoluminescence spectrum (dotted line) and laser output power variation with wavelength (solid line) for the $^4F_{3/2}$–$^4I_{9/2}$ transition. (The photoluminescence spectrum is not corrected for material reabsorption.)

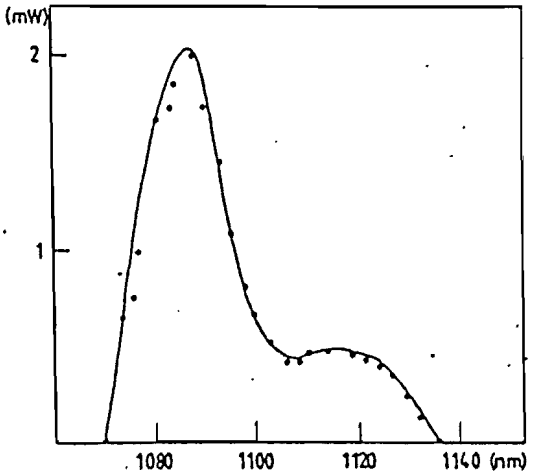

Fig. 3. Laser output power variation with wavelength for the $^4F_{3/2}$–$^4I_{11/2}$ transition.

mirror was chosen to have a reflectivity of approximately 98.5% at 1.08 μm, and the output coupler a reflectivity of approximately 70%. In this case the population of the lower laser level was small, thus giving negligible reabsorption. A fiber length of 2 m was chosen so that the pump power was totally absorbed. The choice of mirrors together with the longer length of the fiber provided sufficient discrimination to suppress operation on the $^4F_{3/2}$–$^4I_{9/2}$ transition.

When the laser was free running without tuning elements it operated at 1.088 μm with a linewidth of 4 nm. Unlike in the case of the $^4F_{3/2}$–$^4I_{9/2}$ transition, the operating wavelength did not change with adjustment of the focusing of the microscope objective. There was no noticeable drop in the output power when the birefringent filter was placed inside the cavity.

The tuning range obtained with the birefringent filter was from 1.07 to 1.135 μm (Fig. 3). The laser linewidth was measured to be 0.1 nm (FWHM). At the peak of the tuning curve the output was 2 mW for 35 mW of absorbed pump power with an absorbed pump power threshold of 12 mW.

The tuning range of 65 nm achieved with this birefringent filter was limited by the inadequate suppression of satellite transmission peaks of the filter, so that at the extreme of the tuning range the wavelength would jump back to near the line center. Tuning on the $^4F_{3/2}$–$^4I_{11/2}$ transition in a fiber laser was previously observed by using a grating,[2] which permitted a slightly greater range, 70 nm, since it was not limited by wavelength hopping. On the other hand, the birefringent filter has permitted more than a 1-order-of-magnitude increase in efficiency over the grating as a result of its much lower insertion loss. An improved tuning range, while maintaining the efficiency, should be possible with a birefringent filter designed specifically for the fiber laser, which, having a higher gain than typical cw dye lasers, needs a better suppression of satellite filter transmission peaks.

A measurement of fluorescence intensity from the

fiber on the $^4F_{3/2}$–$^4I_{13/2}$ transition, at around 1.3 μm, indicated a branching ratio similar to that found in other Nd-doped materials. The possibility of laser action on this transition appeared feasible and was looked for.

To minimize the resonator loss the mirrors (~99% reflectivity at ~1.3 μm) were butted to each end of the fiber. Also, to improve the overlap of the fiber mode with the core, a fiber of longer cutoff wavelength (~1.3 μm) was used, having been pulled from the same preform as the fiber used in the earlier experiments. Based on the performance at 0.9 and 1.08 μm, sufficient inversion should have been available to permit oscillation at ~1.3 μm. This was not observed. The likely explanation for this is excited-state absorption, with the $^4F_{3/2}$–$^4G_{7/2}$ transition as the most probable assignment. To check whether absorption was present in the fiber at ~1.3 μm, a probe beam from a miniature diode-pumped Nd:YAG laser operating on the $^4F_{3/2}$–$^4I_{13/2}$ transition[7] was used. The transmission of this probe beam (which was at either 1.32 or 1.34 μm) through the fiber was monitored while the 590-nm pump beam was modulated by a mechanical chopper. Absorption at both probe wavelengths was observed; it was stronger at 1.32 μm where ~40% absorption for an absorbed pump power of 20 mW was observed, while at 1.34 μm ~12% absorption was observed under similar conditions. The absence of lasing therefore appears to be due to excited-state absorption.

We have demonstrated tuning of a Nd^{3+}-doped fiber laser on two transitions, using a birefringent filter as the tuning element. This is the first report to our knowledge of wavelength tuning on the $^4F_{3/2}$–$^4I_{9/2}$ transition. Compared with a grating-tuned fiber laser,[2] the birefringent filter has permitted an increase of efficiency by more than an order of magnitude. The efficiency under conditions of narrow-line operation is comparable with that obtained from dye lasers, vibronic lasers, and color-center lasers, despite the inhomogeneous broadening of the laser transition. It is therefore anticipated that further narrowing, to single-frequency operation, should not entail any significant reduction in efficiency. Given the possibility of incorporating other dopants into the fiber, thus extending the wavelength range, we believe that fiber lasers can offer convenient and attractive alternatives to existing cw near-infrared lasers.

The research was partly supported by a Science and Engineering Research Council (SERC) grant and the Joint Optoelectronics Research Scheme program. The authors would like to thank the Optical Fibre Group, Department of Electronics and Information Engineering, Southampton University, for providing the doped fiber. I. P. Alcock acknowledges the support of a SERC studentship.

References

1. R. J. Mears, L. Reekie, S. B. Poole, and D. N. Payne, Electron. Lett. 21, 738 (1985).
2. L. Reekie, R. J. Mears, S. B. Poole, and D. N. Payne, IEEE J. Lightwave Technol. (to be published).
3. I. P. Alcock, A. I. Ferguson, D. C. Hanna, and A. C. Tropper, Electron. Lett. 22, 268 (1986).
4. I. P. Alcock, A. C. Tropper, A. I. Ferguson, and D. C. Hanna, Electron. Lett. 22, 84 (1986).
5. S. B. Poole, D. N. Payne, and H. E. Ferman, Electron. Lett. 21, 737 (1985).
6. I. P. Alcock, A. I. Ferguson, D. C. Hanna, and A. C. Tropper, submitted to Opt. Commun.
7. A. I. Ferguson, Electron. Lett. 21, 853 (1985).

Q-switching, mode-locking and tunable operation around 0.9 μm of a neodymium-doped monomode fibre laser

I.P. Alcock
A.C. Tropper
A.I. Ferguson
D.C. Hanna

Indexing terms: Optical fibres, Lasers

Abstract: Recent studies of monomode silica fibre which has rare-earth impurity ions incorporated into the core region have shown that it can exhibit laser action with low threshold and high efficiency when end pumped by an external laser source. In the paper we describe the first demonstration of Q-switching of the $^4F_{3/2}$–$^4I_{9/2}$ Nd^{3+} transition at 0.9 μm using a fibre laser of this type. A birefringent filter has been used to tune the laser output over the range 0.900–0.945 μm. We also report on the performance of the laser at 1.08 μm under conditions of Q-switching and active mode-locking. In Q-switched operation an intracavity acousto-optic modulator was used to generate pulses of 200 ns duration and 8.8 W peak power at repetition rates up to 1 kHz. Active mode-locking of the fibre was accomplished using acousto-optic modulation of the cavity losses at 41.4 MHz, converting the laser output to a train of pulses of subnanosecond duration.

1 Introduction

The operation of a neodymium glass laser in the form of a multimode fibre waveguide was first demonstrated by Stone and Burrus [1] who pointed out that very efficient longitudinal laser pumping could be achieved in such a device. In a recent development of this work monomode optical fibre with impurity doping has been used as a laser gain medium [2–8]. Impurities such as rare-earth ions can be incorporated into the core of an optical fibre without significantly degrading the transmission of the fibre in the spectral windows between the impurity absorption bands [5]. The optical transitions of a rare-earth ion in a fused-silica matrix show strong homogeneous broadening due principally to interaction with high-frequency Si–O bond stretching vibrational modes [9] as well as inhomogeneous broadening associated with the disordered nature of the matrix. The fluorescence spectrum therefore exhibits broad bands which are potentially attractive as tunable laser transitions, except that the gain, which varies inversely with linewidth, is correspondingly small. The remarkable property of the monomode fibre geometry which distinguishes it from conventional glass lasers is that confinement of the pump radiation field within a core of small transverse dimensions can allow intense pumping without associated thermal problems [7]. Moreover, since the interaction length can be extended indefinitely it is possible to make use of all the power available in a pump laser source, even when the pump wavelength falls in the weakly absorbing wing of a rare-earth absorption band. Thus one might expect a monomode fibre laser to achieve oscillation on rare-earth transitions which cannot reach threshold when using bulk glass as the gain medium.

In this paper we describe tunable CW operation of a neodymium monomode fibre laser on the $^4F_{3/2} \rightarrow {}^4I_{9/2}$ transition [8]. The terminal level of this transition is thermally populated and hitherto it has only been operated in pulsed mode in a glass host. Like the 1·5 μm erbium fibre laser [6] this system illustrates the effectiveness of the fibre-laser geometry for low-gain transitions. We also discuss the performance of the fibre laser under Q-switched and mode-locked conditions.

2 Configuration of the fibre laser

All the experiments reported here used silica fibre with a cutoff wavelength of ~1 μm and approximately 0.03% of Nd^{3+} ions in the fibre core. The configuration of the laser cavity is shown schematically in Fig. 1. The laser is pumped with 590 nm radiation from a rhodamine 6G dye laser. Different fibre lengths were needed for the various experiments reported here, and the absorbed pump power varied accordingly. The pump laser beam is launched into the fibre through a high reflector which is

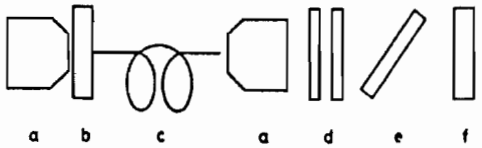

Fig. 1 *Configuration of fibre laser*
a = microscope objective
b = high reflector
c = Nd-doped fibre
d = λ/4 plates
e = intracavity filter or modulator
f = output coupler

Paper 5363J (E13), first received 10th December 1986 and in revised form 18th March 1987

The authors are with the Department of Physics, The University, Southampton SO9 5NH, United Kingdom

optically contacted to the cleaved fibre end. An intracavity × 10 microscope objective is used to produce a collimated output beam and the airgap between this objective and the output coupler allows optical elements such as filters and modulators to be introduced into the laser cavity. In particular, a pair of $\lambda/4$ plates were used to convert the elliptically polarised output of the non-polarisation-preserving fibre to the linear polarisation required by other intracavity components.

3 Tunable operation on $^4F_{3/2}$–$^4I_{9/2}$ transition around 0.9 μm

The spectrum of photoluminescence from the $^4F_{3/2}$ metastable level to the $^4I_{9/2}$ ground multiplet is shown in Fig. 2. This measurement was made on a section of fibre

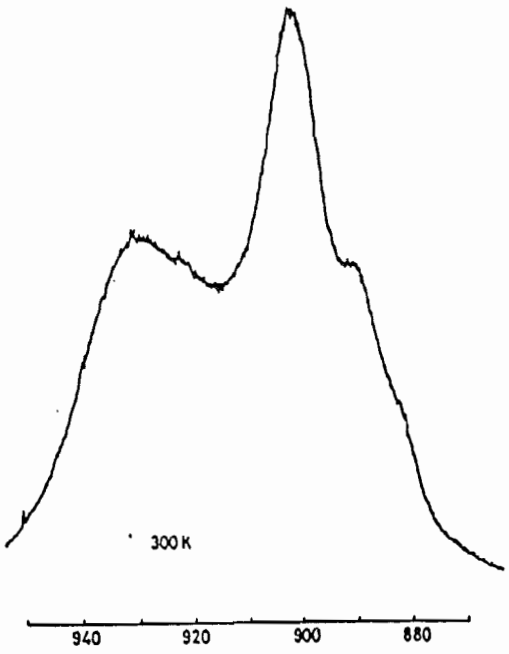

Fig. 2 *Photoluminescence spectrum of Nd ions in fibre preform around 0.9 μm*

preform, and fluorescence which escaped laterally out of the preform core was collected so as to minimise the influence of reabsorption on the spectrum. The band exhibits partially resolved structure corresponding to transitions from the lower energy doublet in $^4F_{3/2}$ to the five doublets composing the $^4I_{9/2}$ multiplet. The shoulder at 890 nm marks the mean energy of transitions to the ground doublet. In thermal equilibrium at room temperature, approximately 30% of the Nd ion population is in the excited state at ~170 cm^{-1} and 6% is in the state at ~480 cm^{-1}, and the fibre therefore exhibits strong attenuation around 903 nm and weaker attenuation around 930 nm owing to thermal population of these excited states.

To observe laser action on this band we used a 1.2 m length of fibre which absorbed only ~53 mW of the available pump power, but which kept cavity losses due to ground-state reabsorption low. Laser action on the $^4F_{3/2}$–$^4I_{11/2}$ transition was suppressed by the high reflector which had 99% reflectivity at 900 nm but only 15% reflectivity at 1.08 μm. An output coupler with 70% reflectivity at 900 nm was used.

A 2-plate birefringent filter was used to produce a tunable output with a spectral bandwidth of 0.06 nm full width at half maximum (FWHM). A particular advantage of this technique is that with $\lambda/4$ plates in the cavity to control the polarisation of the fibre output the Brewster-angled birefringent filter introduces negligible insertion loss. The dependence of output power on wavelength is shown in Fig. 3. where the broken line indicates

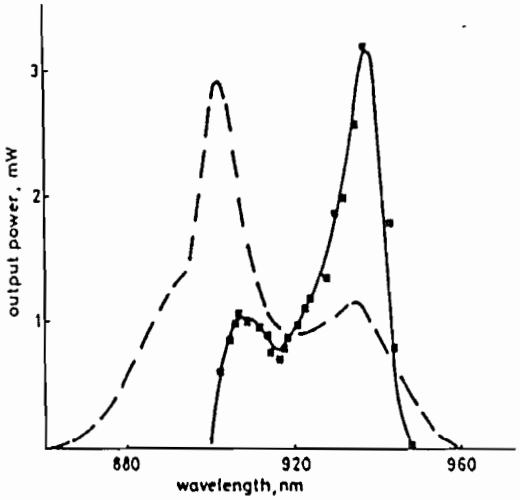

Fig. 3 *Output power versus wavelength for $^4F_{3/2}$–$^4I_{9/2}$ laser transition*
---- *position of photoluminescence band*

the position of the photoluminescence band. At the peak of the tuning curve at ~935 nm the laser reached threshold with 8 mW of absorbed pump power, and with 53 mW of absorbed pump power, 3.2 mW of output power was obtained, representing a conversion efficiency of 6%. This is the same as the conversion efficiency achieved in broadband operation, showing that the homogeneous broadening of this transition is strong enough not to set a limit to the efficiency of narrowband power extraction, at least under CW conditions.

4 *Q*-switched operation

Q-switched operation of the monomode fibre laser has been demonstrated on the 4-level $^4F_{3/2} \rightarrow {}^4I_{11/2}$ neodymium transition [3]. An intracavity acousto-optic modulator (Isomet 1205C-1) was inserted into the cavity between the intracavity microscope objective and the output coupler, thus ensuring a constant pumping rate unaffected by *Q*-switch losses.

For operation at 1.08 μm a 2.3 m length of fibre was used in which the incident pump power of 80 mW was totally absorbed. The reflectivities of the high reflector and the output coupler were 98% and 60%, respectively. Square-wave modulated RF power was applied to the *Q*-switch producing an estimated 40% modulation in the single-pass transmission. During the low-*Q* half cycle the laser was below threshold. Laser output during the high-*Q* half cycle consisted of an initial large spike followed by several smaller spikes and then by continuous-wave action. By altering the duty cycle to shorten the high-*Q* period relative to the low-*Q* period all laser output after the initial large spike could be suppressed, with a corresponding gain in peak power. Fig. 4 shows a typical output pulse obtained at 100 Hz repetition rate with a high-*Q* period of 5 μs. A peak power of approximately 8.8 W was achieved in a pulse of 200 ns duration. The repetition rate could be increased up to ~1 kHz without noticeable loss of peak power.

An estimate of the duration Δt (FWHM) of the Q-switched pulse has been derived from the analysis due to Carlson [9]:

$$\Delta t = \frac{2.48\tau_c}{[x - 1 - lnx]^{1/2}} \quad (1)$$

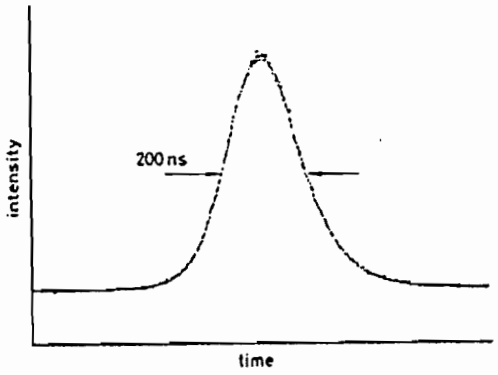

Fig. 4 *Temporal profile of Q-switched pulse at 1.08 μm*

τ_c is the photon lifetime in the resonator in the high-Q state, and x is the ratio of pump rate to threshold pump rate. The photon lifetime was estimated from a measurement of the frequency of relaxation oscillations [11] to be ~35 ns and for this system $x \cong 1.9$. Thus eqn. 1 predicts a duration of 170 ns for the Q-switched pulse, which is close to the experimental value.

Q-switching was also observed with the intracavity modulator replaced by an optomechanical chopper wheel. Remarkably we found that peak powers approaching half those achieved acousto-optically could be achieved, although the switch-on time of the chopper was a few hundred cavity round-trip times and the laser output contained a number of spikes in the high-Q period. This cheap and easy technique recommends itself strongly for applications where optimum pulse shape and peak power are not required.

The same techniques have been used to Q-switch the neodymium fibre laser on the $^4F_{3/2} \rightarrow {}^4I_{9/2}$ transition at 0.9 μm. The photon lifetime is significantly smaller in this system because a shorter fibre, and therefore a shorter resonator, is used, and because the photons suffer ground-state reabsorption. Q-switched pulses of ~70 ns and a few Watts peak power could readily be obtained. However, the Carlson theory cannot be used to predict pulse durations for this 3-level laser transition.

5 Mode-locking

To mode-lock the fibre laser operating on the $^4F_{3/2}$–$^4I_{11/2}$ transition an acousto-optic rhomb mode-locker (Crystal Technology) with Brewster-angled surfaces inserted between the intracavity microscope objective and the output coupler has been used [4]. Since the resonances of the high-Q transducer were highly temperature dependent it was found necessary to mount the mode-locker in a temperature-stabilised enclosure. The output coupler was mounted on a translation stage so that the frequency difference between longitudinal cavity mode beats could be matched to the loss modulation frequency.

The laser output was detected by a Ge photodiode and the amplified photocurrent was fed into a Tektronix 7L14 RF spectrum analyser. With no RF power applied to the mode-locker the laser output contained weak longitudinal cavity mode beats. When RF power at 20.723 MHz was applied to the mode-locker and the cavity length was adjusted to match the loss modulation frequency, the beats became strong and narrower. Eventually higher harmonics appeared and dramatically increased in intensity as the RF power was increased. Fig. 5 shows the comb of RF beat frequencies obtained with

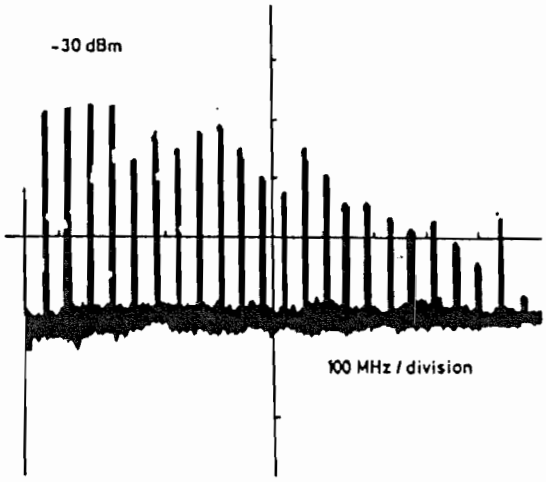

Fig. 5 *Radio-frequency beat spectrum of mode-locked fibre laser*

250 mW of applied RF power. The high frequency rolloff is due to the bandwidth of the amplifier and detector.

The laser output was then observed in the time domain using a fast detector (RCA CA 309709E) and oscilloscope. The laser output consisted of a train of short pulses with a repetition rate corresponding to the cavity round-trip time. Fig. 6 shows a single pulse from

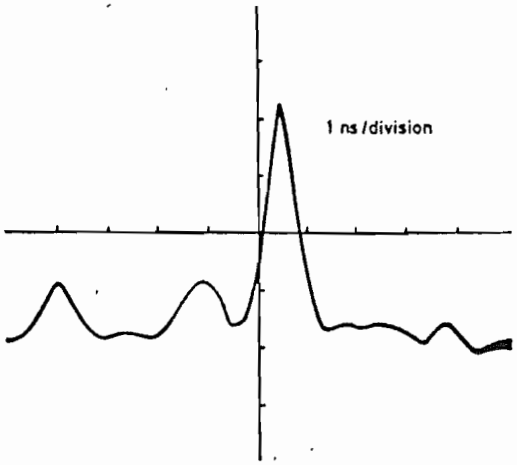

Fig. 6 *Temporal profile of mode-locked laser pulse*

the train, with an FWHM of less than 1 ns limited by the 400 MHz bandwidth of the oscilloscope and an energy of ~17 pJ. The structure around the pulse is believed to be due to étalon effects in the cavity.

The effect of simultaneous Q-switching and mode-locking on the $^4F_{3/2}$–$^4I_{11/2}$ transition was also studied by inserting a mechanical chopper wheel between the mode-locker and the intracavity microscope objective. The output then had the form shown in Fig. 7; a train of short pulses under a Q-switched envelope of ~690 ns duration. Individual pulses in the train are longer than in

the CW case because the build-up time for the Q-switching is not long enough to allow a steady state to be reached. The energy of the largest pulse in the train is ~20 nJ, and its duration is less than 3 ns FWHM.

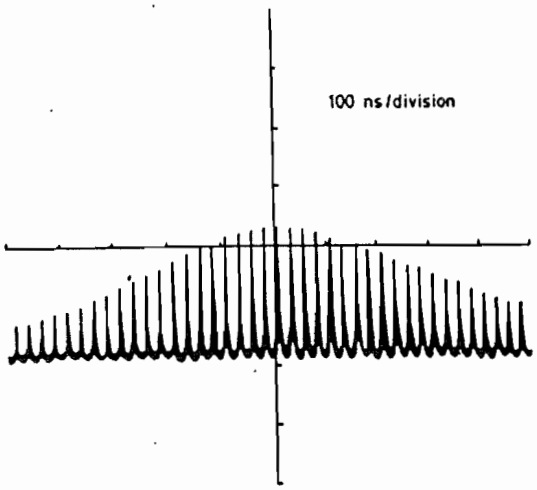

Fig. 7 *Q-switched and mode-locked train of pulses*

So far the potential of the broad gain bandwidth of the neodymium fibre laser for generating short mode-locked pulses has not been fully realised. One technical problem is the difficulty of eliminating feedback into the laser cavity from reflections off the free fibre end, and various possible solutions are currently under investigation. On a more fundamental level, the monomode fibre laser combines a high intensity in the laser radiation field with a long path through the gain medium, so that not only will dispersion play a greater role than in a conventional glass laser but also nonlinear effects such as self-phase modulation and stimulated Raman scattering may become significant. At 1.08 μm such nonlinear processes might be expected to impose limits on the pulse duration and peak pulse power. However, in the negative group-velocity dispersion region the interesting possibility of pulse compression and even soliton propagation in the laser medium arises.

6 Acknowledgments

This work has been supported by a grant from the UK SERC and also in part under a Joint Optoelectronics Research Scheme. The authors are grateful to S. Poole and other members of the Fibre Optics Group in the Department of Electronics, Southampton University, for kindly providing doped fibre, and to D. A. Humphreys of the National Physical Laboratory for the loan of a fast detector. One of us (IPA) acknowledges the support of an SERC studentship.

7 References

1 STONE, J., and BURRUS, C.A.: 'Neodymium-doped silica lasers in end-pumped fiber geometry', *Appl. Phys. Lett.*, 1973, 23, p. 388
2 MEARS, R.J., REEKIE, L., POOLE, S.B., and PAYNE, D.N.: 'Neodymium-doped silica single-mode fibre lasers', *Electron. Lett.*, 1985, 21, (17), pp. 738–740
3 ALCOCK, I.P., TROPPER, A.C., FERGUSON, A.I., and HANNA, D.C.: 'Q-switched operation of a neodymium-doped monomode fibre laser', *ibid.*, 1986, 22, (2), pp. 84–85
4 ALCOCK, I.P., FERGUSON, A.I., HANNA, D.C., and TROPPER, A.C.: 'Mode-locking of a neodymium-doped monomode fibre laser', *ibid.*, 1986, 22, (5), pp. 268–269
5 POOLE, S.B., PAYNE, D.N., and FERMANN, M.E.: 'Fabrication of low-loss optical fibres containing rare-earth ions', *ibid.*, 1985, 21, (17), pp. 737–738
6 POOLE, S.B., PAYNE, D.N., MEARS, R.J., FERMANN, M.E., and LAMING, R.I.: 'Fabrication and characterisation of low-loss optical fibres containing rare-earth ions', *J. Lightwave Technol.*, 1986, LT-4, p. 956
7 ALCOCK, I.P., FERGUSON, A.I., HANNA, D.C., and TROPPER, A.C.: 'Continuous-wave oscillation of a monomode neodymium-doped fibre laser at 0.9 μm on the $^4F_{3/2}$–$^4I_{9/2}$ transition', *Opt. Commun.*, 1986, 58, p. 405
8 ALCOCK, I.P., FERGUSON, A.I., HANNA, D.C., and TROPPER, A.C.: 'Tunable, continuous-wave neodymium-doped monomode-fiber laser operating at 0.900–0.945 and 1.070–1.135 μm', *Opt. Lett.*, 1986, 11, (11), pp. 709–711
9 LAYNE, C.B., LOWDERMILK, W.H., and WEBER, M.J.: 'Multiphonon relaxation of rare-earth ions in oxide glasses', *Phys. Rev. B*, 1977, 16, p. 10
10 CARLSON, D.G.: 'Dynamics of a repetitively pump-pulsed Nd:YAG laser', *J. Appl. Phys.*, 1968, 39, p. 4369
11 YARIV, A.: 'Introduction to optical electronics' (Holt Rinehart and Winston, 1976, 2nd edn.)

Appendix H

Volume 58, number 6 OPTICS COMMUNICATIONS 15 July 1986

MODE-LOCKING AND Q-SWITCHING OF AN OPTICALLY PUMPED MINIATURE Nd^{3+}:YAG LASER

I.P. ALCOCK and A.I. FERGUSON

Physics Department, University of Southampton, Southampton SO9 5NH, UK

Received 24 February 1986

A miniature Nd^{3+}:YAG laser is developed which is optically pumped by a dye laser or a GaAlAs diode laser and can be operated continuously, Q-switched, mode-locked or Q-switched and mode-locked. The continuous-wave laser produced an output power of 23 mW at 1.06 μm for an absorbed pump power of 127 mW from a dye laser operating at 590 nm. Output pulses with an energy of 12 μJ and 140 ns (full width, half maximum) duration at a repetition rate of 1 kHz were achieved by Q-switching the system, while mode-locking produced pulses of 240 ps (full width, half maximum) and 138 pJ of energy at a repetition rate of 245.7 MHz.

1. Introduction

There has been considerable interest in the development of laser pumped miniature Nd^{3+}:YAG lasers both at 1.06 μm and 1.32 μm [1–4] as a source of single frequency radiation. For many applications it is desirable that the power of these lasers be increased or that they produce short pulses while maintaining the reliability and efficiency of an all solid-state source.

We have developed a miniature Nd^{3+}:YAG laser which is optically pumped by a second laser and can be operated continuously, Q-switched, mode-locked or Q-switched and mode-locked. This provides a reliable and versatile source of short and energetic pulses at 1.06 μm. The system can easily be modified to operate at 1.32 μm and 1.34 μm.

2. Results

A schematic diagram of the laser is shown in fig. 1. It consists of a 4 mm diameter by 10 mm long Nd^{3+}:YAG rod with a Nd^{3+} concentration of 1% by weight. One of the plane ends of the rod was coated to provide a high reflector at 1.06 μm with high transmission at 810 nm, and the other was anti-reflection coated. An anti-reflection coated silica lens of 75 mm focal length produced a collimated beam on a plane output coupler

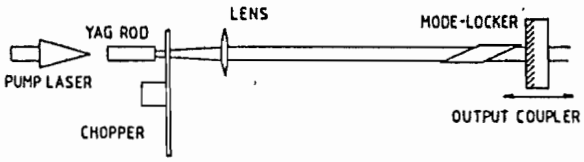

Fig. 1. Schematic diagram of mode-locked and Q-switched Nd:YAG laser.

(R = 93.5% at 1.064 μm), which was mounted on a translation stage. The system was pumped either by a continuous-wave dye laser at 590 nm or by a continuous-wave GaAlAs diode at 808 nm, mode-matched to the cavity. Most of the tests reported here were carried out using the dye laser. When the system was operated continuously the absorped pump threshold power was found to be 5 mW at 590 m, with slope efficiency of 19%. The beam profile was TEM_{00}.

The laser was easily Q-switched by the use of a mechanical chopper placed in the cavity. It was positioned close to the Nd^{3+}:YAG rod where the beam was smallest in order to ensure that the switch on time, 12 μs, was as fast as possible. Fig. 2 shows the Q-switched output of this laser observed using a GaAsP photodiode (RCA CA309709E) and oscilloscope (Tektronix 7A19 amplifier in a 7904 mainframe). The pulse duration was found to be 140 ns with an energy

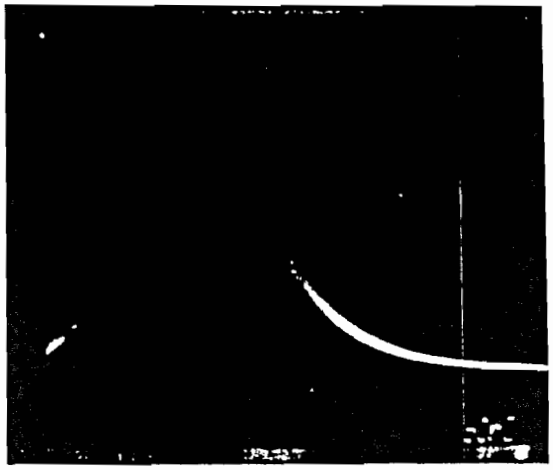

Fig. 2. This shows the output of the laser when Q-switche
Each large division corresponds to 50 ns.

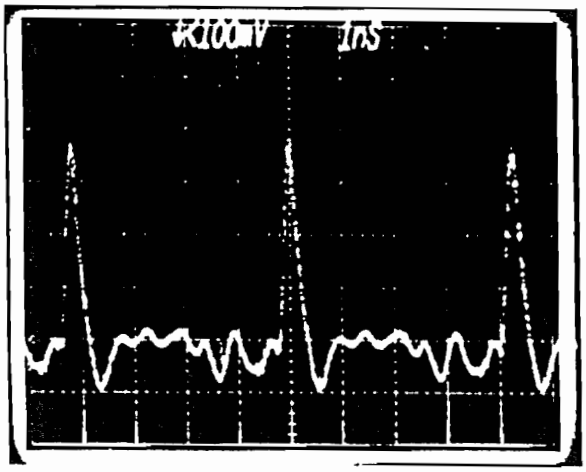

Fig. 3. This shows the mode-locked pulse train at a repetition rate of 245.7 MHz. Each large division corresponds to 1 ns.

of 12 μJ, corresponding to a peak power of 86 W, for an absorped pump power of 130 mW. The pulse energy and duration had a good long term stability although the beating of several longitudinal modes could be seen on the pulse. An acousto-optic modulator has also been used to Q-switch the cavity but resulted in higher threshold and lower pulse energy since the ulator was not designed for intra-cavity work.

When the laser was operated as a mode-locked tem a Brewster angled rhomb mode-locker (Cryst Technology) was placed close to the output coup The mode-locker was of a high-Q variety and driv 122.87 MHz which is the third harmonic of its fu mental resonance.

The output coupler was mounted on a translat stage so that the cavity length could be matched modulation frequency. As the cavity length was sli detuned (~30 μm) the output began to exhibit a strong low frequency spiking behaviour. By adjus the cavity length so that the output appeared fre low frequency oscillations mode-locked pulses of than 400 ps (full width half maximum) were proc without use of a fast oscilloscope. In order to ob the shortest pulses a Tektronix sampling scope w used with the RCA diode to monitor the individ pulses and fig. 3 shows a mode-locked train of pu with a full width at half maximum of 240 ps and energy of 138 pJ.

The system was simultaneously mode-locked Q-switched by combining the chopper and mode-locker in the cavity at the same time. A typical pulse envelope of the mode-locked and Q-switched train is shown in fig. 4 which was recorded using the RCA diode and and oscilloscope (Tektronix 7A19 amplifier in a 7904 mainframe). The pulse envelope had a full width at half maximum of 240 ns and an energy of 10 μJ. The measurement of the pulse duration of each mode-locked pulse was limited by the detection system to less than 800 ps.

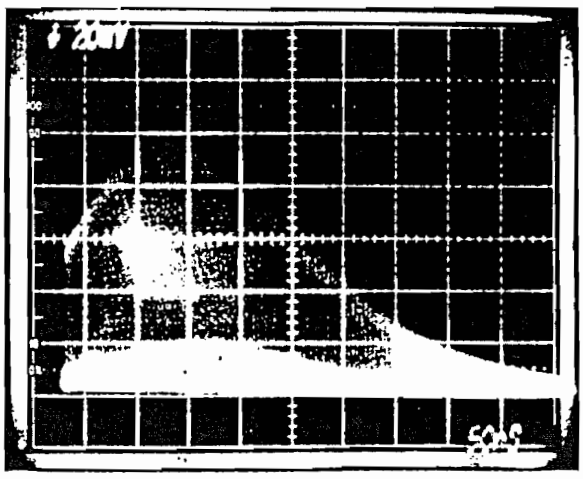

Fig. 4. This shows the mode-locked and Q-switched output of the laser. Each large division corresponds to 50 ns.

The system was not optimised for mode-locked and Q-switched operation as the use of the chopper meant that the pulse shaping took place during the Q-switched build-up period of 10 μs while the gain was unsaturated. This meant that there would not be enough passes through the cavity to achieve a steady state and so the pulses would have been longer than the continuous-wave mode-locked case.

3. Conclusion

We have constructed an efficient miniature Nd^{3+}: YAG laser which can be pumped by a GaAlAs laser diode to provide mode-locked and Q-switched pulses. The system can be easily modified to operate at 1.32 μm. The use of a purpose designed electro-optic or acousto-optic Q-switch should allow the system to be accurately synchronised to an external trigger and the provision of a long prelase period to improve the pulse duration in mode-locked and Q-switched operation. There is also sufficient peak power from this system to enable optical pulse compression in a fibre-grating pulse compressor [5].

Acknowledgement

We should like to thank Photon Control Ltd, Cambridge for the loan of the Nd:YAG rod and D. Humphreys of the National Physical Laboratory. London for the loan of the fast photodiode. The financial support of SERC for this programme is also gratefully acknowledged.

References

[1] B. Zhou, T.J. Kane, G.F. Dixon and R.L. Byer, Optics Lett. 10 (1985) 62.
[2] T.J. Kane and R.L. Byer, Optics Lett. 65 (1985) 65.
[3] A. Owyomg, G.R. Hadley, P. Esherick, R.L. Schmitt and L.A. Rahn, Optics Lett. 10 (1985) 484.
[4] A.I. Ferguson, Electron Lett. (GB) 21 (1985) 853.
[5] B. Nikolaus and D. Griskhowsky, Appl. Phys. Lett. 42 (1982) 1.

References

1. S B Poole, D N Payne & M E Fermann
   Electron Lett v 21 (1985) p 737–738

2. R J Mears, L Reekie, S B Poole & D N Payne
   Electron Lett v 21 (1985) p 738–740

3. I P Alcock, A C Tropper, A I Ferguson & D C Hanna
   Electron Lett v 22 (1986) p 84–85

4. R J Mears, L Reekie, I M Jauncey & D N Payne
   Electron Lett v 23 (1987) p 1026–1028

5. L Reekie, R J Mears, S B Poole & D N Payne
   IEEE J Lightware Technol. LT-4 (1986) p 956–960

6. I P Alcock, A I Ferguson, D C Hanna & A C Tropper
   Opt Lett v 11 (1986) p 709–711

7. I P Alcock, A I Ferguson, D C Hanna & A C Tropper
   Electron Lett v 22 (1986) p 268–269

8. M C Farries, M E Fermann, R I Lamming, S B Poole, D N Payne & A P Leach
   Electron Lett v 22 (1986) p 418–419

9. R J Jacobs & M J Weber
   IEEEJ of QE v 12 (1976) p 102–111

10. W F Krupke

IEEEJ of QE v 10 (1974) p 450–457

11. A W Snyder & J D Love Optical Waveguide Theory

Science Paperbacks Chapman and Hall (1983)

12. C G Young

Proc of the IEEE v 57 (1969) p 1267–1289

13. I P Alcock, A I Ferguson, D C Hanna, & A C Tropper

Opt Comm v 58 (1986) p 405–408

14. Kaye and Laby 14th Edition Longman (1982)

15. C G Young

Appl Phys Letts v 2 (1963) p 151–152

16. T Uchida, S Yoshikawa, K Washio, R Tatsumi, K Tsushima, I Kitano, K Koisumi & Y Ikeda

Jap JAP v 12 (1972) p 126–134

17. S Kishida, K Washio & S Yoshikawa

Appl Phys Lett v 34 (1979) p 273–275

18. J Stone & C A Burrus

Appl Phys Lett v 23 (1973) p 388–389

19. C K Koester & E Snitzer

Appl Opt v 3 (1964) p 1182–1186

20. C J Koester

IEEEJ of QE v 2 (1966) p 580–584

21. M Nakazawa, M Tokuda & N Uchida

J Opt Soc Am v 1 (1984) p 86–90

22. B Di Bartolo

Optical Interactions in Solids

J. Wiley & Sons (1968)

23. M J Weber

Laser Spectroscopy of Solids Editors Y M Yen &

P M Selzer, Springer–Verlag. Springer series on Topics in

Applied Physics v. 49 (1981)

24. J Hegarty & W M Yen

Physical Review Letters v 43 (1979) p 1126–1130

25. J M Pellegrino, W M Yen & M J Weber

J Appl Phys v 51 (1980) p 6332–6336

26. P Avouris, A Campion & M A El-Sayed

The Journal of Chemical Physics v 67 (1977) p 3397–3398

27. R M Macfarlane & R M Shelby

Opt Comm v 45 (1983) p 45–51

28. R M Shelby

Opt Lett v 8 (1983) p 88–90

29. P W Anderson, B I Halperin & C W Varma

Phil Mag v 25 (1971) p 1–9

30. W A Phillips

J of Low Temp Phys v 7 (1972) p 351–360

31. R Reineker & H Morowitz

Chem Phys Lett v 86 (1982) p 359–364

32. D L Huber, M M Broer & B Golding

Phys Rev Lett v 52 (1984) p 2281–2284

33. S K Lyo

Phys Rev Lett v 48 (1982) p 688–691

34. S K Lyo and R Orbach

Phys Rev B v 22 (1980) p 4223–4225

35. R Hegarty, M M Broer, B Golding, J R Simpson & J B MacChesney

Phys Rev Lett v 51 (1983) p 2033–2035

36. H Namikawa, K Arai, K Kumata, Y Ishii & H Tanaka

Japanese J of Appl Phys v 21 (1982) p L360

37. E I Galant, Y N Kondrat'ev, A K Przhevuskii, T I Prokhorova, M N Tolstoi & V N Shapovalor
JETP Lett v 18 (1973) p 372–373

38. R R Jacobs & M J Weber
IEEE J of QE v QE12 (1976) p 102–111

39. M J Weber, D C Ziegler & C A Angell
J Appl Phys v 53 (1982) p 4344–4350

40. M F Digonnet & C J Gaeta
Appl Opt v 24 (1985) p 333–342

41. W Koechner
Solid State Laser Engineering. Springer–Verlag
Springer series on Optical Sciences v.1 (1976)

42. A Yariv
Quantum Electronics 2nd Edition
J. Wiley & Sons (1975)

43. M W Phillips, H Gong, A I Ferguson & D C Hanna
Opt Comm v 61 (1987) p 215–218

44. M Zürn, J Voigt, E Brinkmeyer, R Ulrich & S B Poole
Electron Lett v 12 (1987) p 316–318

45. T Y Fan, G J Dixon & R L Byer

Opt Lett v 11 (1986) p 204–206

46. W G Wagner & B A Lengyel

J of Appl Phys v 34 (1963) p 2040–2046

47. D G Carlson

J of Appl Phys v 39 (1968) p 4369–4374

48. K Washio, K Koizumi & Y Ikeda

IEEE J of QE v QE13 (1977) p 47–53

49. I V Tomov, R Fedosejers & M C Richardson

Rev Sci Instrum v 50 (1979) p 9–16

50. R Fedosejers & M C Richardson

IEEE J of QE v QE16 (1980) p 985–989

51. D J Kuizenga & A E Yariv

IEEE J of QE v QE6 (1970) p 694–708

52. D J Kuizenga, D W Phillion, T Lund & A E Siegman

Opt Comm v 9 (1973) p 221–226

53. A E Siegman & D J Kuizenga

Opto–electronics v 6 (1974) p 43–66

54. D J Kuizenga

IEEE of QE v QE17 (1981) p 1694–1708

55. M Di Domenico Jr

J Appl Phys v 35 (1964) p 2870–2876

56. M E Crowell

IEEE J of QE v QE1 (1965) p 12–20

57. S De Silvestri, P Laporta & O Svelto

IEEE J of QE v QE20 (1984) p 533–538

58. S H Wemple

Appl Opt v 18 (1979) p 31–35

59. J P Tache

Appl Opt v 26 (1987) p 427–429

60. D C Hanna

IEEE J of QE v QE5 (1969) p 483–488

61. H G Danielmeyer & F W Ostermayer Jr

J Appl Phys v 43 (1972) p 2911–2913

Acknowledgements

I would like, in particular, to thank my supervisor Dr A C Tropper for her advice and guidance during the course of this work. Also, I would like to thank Dr D C Hanna and Dr A I Ferguson for their useful discussions and encouragement. My thanks also go to the members of the Optical Fibre Group, especially Simon Poole, at Southampton University for providing the doped fibre and the facility to splice fibres. The financial support of the SERC and the loan of various laser components by Coherent UK is gratefully acknowledged.